MONASH University

Microarray-Based Sensors for Epidermal and Transdermal Diagnostics

Muamer Dervisevic

B.Sc. and M.Sc.
in
Genetics and Bioengineering

A thesis submitted for the degree of

Doctor of Philosophy

at

Monash University

2020

Drug Delivery, Disposition and Dynamics
Monash Institute of Pharmaceutical Science

Copyright notice

Contents

Abstract

Wearable biosensors have received growing worldwide attention due to its wide application in individual and public health monitoring and disease diagnosis. The potential affordability and accessibility of wearable technologies promises fast monitoring of various disease biomarkers which is beneficial not only to patients with chronic diseases, such as diabetes or cancer patients with overwhelming human, economic, and social consequences, but also healthy individuals with high risk to develop a disease. Advancements in microfabrication research have enhanced the development of such wearable sensing devices by providing solutions to some of the challenging problems faced in wearable sensing area. This thesis focuses on the development of micro-structured array-based electrochemical sensing platforms for patient-friendly epidermal and transdermal diagnostics from sweat and interstitial fluid. Microarray-based diagnostics have several advantages over conventional detection methods by promoting compliance and convenience for the patients with non-invasive and minimally invasive painless procedures, avoiding uncomfortable sample collection, and decreasing the possibility of bacterial infections that might occur when conventional needles are used.

In this project, two types of microarrays were used: micropillar arrays (MPA) and microneedle arrays (MNA). MPA and MNA have been used to develop three-electrode wearable patches composed of reference, counter, and working electrodes to be used for the electrochemical detection of clinically relevant biomarkers. Since the sensing platforms come into contact with skin, MPA and MNA are made of biocompatible material silicon which is at the same time a versatile material for nano- and microfabrication. Silicon microarrays were coated with a thin gold layer that

provides electrical conductivity to microarrays as well as a surface for reliable and flexible chemical modifications for the construction of the bio-recognition interface.

Two different sensing approaches have been explored. An enzymatic approach has been used for the detection of glucose in sweat and interstitial fluid using MPA and MNA platforms, respectively, and an immunosensing approach using MNA-based platform designed for the detection of the breast cancer biomarker Erbb2. The MPA patch was successfully applied for the detection of glucose in human sweat showing very good correlation with glucose levels found in blood. *In vivo* application of the MNA in mice shows that the interstitial fluid`s glucose concentrations obtained with the MNA sensor gave very good correlation with the blood glucose levels determined with a commercial glucometer. Regarding the immunosensor work, high-density gold-coated silicon MNA were simultaneously used as biomarker extraction platform and electrochemical transducer, enabling the selective immunocapture of ErbB2, a key breast cancer biomarker, and its subsequent quantification. The sensing platforms presented in this thesis will advance the research undertaken for designing and engineering microarrays as noninvasive and minimally invasive electrochemical wearable sensors by providing solutions when tackling some of the challenges faced.

Thesis including published works declaration

I hereby declare that this thesis contains no material which has been accepted for the award of any other degree or diploma at any university or equivalent institution and that, to the best of my knowledge and belief, this thesis contains no material previously published or written by another person, except where due reference is made in the text of the thesis.

This thesis includes two original papers published in peer reviewed journal. The core theme of the thesis is **"Microarray-Based Sensors for Epidermal and Transdermal Diagnostics"**. The ideas, development and writing up of all the papers in the thesis were the principal responsibility of myself, the student, working within the **Drug Delivery, Disposition and Dynamics at the Monash Institute of Pharmaceutical Sciences**, under the supervision of **Professor Nicolas H. Voelcker, Dr Beatriz Prieto-Simón**, and **Dr Maria Alba**.

The inclusion of co-authors reflects the fact that the work came from active collaboration between researchers and acknowledges input into team-based research.

In the case of *Chapter 2* and *Chapter 4* my contribution to the work involved the following:

Thesis Chapter	Publication Title	Status *(published, in press, accepted or returned for revision, submitted)*	Nature and % of student contribution	Co-author name(s) Nature and % of Co-author's contribution*	Co-author(s), Monash student Y/N*
2	*Skin in the Diagnostics Game: Wearable Biosensor Nano- and Microsystems for Medical Diagnostics*	Published	*55%* *Concept, literature research and writing first draft*	• *M. Alba 25%* *Manuscript preparation* • *B. Prieto-Simon 10%* *Manuscript preparation* • *N.H. Voelcker 10%* *Concept, manuscript editing*	No No No
4	Transdermal Electrochemical Monitoring of Glucose via High-density Silicon Microneedle Array Patch	Published	70% Concept, method development, data collection and analysis, and writing first draft	• *M. Alba 10%* *Research supervision* *Manuscript preparation* • *L. Yan 6%* *help in experiment set up* • *M. Senel 2%* *help in experiment set up* • *T.R. Gengenbach 2%* *help in experiment set up* • *B. Prieto-Simon 5%* *Research supervision* *Manuscript preparation* • *N.H. Voelcker 5%* *Concept, research supervision* *Manuscript editing*	No No No No No No

I have renumbered sections of submitted or published papers in order to generate a consistent presentation within the thesis.

Student name: Muamer Dervisevic

Student signature: **Date:**

I hereby certify that the above declaration correctly reflects the nature and extent of the student's and co-authors' contributions to this work. In instances where I am not the responsible author I have consulted with the responsible author to agree on the respective contributions of the authors.

Main Supervisor name: Nicolas H. Voelcker

Main Supervisor signature: **Date:**

Publications

1. **Dervisevic, M.**; Alba, M.; Yan, L.; Senel, M.; Gengenbach, T.R.; Prieto-Simon, B.; Voelcker, N.H. Transdermal Electrochemical Monitoring of Glucose via High-density Silicon Microneedle Array Patch. *Advanced Functional Materials, **2021**, 2009850.*

2. **Dervisevic, M.**; Alba, M.; Prieto-Simon, B.; Voelcker, N.H. Skin in the Diagnostics Game: Wearable Biosensor Nano- and Microsystems for Medical Diagnostics. *Nano Today, **2020**, 30, 100828.*

Publications during enrolment:

3. Senel, M.; Dervisevic, E.; Alhasse, S.; **Dervisevic, M.**: Alachkar, A.; Cadarso, V.J.; Voelcker, N.H. Microfluidic Electrochemical Sensor for Cerebrospinal Fluid and Blood Dopamine Detection in a Mouse Model of Parkinsons Disease. *Analytical Chemistry, **2020**, 92, 12347-12355.*

4. **Dervisevic, M.**; Shi, Q.; Alba, M.; Prieto-Simon, B.; Cheng, W.; Voelcker, N.H. Enzyme-like Electrocatalysis from 2D Janus Gold Nanograss-Nanocube Assemblies. *Journal of Colloid and Interface Science, **2020**, 575, 24-34.*

5. Senel, M.; **Dervisevic, M.**; Alhassen, S.; Alachkar, A.; Voelcker, N.H. Electrochemical Micropyramid Array-based Sensor for in Situ Monitoring of Dopamine Released from Neuroblastoma Cells. *Analytical Chemistry, **2020**, 92, 7746-7753.*

6. Dervisevic, E.; **Dervisevic, M.**; Wang, Y.; Malaver-Ortega, L.F.; Cheng, W.; Tuck, K.L.; Voelcker, N.H.; Cadarso, V.J. Highly Selective Nanostructured Electrochemical Sensor Utilising Densely Packed Ultrathin Gold Nanowires Film. *Electroanalysis, **2020**, 32, 1850-1858.*

7. Senel, M.; **Dervisevic, M.**; Esser, L.; Dervisevic, E.; Dyson, J.; Easton, C.D.; Cadarso, V.J.; Voelcker, N.H. Enhanced Electrochemical Sensing Performance by *In Situ* Electrocopolymerization of Pyrrole and Thiophene-Grafted Chitosan. *International Journal of Biological Macromolecules, **2020**, 143, 582-593.*

8. Senel, M.; **Dervisevic, M.**; Voelcker, N.H. Gold Microneedles Fabricated by Casting of Gold Ink Used for Urea Sensing. *Materials Letters, **2019**, 243, 50-53.*

Acknowledgements

Firstly, I would like to thank and express my deepest appreciation to my supervisors Professor Nicolas H. Voelcker, Dr Beatriz Prieto-Simon, and Dr Maria Alba for their patience, support, and guidance throughout my Ph.D. journey. Many thanks to all of you for your useful critique, assistance, and suggestions that you have provided during the process of writing my thesis, manuscripts, and designing experimental work. I would also like to thank you for demonstrating how to set high standards and be creative in my work.

I would like to thank to Dr Tony Yan for his help with *in vivo* studies, Nazia Tabassum for her help in fabrication of micropillars, Prof. Mehmet Senel for providing Fc-PAMAM as well as for his support during my Ph.D. study, and to the Volcker group members, especially those at Melbourne Center for Nanofabrication (MCN); Raj Minhas, Sanduru Krishnan, Stella Aslanoglu, Dr Eduardo Ceron, and Dr Amane Shiohara. Also special thanks to MCN process engineer Dr Ricky Tjeung, and Dan Smith.

I am grateful to my family who nurtured and provided education to me and who has always been very understanding and supportive. I wish to express my deep and sincere gratitude to Zahid and Bahrija Ramulic for their company, support, and their effort in making our stay in Australia pleasant and joyful.

My deep and sincere gratitude and many thanks to my wife, friend, and coworker Esma Dervisevic for her unparalleled love, encouragement, and unconditional support over all of these years and special thanks for her scientific advice and suggestions.

Thanks to the Monash University for funding my studies and research with the Monash University Graduate Scholarship and Monash International Postgraduate Research Scholarship. Thanks also to the Probing Biosystems Future Science Platform of Commonwealth Scientific and industrial Research Organization (CSIRO) for funding my research and for providing me with CSIRO Postgraduate Research Scholarship.

Chapter 1: Introduction

1.1 Introductory Background

Health monitoring system can benefit an individual by providing early diagnosis, potentially becoming lifesaving in progressive diseases such as diabetes,[1] and cancer.[2] Early diagnosis can increase the treatment efficiency, life expectancy, and the overall life quality.[3] In contrast to health monitoring systems where the presence of a disease is being investigated, patient monitoring systems monitor vital signals including heart rate and blood pressure, in order to evaluate the treatment efficacy and warn against a life threatening condition.[4] In both systems, diagnosis relies on traditional methods of analysis that priorities quality and reliability of the results over the processing time.[5] However, there is an increasing demand for providing personalized, easy to implement, specialized, rapid, and affordable diagnostic approaches to the healthcare sector due to several reasons, which include but are not limited to: the insufficient healthcare providers, aging population, increasing number of patients with chronic diseases, patients with disabilities facing mobility issues, and infectious disease outbreaks.[6,7]

Point-of-care diagnostic technology can benefit both health monitoring and patient monitoring systems due to its ability to provide on-site fast detection of a target biomarker without requiring specialized equipment and highly skilled operational personnel. Wearable sensing technology has attracted enormous academic and industrial research interest because of its potential to provide point-of-care testing in a continuous, convenient, noninvasive, and real-time fashion when being physically attached to the body of the individual.[8] Today, a wide range of wearable sensors performing electrophysiological measurements are already commercially available to track heart rate, sleep or physical activity. Their affordability thus accessibility and practicality, combined with reliable detection capability, capture significant interest in

using these technologies from both healthcare provider and for home settings.[9] However, molecular wearable sensors, which are able to monitor molecular markers of physiology, pathology, or therapy, demand additional research to reach the consumers. These sensors require more sophisticated transducer technology due to having an interface with a body fluid, which can provide the molecular markers, when performing efficient sensing.

Most wearable sensing devices utilize electrochemical methods due to their suitability for continuous monitoring in a wide range of applications and miniaturization, high performance, and affordability.[10] Those sensors involve an electrochemical transducer which converts chemical and biological information into electrical one. These sensors contain a chemically and biologically selective layer that interacts with the target analyte or biomarker and is used to relate the concentration (or presence) of the targeted compound with the changes observed in the electrical signal, which can be in the form of current, resistivity, or potential.[11] A biomarker is any substance, structure, or process that can be measured in the body or its products and can influence or predict the incidence of outcome or disease.[12] Electrochemical sensing has been used to monitor biomarkers found in various biofluids including tears, sweat, saliva, and skin interstitial fluid by overcoming the challenges regarding the complex biochemical nature of these biofluids, which can limit the required sensing performance.

Progress in micro- and nanotechnologies have greatly benefited the development of wearable biosensors because of the solutions they offer when tackling sensitivity, miniaturization, and cost-related problems. The high surface area to volume ratio allows amplified signals, improved catalytic properties and higher electrical conductivity, which result in enhanced sensitivity. Moreover, they have the

potential to reduce foreign body and immune responses, leading to longer sensor working lives.[9]

In this thesis, the application of microstructured arrays as wearable electrochemical sensing devices for the monitoring of biomarkers found in sweat and skin interstitial fluid (ISF) has been explored. A micropillar-based (MPA) wearable sensing patch was fabricated, optimized, and used to monitor glucose in human sweat. A second sensing patch containing microneedle arrays (MNA) was also developed and optimized for the detection of first glucose, and second a breast cancer biomarker (ErbB2), both found in skin interstitial fluid. On the one hand, the detection of glucose using the developed wearable platforms promises technology adoption by diabetic patients, because it can be translated into an affordable point-of-care testing device capable of real-time and continuous monitoring. On the other hand, the application of a wearable device to the detection of a cancer biomarker can provide a better understanding of, and lead to one step closer to, cancer diagnosis based on biomarkers found in skin interstitial fluid using a point-of-care device.

1.2 Hypothesis and Specific Objectives

This thesis builds on the hypothesis that sweat and ISF contain biomarkers that can be used for diagnostics just as blood is, with the benefit of being accessible without reaching blood vessels or nerve bundles, and that microarrays can be engineered in the form of highly sensitive and selective wearable electrochemical sensing platforms to interact with any of these body fluids for the detection and quantification of biomarkers. The main objective of this thesis is to develop microarray-based sensing platforms with the potential to facilitate disease diagnostics and health monitoring without causing any pain or risk of any type of infection.

Specific objectives of the thesis are to:

1. Design and fabricate silicon microarray structures suitable for targeting sweat or ISF.
2. Develop wearable sensing patch by integrating microarrays into three-electrode system suitable for effective electrochemical sensing.
3. Modify the surface chemistry of the working electrode according to the specific application and to characterize and optimize the sensing patch.
4. Assess the analytical performance of wearable platforms and validate wearable patches in tailored application scenarios.

1.3 Scope and Structure of Thesis

Chapter 2 reviews current advances on the development of skin-interfaced biosensors for the determination of physiological biomarkers from different skin layers in great detail. This chapter starts with an overview of the anatomy of the skin and the properties of the biofluids therein contained i.e. sweat, ISF, and blood. The chapter continues discussing the progress in biosensors targeting different layers of the skin, divided into three parts; i) wearable sweat-based biosensors; ii) transdermal biosensors, and iii) subcutaneously implanted biosensors. Each subsection focuses on recent scientific and technological advancements in the field of wearable biosensing micro- and nanosystems by highlighting critical challenges as well as providing information on how these challenges are being addressed by the research community.

Chapter 3 reports the fabrication and optimization of a wearable glucose-sensing patch utilizing a high-density silicon micropillar array for the noninvasive monitoring of glucose levels in human sweat. This sensing patch is composed of three-electrode system containing reference, counter, and working electrodes made of silicon MPA. This chapter addresses some of the challenges faced with wearable technology by providing a solution to one of the recurrent issues faced by epidermal sensors: loss of the recognition element (e.g. enzyme) when exposed to mechanical friction induced between skin and electrode surface. The chapter describes detailed fabrication, characterization, optimization, and successful real sample application of the wearable sensor in monitoring of glucose in human sweat.

Chapter 4 exploits the use of a high-density MNA patch for transdermal monitoring of glucose in ISF. Here, the fabrication, optimization, and application of MNA-based three-electrode system consisting of counter, reference, and working electrodes is described in details. Current technology for blood glucose level monitoring is mainly based on the invasive finger-prick extraction of a small drop of blood using a lancet and measuring via handheld glucometers, which is not conducive to continuous measurements. ISF is gaining attention as an alternative biofluid. Its biochemical composition is very similar to that of blood and it can be monitored in a continuous manner via minimally invasive methods that cause no pain and minimize any risk of infection. The electrodes consist of arrays of microneedles, which are the downsized form of conventional hypodermic needles, with few hundred μm in length making them less invasive and enabling monitoring without causing pain or discomfort. The developed MNA patch provides a high surface area to interface transdermal ISF, facilitating the measurement of glucose at physiologically relevant levels without

reaching the blood vessels or nerve terminations. Glucose detection and quantification analysis carried out *in vitro* demonstrated high selectivity and sensitivity of the microneedle patch. *In vivo* application of the microneedle array in mice showed very good correlation between the ISF glucose concentrations obtained with the MNA patch and the blood glucose levels determined with a commercial glucometer. This microneedle-based sensing system hence provides an alternative transdermal diagnostic tool to the existing invasive techniques.

Chapter 5 reports a different application of the high-density silicon MNA that involves the simultaneous usage of the patch as biomarker extraction platform and electrochemical transducer, enabling the selective immunocapture of ErbB2, a key breast cancer biomarker, and its subsequent quantification. The analytical performance of the device was tested in artificial ISF, which exhibited a linear response over a wide concentration range (from 50 to 250 ng/mL), with a detection limit of 25 ng/mL adequate to detect ErbB2 breast cancer biomarker in healthy individuals as well as in breast cancer patients. The immunosensor showed excellent selectivity towards Erbb2 in the presence of glucose, glycine, T4 bacteriophage, and insulin. As a proof of concept, the immunosensor demonstrated its ability to successfully extract and quantify ErbB2 from a phantom gel skin model that mimicked the epidermis and dermis layers. The uniqueness of this sensing platform combining direct biomarker transdermal extraction and quantification opens up new avenues towards the development of high-performing point-of-care devices for cancer diagnosis and prognosis.

Finally**, Chapter 6** summarizes the contribution of this thesis to the development of wearable biosensors based on high-density microarrays, with smart chemical modifications, and their application to the electrochemical sensing of model biomarkers. A future perspective of epidermal and transdermal biosensors in diagnosis and health monitoring is also provided.

1.4 References

(1) Fonseca, V. A. Defining and characterizing the progression of type 2 diabetes, *Diabetes Care* **2009**, *32 Suppl 2*, S151-S156.

(2) Costantini, A.; Corny, J.; Fallet, V.; Renet, S.; Friard, S.; Chouaid, C.; Duchemann, B.; Giroux-Leprieur, E.; Taillade, L.; Doucet, L.; Nguenang, M.; Jouveshomme, S.; Wislez, M.; Tredaniel, J.; Cadranel, J. Hyper-progressive disease in patients with advanced non-small cell lung cancer (NSCLC) treated with nivolumab (nivo), *European Respiratory Journal* **2018**, *52*, PA2808.

(3) Cheng, M.; Zhu, G.; Zhang, F.; Tang, W.-l.; Jianping, S.; Yang, J.-q.; Zhu, L.-y. A review of flexible force sensors for human health monitoring, *Journal of Advanced Research* **2020**, *26*, 53-68.

(4) Gardner, R. M.; Shabot, M. M. In *Medical Informatics: Computer Applications in Health Care and Biomedicine*, Shortliffe, E. H.; Perreault, L. E., Eds.; Springer New York: New York, NY, 2001, pp 443-484.

(5) Drenck, N.-E. Point of care testing in Critical Care Medicine: the clinician's view, *Clinica Chimica Acta* **2001**, *307*, 3-7.

(6) Majumder, S.; Deen, M. J. Smartphone Sensors for Health Monitoring and Diagnosis, *Sensors (Basel)* **2019**, *19*, 2164.

(7) Lingervelder, D.; Koffijberg, H.; Kusters, R.; IJzerman, M. J. Point-of-care testing in primary care: A systematic review on implementation aspects addressed in test evaluations, *International Journal of Clinical Practice* **2019**, *73*, e13392.

(8) Guk, K.; Han, G.; Lim, J.; Jeong, K.; Kang, T.; Lim, E.-K.; Jung, J. Evolution of Wearable Devices with Real-Time Disease Monitoring for Personalized Healthcare, *Nanomaterials (Basel)* **2019**, *9*, 813.

(9) Dervisevic, M.; Alba, M.; Prieto-Simon, B.; Voelcker, N. H. Skin in the diagnostics game: Wearable biosensor nano- and microsystems for medical diagnostics, *Nano Today* **2020**, *30*, 100828.

(10) Bandodkar, A. J.; Wang, J. Non-invasive wearable electrochemical sensors: a review, *Trends in Biotechnology* **2014**, *32*, 363-371.

(11) Antuña-Jiménez, D.; Díaz-Díaz, G.; Blanco-López, M. C.; Lobo-Castañón, M. J.; Miranda-Ordieres, A. J.; Tuñón-Blanco, P. In *Molecularly Imprinted Sensors*, Li, S.; Ge, Y.; Piletsky, S. A.; Lunec, J., Eds.; Elsevier: Amsterdam, 2012, pp 1-34.

(12) Strimbu K, Tavel J.A. What are biomarkers? *Current Opinion in HIV and AIDS* **2010**, 5(6), 463-466.

Chapter 2: Skin in the Diagnostics Game: Wearable Biosensor Nano- and Microsystems for Medical Diagnostics

Declaration

This chapter was published as Dervisevic, M.; Alba, M.; Prieto-Simon, B.; Voelcker, N.H. Skin in the Diagnostics Game: Wearable Biosensor Nano- and Microsystems for Medical Diagnostics. *Nano Today, **2020**, 30, 100828.*

2.1 Introduction

Wearable biosensing devices are arguably the potential next frontier of wearable technologies for fitness as well as individual and public health monitoring.[1-5] Today, a wide range of wearable devices are commercially available to track heart rate, sleep or physical activity. However, the development of wearable devices able to provide information at the molecular level is still at its infancy. The potential affordability and accessibility of such technologies raise interest in personalized medicine not just from the perspective of patients and physicians but also from healthy individuals. Fast growing research on wearable technologies brings us a step closer towards revolutionizing medical practice and healthcare systems to be more proactive rather than just reactive. The main aim of on-body monitoring is to provide continuous information associated with the physiological state of the individual by detecting specific biomarkers of physiology, pathology, or even the effect or effectiveness of therapy. A biomarker is a substance that can be found in body fluids, and whose presence or variation in concentration influences or predicts the incidence or outcome of disease. Biomarkers can range from electrolytes (K^+, Ca^{2+}), to metabolites (glucose, lactate, creatinine), to hormones (cortisol), proteins (interleukins, cytokines) or oligonucleotides (microRNA). Their presence or concentration level may be related to various health conditions, including diabetes (glucose), cystic fibrosis (Cl^-), stress (cortisol), cancer (cytokines) or inflammation (microRNA). For nearly every disease

marker, specific diagnostic methods are available but unfortunately, they are predominantly based on body fluid sampling and analysis through standard laboratory assay techniques.[2] Polymerase chain reaction (PCR), enzyme-linked immunosorbent assay (ELISA), flow cytometry, mass spectrometry, radioimmunoassay, and immunohistochemistry are some of the conventional methods employed to analyze bodily fluids in pathological labs. These methods have enabled the accurate diagnosis of a range of diseases at earlier stages, lowering healthcare costs and providing better health outcomes. They are also routinely used as tools to monitor efficacy of therapies and manage health conditions. Among these techniques, ELISA as an immunoassay and PCR as molecular diagnostic should be considered as the gold standard. Indeed, their development has importantly contributed to the improved screening, detection, monitoring and treatment of, for example, cancers, infectious diseases, and genetic and hormonal disorders. Despite the reliable detection, they remain to be costly and time-consuming, requiring specialized personnel and sophisticated, bulky instruments. This confronts us with the challenge on how to replace these conventional diagnostic methods by wearable devices and translate them into clinical practice. First, highly selective and sensitive biosensors need to be integrated on wearable platforms to continuously measure the levels of specific biomarkers. Following this, the large amount of data generated by these biosensors will need to be properly processed and analyzed to produce a baseline of health state of the user or even a population. The combination of data collection and analytics will enable individualized monitoring of developing health conditions, guidance of therapeutic decisions, management of chronic diseases, and assistance to physicians to predict and prevent diseases.[1]

Over the last two decades, strong efforts have been devoted to exploiting the opportunities that the skin offers in the diagnostics game in both academic and

industrial settings. Although being of high complexity, the skin is the most accessible organ and an important source of biomarkers that could be related to different diseases. These biomarkers may be found in different biofluids accessible from the skin, such as sweat, interstitial fluid (ISF) and blood. The potential is enormous. But the realization of wearable biosensing devices that enable the selective, accurate detection of molecular markers in bodily fluids is still very limited. Today, developed wearable biosensing technology is mostly monopolized by continuous glucose monitoring devices. Some of these devices have recently entered the market and already exceeded US$1 billion in market value.[5] Spurred by the large and growing market for glucose monitoring market for diabetic patients, several other continuous glucose monitoring systems are in the development pipeline and are rapidly progressing towards marketed products. These devices have been conceptualized as noninvasive, minimally invasive or implantable systems. For example, Glucotrack (Integrity Applications), which was approved by European Union (EU) in 2016, is a noninvasive glucose device in the form of an ear clip. This device measures glucose levels in the earlobe tissue and can be used for up to 6 months with working range from 3.9 to 27.8 mM at a cost of ~US$100 per ear clip. Furthermore, a few other devices based on minimally invasive approaches have been approved in recent years by the U.S. Food and Drug Administration (FDA). Dexcom G6 CGM (Dexcom) and FreeStyle Libre (Abbott) are two examples. Both wearable platforms are transdermal patches that target ISF glucose and rely on electrochemical transduction mechanisms. Dexcom and Abbott patches measure glucose continuously for up to 10 days with working range from 2.22 to 22.2 mM and 14 days from 2 to 27.8 mM, respectively. The current cost of these patches ranges from US$90 to US$110 per patch. In addition, some patches like the Dexcom one requires self-calibration two times a day. Very

recently (June 2019), the FDA granted approval to the first continuous glucose monitoring system based on optical methods. Eversense (Senseonics) relies on fluorescence mechanisms to measure ISF glucose for up to 90 days providing glucose readings between 2.22 to 22.2 mM. The device comes in the form of a small stick implant. The Eversense implant costs ~US$99 excluding insertion and removal or replenishing the implant. Sweat wearable biosensing promises to enable more cost-efficient, less invasive glucose monitoring, but the technology is still in an earlier phase of development.[6] However, commercialization of these sensors can certainly be expected in near future. Despite the medium- to long-term monitoring ability in a minimally-invasive manner, most of these wearable devices still require large scale validation studies and development of manufacturing technologies to decrease the cost. In addition, except for glucose, currently there is no reliable sensor for the long-term detection of any other analyte.

Micro- and nanotechnologies are playing a central role in advancing the wearables field.[6] Their potential to address some of the sensitivity, miniaturization, and cost-effectiveness challenges is promising. Micro- and nanoscale materials display attractive physicochemical properties derived from their small size. The high surface area to volume ratio allows amplified signals, improved catalytic properties and higher electrical conductivity, which may result in enhanced biosensing sensitivity.[7] Nanomaterials also show exceptional optical properties. These have been exploited in the realization of highly sensitive fluorescence and surface-enhanced Raman scattering (SERS) biosensors. Metallic nanoparticles, silicon nanowires or carbon nanomaterials are some examples of nanomaterials that have been actively investigated for their application in biosensing. Micro- and nanotechnologies also make miniaturization an attainable task. Biosensing transducers can be designed at

the nanoscale. But even if they need to be designed at a larger scale, micro-sized (or even macro-sized) components can also incorporate nanostructured surfaces or materials within multi-scale platforms. Due to their small size, micro- and nano-biosensing systems also have the potential to reduce foreign body and immune responses, leading to longer sensor working lives. Nanostructured materials are used to provide large active surface area and, in some cases, to boost the electrical conductivity, thereby enhancing the sensitivity of the biosensing system.[8]

This chapter summarizes the current advances on the development of skin-interfaced biosensors for the determination of physiological biomarkers from epidermal, dermal and subdermal fluids (Figure 2.1). Wearable sensors that measure body signals such as heart rate and pressure or wearable motions accelerometers have been extensively reviewed elsewhere and are not covered here.[9] This chapter is divided into three major parts describing on-body measurements at different skin sections, namely epidermis, dermis and hypodermis. The first part summarizes progress in wearable sweat-based biosensors; the second one compiles the advances in transdermal monitoring; and the last part covers subcutaneously implanted biosensors. Every part of this chapter focuses on recent scientific and technological advancements in the field of wearable biosensing micro- and nanosystems by highlighting critical challenges as well as providing information on how these challenges are being addressed by the research community. In each section, representative examples are provided in order to illustrate the sensing components and working principles of the biosensors. Additionally, their limitations and unique features are highlighted and critically discussed. Lastly, a concluding section summarizes the barriers and opportunities in the field and anticipates future research directions. However, before discussing the latest advances in wearable biosensors

and in order to better understand the biological and technological context, a brief insight into skin anatomy and the challenges associated with skin biosensing is given.

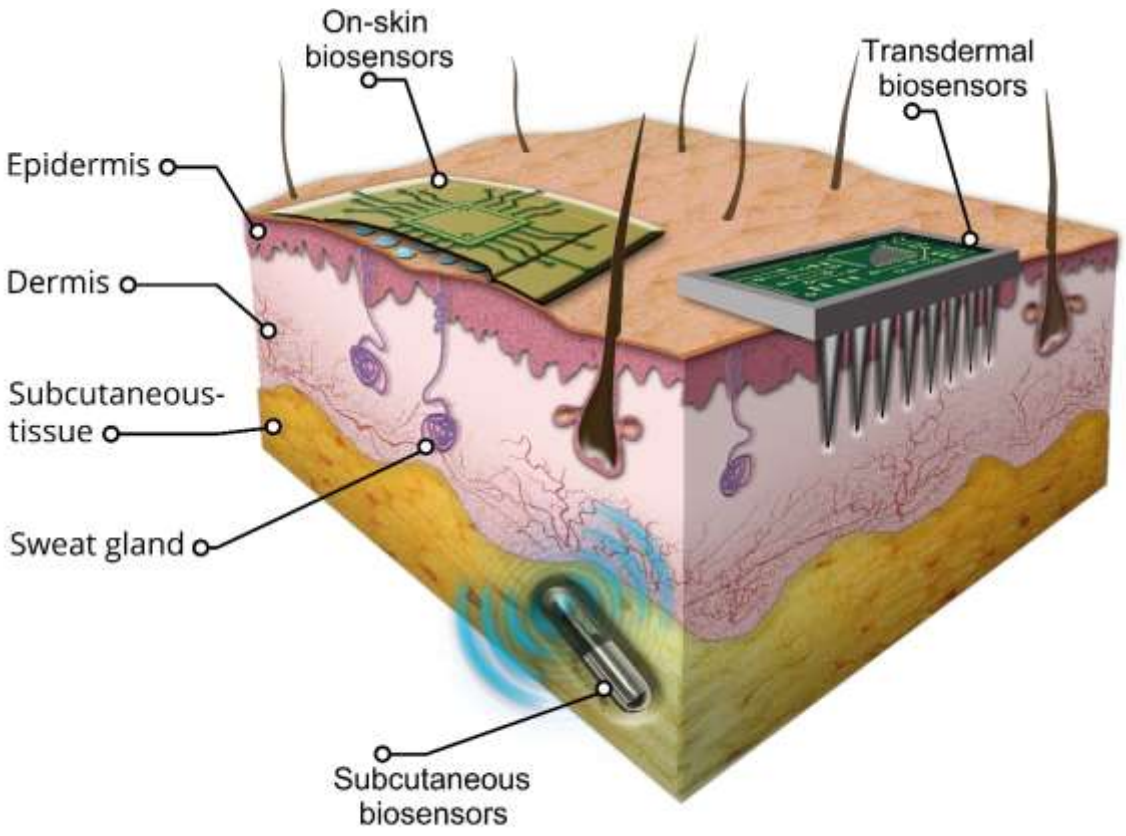

Figure 2.1: Schematic illustration of skin layers and different wearable devices their applications.

2.1.1 Skin Anatomy and Accessible Fluids for Wearable Biosensing

The skin is the largest and most accessible organ in the human body. The biofluids contained in skin are a rich source of biomarkers which are of value not only in diagnosis and monitoring of diseases, but also in profiling an individual's well-being. Nonetheless, the skin is a very complex organ and, in order to better exploit this tissue

for salient biosensing opportunities, understanding of the physiology and the microanatomy of the skin is necessary.

The skin is essential to protect the underlying tissue from external biological, chemical and physical aggressions. It also prevents the loss of body fluids, helps to regulate the body temperature, serves as sensory organ for the surrounding environment, and plays an essential role in the production of antimicrobial peptides and vitamin D.[10] This organ is composed of three main layers: epidermis, dermis, and hypodermis (Figure 2.1). The epidermis, with an average thickness of 150 µm,[11] is a stratified epithelium located in the outermost layer of the skin which continuously renews itself.[12] The outermost layer of the epidermis is the stratum corneum (SC) and is primarily composed of anucleate cells (corneocytes), which mainly provide a hydrophobic barrier to environmental pathogens.[13] The second skin layer is the dermis, located between the epidermis and the subcutaneous tissue or hypodermis. The dermis layer is divided into two regions, the papillary dermis region which is adjacent to the epidermis layer and an underlying thicker region, the reticular dermis.[14] The thickness of the dermis ranges from 500 to 2000 µm depending on its location on the body.[11] The boundary located between the epidermal and dermal layers is called dermoepidermal junction where epidermal basal cells are attached to the basement membrane. This porous membrane provides a space for nutrients and exchange of fluids [10] and acts as a reservoir for molecules required for various biological purposes such as immunity and wound healing.[13] Beneath the dermis and above the muscle is the hypodermis, mostly composed of adipocytes or fat cells, which contains a network of fibrous septa made of blood vessels, lymphatic vessels and collagen. Vascular and nerve structures can be found in the hypodermis and in deeper parts of the dermis layer where blood vessels are supplied by branches of musculocutaneous and

cutaneous arteries coming through the hypodermis whereas nerves course through the dermis in nerve bundles.[10] The space outside the parenchymal cells, blood and lymphatic vessels is called the interstitial space, or interstitium and is filled with ISF.

The skin therefore offers non-invasive access to three different biofluids namely sweat, ISF and blood. These fluids may be very different in nature, but all three comprise a wealth of biochemical information that may provide indication of an individual's health state.

Easy access and sampling of sweat makes it very convenient for wearable sensing. It plays an important physiological role in thermoregulation, moisturization, immune defense, and electrolyte and pH balance.[15] Sweat is secreted by eccrine glands after neurotransmitter stimulation and conducted to the skin surface through dermal ducts.[1,15] Acetylcholine is the main neurotransmitter responsible for sweat stimulation, causing release of Ca^{2+} which in turn causes water, Na^{+} and Cl^{-} ions to flow into the lumen and induce the generation of sweat. Apart from water, Na^{+} and Cl^{-} ions, the secreted sweat also contains metabolites, hormones, proteins and peptides.[16] Although the partitioning mechanisms at play are yet poorly understood, it has been hypothesized that analytes contained in sweat passively or actively diffuse from neighboring blood or ISF at levels ranging from mM (urea, lactate) to µM (glucose) to nM or pM traces (proteins).[1] In addition, it is worth noting that a variation in sweat composition profile may be expected depending on the mechanism of stimulation, whether heat, exercise, stress or a chemical stimulus is responsible for its generation.[17,18]

ISF is another source of valuable biomarkers but it has been traditionally difficult to sample from the human body. This fluid surrounds parenchymal cells, blood and lymphatic vessels, and it is formed by extravasation of plasma from capillaries. ISF

constitutes 45% of the volume fraction of the human skin and it can be seen as a combination of serum and cellular materials. The ISF plays important roles in the transport of signaling molecules between cells and also in carrying antigens and cytokines to local draining lymph nodes for immune regulation. It is furthermore involved in the transport of nutrients and waste between blood capillaries and cells.[19] ISF is not just a passive conduit for the flux of solute and fluids, it actually functions as highly dynamic and complex structure having profound influences on fluid exchange.[20] The fluid exchange between the vascular and interstitial compartments is regulated by hydrostatic and oncotic (protein-induced osmotic) forces operating within the extracellular matrix (ECM) and lymphatics, and across microvascular walls.[20] Impelling forces of fluid flux through the interstitial space are essential for protein transport from blood to interstitial cells, because proteins are too large to diffuse through the crosslinked ECM.[20] Tran and co-workers study on proteomics characterization of dermal ISF demonstrated that the protein composition in ISF matches approximately 93% with that found in serum and plasma.[13] However, it has also been reported that the concentration of proteins and ions are about one-third lower in ISF than in blood. The concentration of glucose in ISF is, however, identical to that in blood in steady-state conditions, but there may be a lag time immediately after glucose intake due to the kinetics of diffusion.[21]

Blood is the most commonly sampled fluid for clinical diagnosis and its proteome has been well studied.[22,23] However, access to blood has been traditionally limited by the requirement for trained healthcare professionals when drawing venous blood or by the patient's apprehension when collecting finger-prick blood samples. Although blood contributes to only 5% of the skin volume fraction, it can be non-invasively collected from the skin. The dermis is a highly vascularized region and here

is where the majority of the blood vessels are located. These vessels supply blood and nutrients to the other layers of the skin through small capillaries. Significant differences have been found between systemic and capillary blood in the levels of total proteins, bilirubin and certain ions (Ca^{2+}, Na^{+}, Cl^{-}), whereas the concentrations of other analytes such as glucose, urea and K^{+} are practically identical.[24]

As illustrative examples, Table 2.1 shows a list of selected biomarkers representing ions, metabolites, hormones and proteins classes. They are listed together with the concentration found in blood, ISF and sweat found of healthy individuals. For most biomarkers of low molecular weight (i.e. < 400 Da) such as ions, metabolites and hormones, their ISF concentration is very similar to blood. This is due to rapid diffusion through the capillary walls. However, for higher molecular weight species, capillary walls have a filtering effect.[5] As the molecular weight increases, the diffusion rate from blood into ISF decreases. A conversion factor may be required to determine the diluted concentration of these high molecular weight proteins in the ISF.[5,25] The ratio between biomarker concentration in sweat and blood/ISF may be much more complicated to correlate. As mentioned before, analyte concentration in sweat greatly depends on the sweat secretion rate and dilution effect. Some studies have suggested that the molecular weight of the analyte, as well as its lipophilicity, play a strong role in partitioning mechanisms in sweat.[5] For example, hydrophilic glucose (180 Da) is found in sweat at about 1% concentration of that in blood. But concentration of hydrophobic cortisol (362 Da) in sweat shows a good correlation with blood levels. Protein concentration in sweat can be as high as tens of μM for those actively secreted. But passively transported proteins are typically found in sweat at concentration levels below 0.1% of those in blood.[5]

Table 2.1: Comparison of several analytes' concentrations found in blood, ISF and sweat.

		Blood	ISF	Sweat
Ions	Na^+	135-145 mM*	Similar to plasma	10-90 mM [26,27]
	K^+*	3.5-5.5 mM*		2-10 mM [27]
	Cl	95-110 mM*		14-48 mM [28]
	Ca^{2+}	>2.6 mM*		0.37 mM [29]
Metabolites	Glucose*	3.6-6.0 mM*	Similar to plasma	36-60 µM [32]
	Lactate	0.5-10 mM		5.0-20 mM [33]
	Urea*	3.0-7.5 mM*		13-24 mM [34]
	Cholesterol*	<3.5 mM*		-
	Uric acid	0.12-0.45 mM [30]		25-36 µM [34]
	Ascorbic acid	30-80 µM [31]		10-50 µM [35,36]
Hormones	Cortisol	Morning 193-773 nM [37] Afternoon 55-496.6 nM	Similar to plasma	20-500 nM [38]
Proteins	Cytokines	pM to nM	80 % of plasma	<0.1% of plasma
	Antibodies e.g. IgA	0.4 -16 mg/mL ~262 mg/mL[39]	15-25 % of plasma	0.1-10 ng/mL[40]

*****values obtained from Melbourne Pathology biochemical analysis test

2.1.2 Challenges for Wearable Biosensing

The translation of wearable biosensors into routine technology that offers comprehensive information about the physical activity and health state of an individual is imminent. This foreseeable achievement is arguably spurred by the accurate and robust quantification of biomarkers present in skin biofluids. However, for the successful development of wearable biosensors, multiple challenges and technological gaps still need to be addressed. Some of these critical challenges relate to data acquisition and processing, communications, power supply, wearability (stretchability, bendability), and security, and those are not reviewed here. We refer the reader to several excellent reviews which focus on these topics in detail.[41-45] We will instead emphasize on the key challenges that this field is still facing in terms of

biosensor design, that is, the physical and chemical aspects of its elements, and its consequential sensing attributes.

The ability of the biosensing platform to interface with the skin causing minimal disruption of the tissue and its microenvironment whilst remaining fully functional is one of the most important challenges in the development of wearable biosensors. This is intrinsically linked to its biocompatibility as well as its anti-fouling characteristics. These features will ultimately govern the biosensor stability and, subsequently, its lifetime for long-term applications. Depending on the nature of the wearable device and the analyte of interest, desirable lifetimes range from a few minutes to several months. For example, disposable sweat biosensors for the detection of illicit drugs may need to be used for only a few minutes. Implantable devices, however, should remain functional for at least few weeks (e.g. Dexcom G6), and ideally several months (e.g. Eversense) or even years. The degree of biocompatibility will depend on many factors including biosensor geometry, size and water content. Most importantly, it will be greatly influenced by the bulk and surface chemical properties of the material. The material should be selected to not cause inflammation and to minimize biofouling. The effect that the accumulation of chemical and biological species has on the biosensor performance may be critical. Hydrophilic, flexible materials such as polymeric chains (e.g. polyurethane,[46] polyethylene glycol (PEG),[47] zwitterionic polymers,[48]) have been extensively investigated as coating layers because of their non-inflammatory, non-toxic as well as anti-fouling properties. Additionally, from a practical perspective, attention should also be paid to minimizing the need for calibration and to render operation by the end user as simple as possible. Usually, continuous monitoring of biomarkers requires an initial calibration, and in many occasions, also a recalibration at regular time intervals. Hence, researchers have focused their efforts in developing

one-point calibration biosensors considering a zero baseline.[49,50] Reduced biofouling will facilitate the use of biosensors for continuous monitoring and, ultimately, minimize calibration requirements.

The application of transdermal and subdermal devices inevitably involves certain damage to the tissue and therefore those devices must meet the highest requirements in biocompatibility. Furthermore, in the long-term applications based on transdermal or implantable systems, a foreign body response will ensue after the device is inserted. This response may result in drastic change in the microenvironment and in macrophage and lymphocyte attack,[51] which will most likely affect the biosensor signal. Moderation of the foreign body response may be achieved by using active layers for reduction of reactive oxygen species [52] or by introducing nano-topographical modifications on the biosensor surface.[53] Attempts have been made in terms of incorporating anti-inflammatory agents such as dexamethasone into hydrogel-based sensors to control inflammation at the biosensor application site.[54] Surface modifications employed in the biosensor design will not only improve the biocompatibility but also the bioreceptor stability, and ultimately the response reliability and the lifetime of the device. Stable biosensors have been successfully built by coupling the biorecognition element with various nanomaterials (e.g. quantum dots, carbon nanotubes),[55] hydrogels (e.g. chitosan, gelatin) [56,57] or others through a range of chemical and physical immobilization protocols.[58] We are still not at the point of being able to 'dial in' material and surface modification approach, and hence those parameters should only be chosen after initial *in vitro* and ideally *in vivo* tests.

The selectivity of the biosensor will determine the preferential detection of the target analyte versus other interfering species. Affinity-based biosensors and catalytic biosensors, where a bioreceptor specifically interacts or reacts with a target analyte,

are regarded as highly selective and specific and it is this principle that many biosensors rely on. Among the catalytic biosensors, enzyme sensors have continued to be forerunners in the development of wearable sensors due to their excellent selectivity and ability to provide continuous measurements without the need to regenerate their surface.[17,59] The biological response induced by the enzymatic reaction with the analyte can be translated into measurable signals that have allowed qualitative and quantitative analysis of a range of clinical biomarkers. One intrinsic problem of enzymatic systems is that enzymes are proteins sensitive to their microenvironment and factors such as oxygen level, pH, temperature and ionic strength can affect their structure and thus their activity, and subsequently the sensor's response.[60] In addition, enzyme activity often diminishes over time.[61] Affinity-based biosensors, such as immunosensors, DNA sensors or aptamer-based sensors display high target affinity and specificity based on precise three-dimensional complementarity. Nevertheless, high affinity systems are difficult to implement into continuous monitoring devices mainly due to their limited reusability. The main reason for this is that the *in situ* regeneration of the biorecognition element, particularly in wearables or implantables, is extremely difficult to realize. In recent times, important research efforts have been devoted to engineering bioreceptors, not only to create new libraries of novel synthetic and semi-synthetic bioreceptors, but also to manipulate their binding affinity. Engineering of antibody and DNA aptamer structures has enabled the possibility to control their binding properties,[62] so that a biosensor can be potentially regenerated and reused. Biosensors can also be regenerated by overcoming the attractive forces between bioreceptor and its cognate analyte via various treatments including chemical, thermal and electrochemical regeneration.[63] In this regard, synthetic bioreceptors such as DNA aptamers [64] have showed higher

reversibility over a number of bind-release cycles than antibodies.[65] Despite the substantial challenges presented by affinity-based wearable biosensors, there is a considerable interest in developing this technology due to the plethora of clinically validated targets that can be detected by these assays.[66]

Efforts should also be devoted towards improving the biosensor sensitivity. The physiological levels of many key biomarkers are usually precisely regulated and their presence in skin biofluids occurs over defined concentration ranges. Thus, it is a requirement that the wearable biosensor responds acutely to small but relevant changes in bioanalyte levels. This may not be a priority in applications that seek binary information, such as the detection of illicit drugs, but it is of special importance in continuous monitoring applications where tracking the change of the concentration profiles of biomarkers is critical. Likewise, the biosensor should present a limit of detection (LOD) relevant to physiological conditions. For example, a biosensor that monitors glucose from ISF should be able to detect amounts as low as 3.6 mM (see Table 2.1). But for clinically relevant glucose detection in sweat, biosensors need to be designed to improve the LOD by two orders of magnitude. This is, they need to be able to detect amounts as low as 0.036 mM. The incorporation of nanomaterials such as carbon nanotubes, metallic particles or quantum dots can significantly amplify the biosensor's response signal and therefore improve the sensitivity as well as lower the LOD.[67,68] Engineering of the bioreceptor immobilization can also lead to increased sensitivities. Oriented antibody immobilization strategies have been demonstrated to maximize the biosensor sensitivity.[69,70] Moreover, engineered bioreceptors such as antibody fragments or nanobodies® have been shown to overperform compared with natural antibodies.[71] Nonetheless, certain biomarkers are present in extremely low concentrations in body fluids. For example, cytokines can be found in ISF in nanomolar

concentrations, but their concentration in sweat lies in the sub-picomolar range. Although low-picomolar detection of cytokines have been achieved in lab settings,[72] the translation of these highly sensitive methods into wearable devices is still under development.

Furthermore, despite the fact that the skin is the most accessible organ in the human body, the non-invasive collection of skin biofluids remains a challenge. Skin biofluids in large enough amounts have been typically sampled using complex, time-consuming procedures (i.e. microdialysis, microperfusion, and iontophoresis) that usually involve discomfort, risk of infection, specialized equipment and trained professionals. Currently, the minimally-invasive collection of several microliters of skin biofluids that allow the reliable, accurate detection of analytes in their physiological range is still under development. Skin patches have typically relied on diffusion, capillary action, osmosis and pressure-driven convection for the collection of bodily fluids.[73] The use of adsorbing materials such as woven textiles [74] or porous hydrogels [17] has been widely explored in wearable settings due to their ability to capture and store bodily fluids, although these materials do not allow precise control over the collected and stored volume. Sweat sampling faces additional challenges such as flow rate variations, sweat dilution, sample evaporation and external contamination.[75] Integration of sweat biosensing devices with microfluidics [76,77] or micro-iontophoretic systems [18] are some of the current approaches employed to gain control over sweat storage, sweat rate and biodegradation or evaporation.

Micro- and nano-technologies have given rise to opportunities in developing miniaturized wearable biosensors that allow operation with low volumes of samples and integrate several functions into a single device. Microfluidics, micro-/nano-patterning techniques and thin film deposition methods are some of the technologies

that have allowed the creation of devices measuring only a few millimeters. The design of transducers has greatly benefited from the advances on these miniaturized technologies. Today, electrochemical and optical transducers can be easily miniaturized to the micro-or nano-scale. But to complete the biosensing function, these transducers require usually bulky readout systems. In this context, certain technologies may be placed in an advanced position with respect to others. For instance, electrochemical biosensors require reduced volume of sample and simple electronics. This has allowed the realization of several portable electrochemical biosensors, where the best example is the glucometer. Optical biosensing, in addition to a readout system, require an external light source to induce a measurable optical response, which makes miniaturization a more challenging task. To address this limitation, in recent times researchers have proposed is to integrate readout systems into smartphones to reduce overall size and enable portability.[78,79] Smartphones not only have LED flashes that may be used as illumination sources, but CMOS-based cameras can also be used as signal detectors. They can also process signals and have connectivity, which may promote their application into wearable biosensing.

2.2 On-skin Biosensors

Sweat is the body fluid easiest accessed and therefore suitable for on-skin monitoring devices. This medium can provide a wealth of information related to the body's physiological state and eventually about the health of the patient. For this reason, sweat is one of the most targeted biofluids for the development of non-invasive wearable biosensors. Up to date, various sweat biosensors for monitoring of analytes such as Na^+, Cl^-, K^+, Ca^{2+},[80] Zn^{2+}, Cd^{2+}, Pb^{2+}, Cu^{2+}, Hg^+,[81] glucose,[82] lactate,[33] uric acid and ascorbic acid,[36] ethanol,[83] cortisol [84] etc. have been reported. Although sweat is rich in different types of metabolites and electrolytes which are potential disease markers, extensive effort is still required to tackle the problems involved in its use. These problems are mostly associated to the low rates of sweat production at resting heart rate. Sample evaporation at body temperature, dependence of biomarker concentration on sweat production rate and mechanism, and cross-contamination with molecules already on the skin surface, such as those contained in cosmetics, cause additional problems. In this section, advances in wearable sweat biosensors will be discussed based on the approaches employed to generate this fluid. We can distinguish between naturally occurring (i.e. through physical exercise, thermal heating or stress) and stimulated (i.e. iontophoresis) sweat secretion. The way the fluid is generated will shape the biosensor design in its sampling, sensing and device technology.

2.2.1 Sweat Biosensors

As mentioned before wearable skin-interfaced biosensors provide a non-invasive alternative to conventional diagnostics methods that require blood sampling. Acquiring a blood sample through invasive methods has the potential to cause physical trauma and infection, and usually requires the assistance of a trained healthcare professional.[85] Early investigations on sweat biosensors focused on developing skin-interfaced platforms able to capture sweat during exercise and detect a single bioanalyte. First, tattoo-like approaches were established; later, these were integrated with microfluidics. In recent years, the sweat biosensing proof-of-concept has been extensively validated and numerous skin-interfaced biosensors have been developed based on various detection mechanisms, substrates, nanomaterials, and target analytes.[17,81,82,86,87] Among different types of wearable devices that can analyze sweat directly [17,82,84,86-90] or via their integration with microfluidics,[33,38,77,91] various transduction mechanisms have been utilized including electrochemical and optical ones. Today, some of these wearable biosensors can provide multiplexed information, not only for the simultaneous quantification of multiple biomarkers,[17] but also for maximizing accuracy by tracking other parameters such as temperature, humidity and/or pH.[82] On the other hand, recent developments have combined sensing and drug delivery features via closed-loop systems, which feature self-triggered drug release mechanisms when certain levels of targeted analyte are reached. For example, glucose monitoring may lead to an automatically determined insulin delivery.[82] Regarding the targeting analytes, although sweat contains numerous ions, metabolites and even small amounts of large biomolecules, glucose has been the most commonly studied biomarker in sweat technology and we will therefore extensively review the advances on glucose sweat sensing devices.[17,82,86,87,89,92]

Electrochemical sensing is the most common method used in wearable sweat analysis due to its high sensitivity and simplicity. Recently Lee et al. reported an electrochemical multilayer wearable biosensor for glucose monitoring with multistage transdermal drug delivery for management of diabetes mellitus.[82] The wearable biosensing patch (Figure 2.2a-c) is composed of an ultrathin and stretchable substrate that accommodates various sensors for glucose, humidity, pH, and temperature, and an integrated microneedle array for controlled drug delivery. Glucose monitoring starts with sweat uptake in a porous layer where the humidity sensor is used to measure the critical amount of sweat. When sufficient amount of sweat is present in the sweat-uptake layer, detection of glucose and measurement of pH levels occur. Glucose detection was performed on an electrodeposited nanoporous Au working electrode modified with a mix of glucose oxidase enzyme (GOx), chitosan-graphene and bovine serum albumin. The Au nanoporous structure provided a large electroactive surface area and enhanced H_2O_2 catalytic activity, enabling glucose detection in the range of 10 μM to 1 mM which covers typical glucose concentrations in sweat from hypoglycemic to hyperglycemic states.[32,82] Metformin drug was loaded into temperature-sensitive nanoparticles incorporated into an array of hyaluronic acid hydrogel microneedles. Two types of temperature-sensitive nanoparticles were used with melting temperatures of 40ºC and 45 ºC, respectively, which makes them ideal for temperature-dependent stepwise drug delivery. Integration of the microneedle array with heaters afforded controlled thermal actuation and multistep and triggered drug release through the microneedles in response to an individual's glucose levels. The external part of the wearable device was covered with an elastomeric silicone patch to protect it from the ambient humidity and prevent delamination during skin deformation. The wearable glucose device was applied on human subjects and was

able to detect glucose and measure the skin temperature simultaneously (Figure 2.2c). Unique features of this sensing platform are combination of different sensors for accuracy improvement, incorporation of nanomaterials for improvement of sensitivity and providing suitable environment to the enzyme, as well as combination of monitoring system with drug delivery for diabetes management. Only limitation to this work is lack of wireless system which would drastically ease real application experiments.

In addition to flexible substrates, wearable biosensors need flexible printed circuit electronics which can be easily integrated into the plastic substrates to facilitate adhesion to different parts of the body without affecting the signal quality because of possible deformation in the substrate.[93] Example of such flexible printed circuit was recently reported by Gao et al..[17] Figure 2.2d-f illustrates a mechanically flexible wearable device based on an integrated sensor array for *in situ* multiplexed perspiration analysis with a flexible circuit board for complex signal processing. The device has the ability to selectively and simultaneously screen targeted metabolites (glucose, lactose) and electrolytes (K^+, Na^+). Multiplexing biosensors on a single wearable device can collect more detailed information about the patient's physiological state. The described flexible electrode sensor array enables amperometric enzyme-based sensing of glucose and lactate, and potentiometric sensing of K^+ and Na^+ via ion-selective electrodes. Enzymatic sensors for glucose and lactate detection were prepared by drop-casting a mixture of enzyme (GOx or lactate oxidase, LOx), chitosan and single-walled carbon nanotubes (SWCNT) onto Prussian Blue (PB)-modified Au electrodes. The thickness of the PB film is key to tune the sensitivity and linear response range, while SWCNTs contribute to enhance the mediated electron transfer. SWCNTs have excellent electrical conductivity and large surface area which make

them popular as an electrode or surface integrated active nanomaterial [94] for enhancing the sensitivity of wearable biosensors. Incorporation of temperature sensors made of Cr/Au metal microwires provided real-time calibration of the glucose and lactate sensor readings. While worn on the wrist (Figure 2.2h) and forehead of a human subject exercising on a cycle ergometer, the sensor array was able to measure changes in analyte concentration for different sweat rates.[95] Distinctive characteristic of this work is flexible printed circuit electronics which enables signal processing of two measurement techniques, amperometry and potentiometry, in multiplexing. Through this system, once more is illustrated that additional sensors for accuracy improving is very important in sweat sensing same as incorporation of nanomaterials which not just increases conductivity and surface area but also enhances mediated electron transfer.

Field-effect transistor (FET)-based devices stand out in biosensor research due to their attractive properties such as low-cost manufacturing, mass production capability and sensitivity.[96] FET devices are three-terminal semiconductor devices which are composed of source, drain, and gate electrodes. The working principle of FET biosensors is that the electrical conductance of the sensing component between the source and the drain changes with the specific binding of biomolecules or chemicals onto the surface.[97] For instance, enzyme-based FET biosensors work on the principle that the enzymatic reaction affects the charge at the gate surface and produces a signal change that scales with substrate concentration.[97] Liu et al. recently [86] proposed a FET-based wearable device based on a flexible In_2O_3 nanoribbon (Figure 2.2g and h) fabricated by sputtering ~20 nm thick In_2O_3 on 5 μm flexible polyethylene terephthalate (PET) substrate, after which Au was sputtered to coat source, drain, and side gates. A SonoPlot printer deposited a mixture of chitosan, GOx

and SWCNT on the source and drain pads. Integrating two side gate electrodes coated with Au between four In_2O_3 nanoribbons afforded a FET device with an Ag/AgCl reference electrode positioned in the middle of the device. The additional side gate also coated with Au served to monitor changes in the device potential. The performance of the FET glucose biosensor was tested using human body fluids such as sweat and tears. The sensor showed a LOD of 10 nM being able to distinguish between glucose levels in real human sweat before and after a meal. From this example it can be clearly seen how important nanofabrication is for device miniaturization which is required in wearable sensing technology. Although, sensor has impressive working range in glucose detection of 1 nM to 1 mM it still has to be incorporated in wearable flexible electrical circuit which could be challenging due to the size of the electrodes.

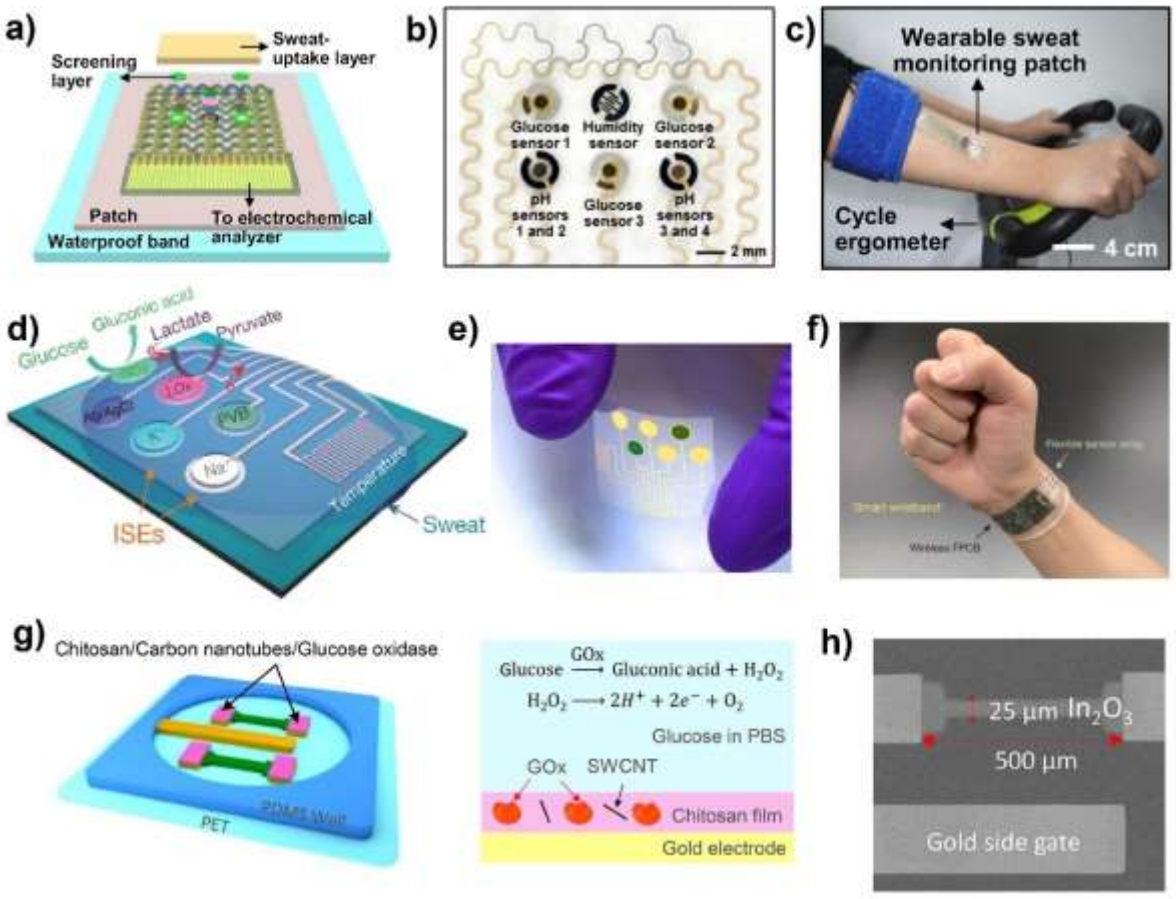

Figure 2.2: Wearable skin-interfaced biosensors for sweat monitoring. **a)** Schematic illustration and **b)** optical image of a sweat analysis biosensor array with glucose, pH, and humidity electrodes, **c)** wearable patch attached on subject's forearm while using cycle ergometer, adapted from Ref. [82] Copyright (2017) American Association for the Advancement of Science, **d)** schematic illustration of a sensor array device for glucose, lactate, Na^+, K^+ and temperature sensing**, e)** optical image of a flexible electrode array and**, f)** wearable device applied on human wrist for glucose, lactate, K^+ and Na^+ detection, adapted with permission from Ref. [17] Copyright (2016) Springer Nature**, g)** schematic illustration of pH and glucose sensing device and working principle of the biosensor, **h)** SEM image of an In_2O_3 nanoribbon device for glucose detection, adapted with permission from Ref. [86] Copyright (2018) American Chemical Society.

The aforementioned studies were able to overcome several important challenges faced when developing devices for direct sweat analysis. Thanks to the incorporation of additional sensors self-calibration increased the reliability of the sensor when ambient conditions such as pH and temperature changed. On the other hand, flexible substrates and electronics overcame the mechanical stress caused by body movement that can lead to device delamination and loss/damage of immobilized bioreceptors due to friction.[93] Nevertheless, flexible sweat biosensors coupled to the skin still do not address the problems related to sample evaporation and sweat rate effects. In order to address these issues, microfluidic systems have been integrated into skin-interfaced biosensors. These wearable devices work on the principle of ensuring adhesion to the skin surface, while collecting sweat from naturally occurring pores and routing the sample towards the biosensing area using micro-channels and/or reservoirs.[16] These flexible microfluidic devices enable the collection and storage of sweat, and allow the analysis of multiple analytes by using different detection techniques that mainly include colorimetric and electrochemical approaches.

Recently, Wang's team introduced the first soft microfluidic platform for epidermal electrochemical sensing of sweat metabolites glucose and lactate.[77] The platform is composed of two soft PDMS layers, the first containing the three-electrode system (working, counter and Ag/AgCl) and the second one with the microfluidic channels and the detection reservoir. The device interfaces with sweat glands across the skin to fill the microfluidic device with sweat (Figure 2.3a). Photo-lithography was used to pattern sensors and interconnect layers after which those patterns were coated by nanolayers depositing 10 nm Ti, 550 nm Cu, 20 nm Ti and 200 nm of Au using e-beam evaporator. Later on, these nanolayer Au based connectors were screen-printed with Prussian blue-modified carbon ink for working and counter

electrodes, and for reference Ag/AgCl ink was used. The working electrode was modified with entrapped LOx or GOx for lactate and glucose sensing, respectively. This study demonstrates the successful combination of mico- and nanofabrication technologies with printed electronics. The microfluidic device was tested on human subjects where on-body electrochemical flow detection capabilities of lactate and glucose were successfully demonstrated (Figure 2.3b). However, interfaces of microfluidic device with sweat glands across the skin should be investigated in more details since dynamic of the skin can drastically vary from patient to patient.

Koh et al. [91] reported a wearable multifunctional microfluidic device for capture, storage and colorimetric sensing of pH, glucose, lactate, and Cl^-. The device consists of a multilayer stack of three subsystems (Figure 2.3c); a skin compatible adhesive layer with integrated micro-machined opening for sweat collection, a sealed collection of microfluidic channels and four reservoirs with integrated color-responsive chemicals for colorimetric detection, and a near field communication (NFC) electronics for wireless communication with an external device. Their channel design avoids backpressure and allows free fluid flow. Commercially available colorimetric D-lactate and Cl^- kits, and pH indicator solution were used for colorimetric sensing. The glucose sensor was prepared with a mixture of GOx, horseradish peroxidase (HRP), trehalose and potassium iodide. A smartphone interface (Figure 2.3d) extracting RGB color information from the sensory parts of the device was used to interpret the analytes concentration. The soft wearable microfluidic device was successfully used to monitor targeted sweat analytes on human subjects during intense physical activities. Since it is only tested on subjects during exercise, limitation of this sensing platform is that it does not address problem regarding low and inconsistent sweat volume rate. Before

commercialization of such colorimetric wearable sweat devices sweat rate volume would be one of the main problems to address.

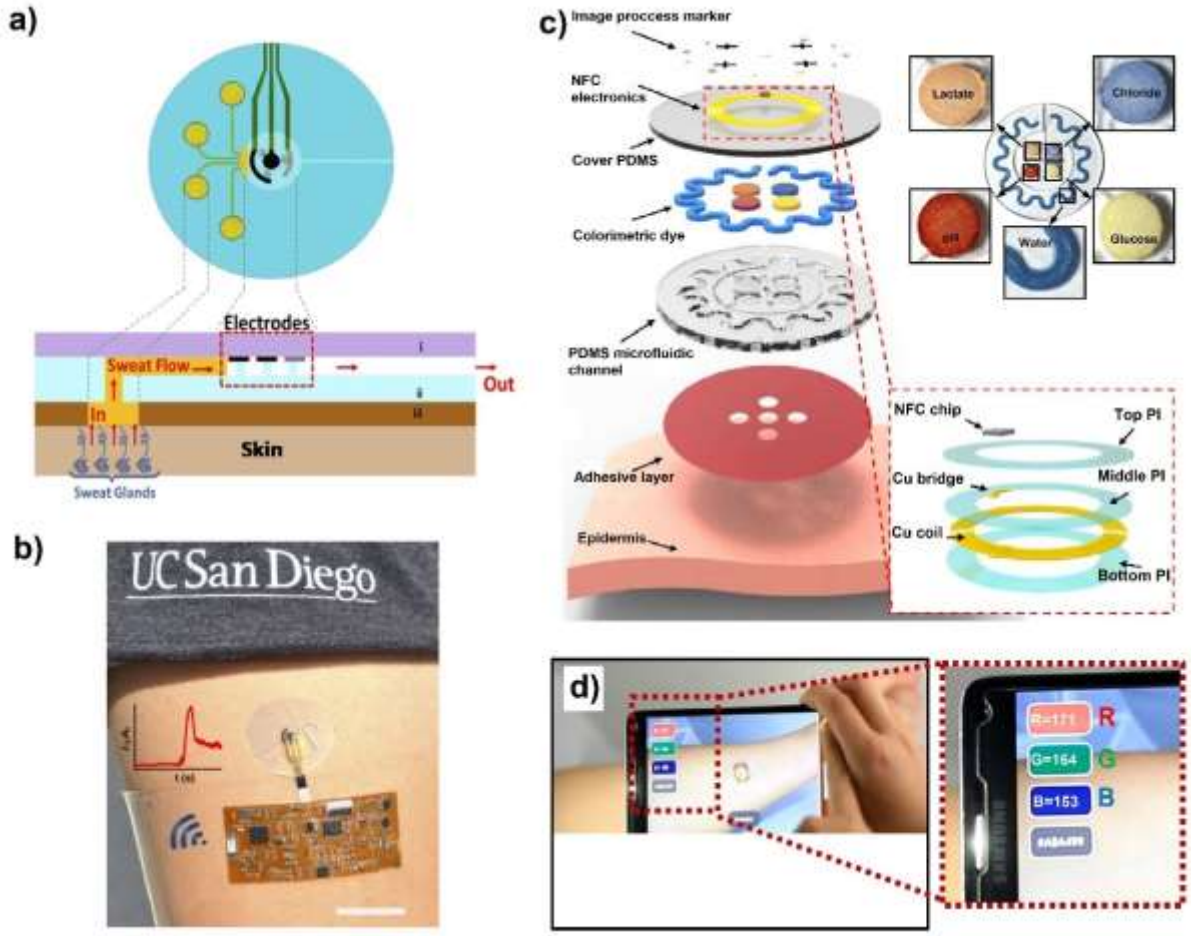

Figure 2.3: a) Schematic illustration of an electrochemical microfluidic device for glucose and lactate detection, **b)** optical image of the microfluidic device integrated with electronic board for wireless transfer of data, adapted with permission from Ref. [77] Copyright (2017) American Chemical Society. **c)** Schematic illustration of a microfluidic sweat device and its NFC system for colorimetric detection of pH, glucose, lactate and Cl^-, **d)** demonstration of NFC between device and smartphone launch software, adapted with permission from Ref. [91] Copyright (2016) American Association for the Advancement of Science.

Despite the great progress recently made in the development of skin-interfaced biosensors for sweat generated through exercise or local heating, the limitations associated with the low and inconsistent volume rate, together with the poorly understood relationship between secretion rate and partitioning profile, have encouraged investigations in alternative processes to stimulate sweat generation. In this context, iontophoretic stimulation has emerged as a preferred method to overcome challenges related to the non-continuous production of sweat. In the following section, wearable devices that use iontophoresis to induce sweat secretion, followed by electrochemical sensing of the analyte in the secreted sweat will be discussed. Additionally, ISF can also be extracted to the outer skin surface through a similar mechanism, the so-called reverse iontophoresis. Wearable biosensing platforms based on this approach will be also reviewed.

2.2.2 Iontophoresis-based Biosensors

Secretion of sweat during exercise is approximately 20 nL per gland per min,[16] varies between individuals and is related to the intensity of physical activity, fitness and hydration level.[1] While sweat sourced during physical exercise is appropriate for fitness monitoring, the lack of its continuous secretion in elderly patients or during less active physical states makes sweat insufficient for continuous medical monitoring. This issue can be addressed by iontophoresis. By applying a mild electric current across the skin, iontophoresis facilitates the release of sweat-inducing small molecular drugs into the dermis, where sweat glands are located. Acetylcholine, methacholine and pilocarpine are examples of sweat-inducing drugs used in iontophoresis, each providing a specific sweat secretion profile. Iontophoresis devices require additional two electrodes, anode and cathode, for current application. These electrodes are

typically modified with hydrogels, where anode's hydrogel contains the sweat-inducing drug. Electrical current flow from anode to cathode triggers the movement of drug molecules from hydrogel under the skin, following current flow, through epidermal layer and into the dermis where stimulation of sweat glands occurs (see Figure 2.4a). Thus, sweat is secreted regardless of the physical activity status.[1]

Conversely, in reverse iontophoresis, a mild current is applied between the anode and cathode to facilitate ionic migration across the skin epidermal and dermal layers towards the cathode. This technique has been employed to enrich the content of biomarker molecules in sweat.[98,99] The negative charge of the skin at neutral pH is responsible for its permselectivity to cations. This forces an electro-osmotic flow of ISF from the dermis layer towards the outermost epidermal layer that causes electrophoretic transportation of neutral molecules such as glucose to the skin surface [99] (Figure 2.4a). Iontophoresis-based techniques have been used in combination with electrochemical sensing for the monitoring of cystic fibrosis,[18] alcohol,[56] lactate,[17] glucose,[17,98-101] and urea [102,103] from sweat.

Emaminejad et al. recently reported an integrated wearable platform that combines autonomous sweat production via iontophoresis and detection of glucose, Na^+ and Cl^- levels, ontrolled by a wireless flexible printed circuit board (Figure 2.4b).[18] Healthy subjects and cystic fibrosis patients showed significant differences in their Na^+ and Cl^- levels (26.7 and 21.2 mM for the healthy individuals, and 82.3 and 95.7 mM for CF patients, respectively). Those results were consistent with tests performed *ex situ* using collected sweat samples. Unique quality of this work is autonomous sweat production via iontophoresis using wireless flexible printed electronics. Although, working range for glucose detection can easily analyze glucose concertation in healthy

individuals (see Table 2.1) further improvements in working range should be extended if glucose is to be detected in diabetic patients.

A commercial example of reverse iontophoresis in a wearable device for semi-continuous electrochemical glucose monitoring is the GlucoWatch by Cygnus Inc..[104,105] Its commercialization was discontinued upon consumers complaints about skin burns caused as a result of repeated high current applications. This problem was overcome by Chen et al. in their recent report on the application of reverse iontophoresis for electrochemical glucose monitoring [100] with an ultrathin skin-like based sensor powered by a paper battery. The paper battery is used to power reverse iontophoresis by generating a mild current flow through the dermis layer, from the anode to the cathode. During this process high-density positively charged hyaluronic acid (HA) located underneath the anode is repelled into the ISF. As a result, the ISF osmotic pressure rises, affecting the equilibrium between ISF filtration and reabsorption, and thus contributing to an increase in the intravascular blood glucose extracted from the vessel and driven to the skin surface. The high glucose concentration in ISF speeds the flux of the reverse iontophoresis up, and thus low applied currents suffice, minimizing the risk of skin irritation and pain for the user (Figure 2.4c). The skin-like biosensor suitably conformed to the skin and accurately measured the glucose driven to the skin surface thanks to a multilayered structure consisting of a 80 nm PMMA layer, a 1.6 µm polyimide layer, a 100 nm nanostructured Au film, and a 51.8 nm PB layer on which GOx was entrapped in a 1 µm chitosan membrane (Figure 2.4d). The nanostructured pattern of the Au layer transferred to the electrocatalytic and enzymatic layers provided a large surface area to perform both enzymatic and electrocatalytic reactions, contributing to the high sensitivity (130.4 µA/mM) and low LOD (5 µM) achieved. *In vivo* obtained data using the skin-like

biosensor correlated well with measurements performed by a conventional finger-prick glucometer. Results *in vivo* confirmed there were no signs of irritation, inflammation or pain using this reverse iontophoresis-based glucose biosensor.

In order to increase consistency of analyte extraction via reverse iontophoresis, a path-selective graphene-based glucose monitoring platform was recently developed by Lipani et al..[106] This platform consists of GOx hydrogel reservoirs into which ISF is drawn via electroosmosis and the systemic glucose there is quantified by an electrochemical biosensor made of a graphene-based film decorated with Pt nanoparticles (Figure 2.4e). The graphene-Pt nanocomposite enhances the sensitivity due to its high conductivity and large surface area, and is suitable for integrating high-resolution patterns into wearable devices using standard microfabrication techniques. The nanocomposite-based glucose biosensor provided a sensitivity of 37 μA/mM/cm^2 and low LOD of 0.76 μM. The patch consists of an array of small electrodes (Figure 2.4f) having sizes suitable for extraction of ISF from single hair follicles which decreases resistance and improves reproducibility of ISF extraction. *In vivo* tests of the device demonstrated continuous measurements of glucose concentration for six hours. However, further optimizations are required prior to commercialization. Those include the operation lifetime of the sensor which can be addressed by improving stability and catalytic activity of materials nanostructures, and increasing the detection range of the sensors. Normal glucose level in sweat ranges from 36 to 60 μM (see Table 2.1) where proposed device operates from 8 to 25 μM range. Furthermore, long-term reliable operation of the sensor can be improved by shielding the sensor surface by filters, selective or durable solid membranes, and cleaning or renewing sensing elements or membranes.[107]

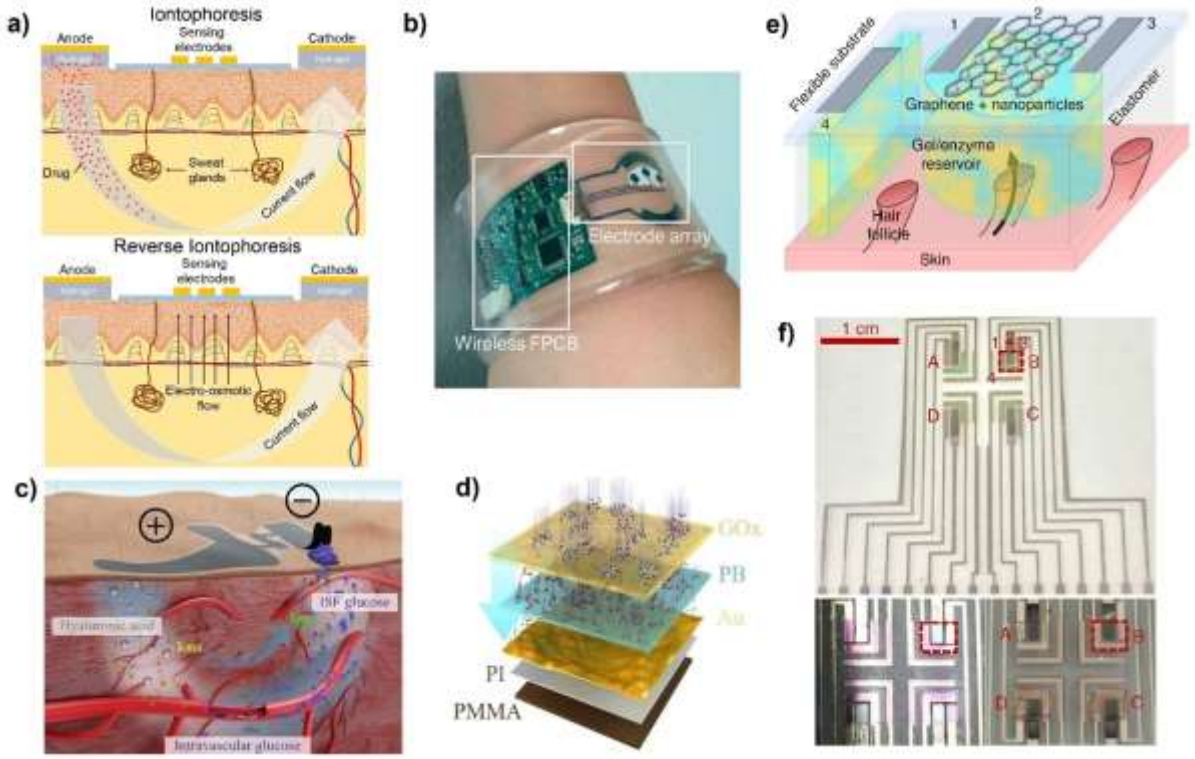

Figure 2.4: a) Schematic illustration of the iontophoresis and reverse iontophoresis processes. **b)** Autonomous sweat extraction, Na^+ and Cl^- sensing platform composed of a wireless flexible printed circuit board and an electrode array, adapted from Ref.,[18] **c)** schematic illustration of a wearable paper battery-powered device for non-invasive electrochemical monitoring of glucose from ISF, **d)** schematic of the multiple layers of an electrochemical skin-like glucose biosensor, adapted from Ref. [100] Copyright (2017) American Association for the Advancement of Science, **e)** reverse-iontophoresis based sensing-patch utilizing graphene-Pt nanoparticles pixel arrays for glucose monitoring (electrodes: 1 and 4 used for glucose extraction, 1, 2, and 3 for glucose detection), **f)** flexible and fully integrated graphene-based pixel array, adapted with permission from Ref. [106] Copyright (2018) Springer Nature.

Whilst both iontophoresis and reverse iontophoresis [18,56,98,102,106,108-111] have demonstrated strong potential for non-invasive monitoring of small molecules such as glucose,[18,98,106,108,112] urea,[102,112] alcohol,[56,108] Na^+ and Cl^-,[18] they are limited by several drawbacks that have yet to be resolved. First, the need to repeatedly apply current and the associated risk to cause skin discomfort and pain. Second, the long (e.g. 20 min) pre-measurement time [100] that is not conducive to continuous monitoring. Third, this one being specific to iontophoresis, the need to incorporate sweat-inducing agents that could lead to adverse effects for long term usage.

Table 2.2 summarizes the most recent wearable devices applied for the detection of single or multiple analytes in sweat, the nanomaterials used for sensor construction and their analytical performance. The main drawback of sweat is that not all the important biomarkers are accessible in this type of biofluid (see Table 2.1). In order to detect biomarkers which for example can facilitate early prevention or treatment of cancer or even increase life quality of chronic patients, one needs to take a closer look in deeper layers of the skin. And this can be achieved by means of transdermal or subcutaneous monitoring technology.

Table 2.2: Examples of the most recently developed wearable sweat and iontophoresis-based biosensors.

	Biosensing electrodes materials	Targeted analyte	DM	Detection limit (M)	Detection range (M)	Ref.
Sweat biosensors	pAu-chitosan-graphene/GOx	*Glucose*	Amp.	NR	$10 \times 10^{-9} – 1 \times 10^{-3}$	82
	In_2O_3- Au/chitosan-SWCNT/GOx	*Glucose*	FET	10×10^{-9}	$10 \times 10^{-9} – 1 \times 10^{-3}$	86
	Au-chitosan-CNT/GOx	*Glucose*			$0 – 200 \times 10^{-6}$	
	Au-chitosan-CNT/LOx	*Lactate*	Amp.	NR	$2 – 30 \times 10^{-3}$	17
	ISE-K^+ membrane	K^+			$2 – 16 \times 10^{-3}$	
	ISE-Na^+ membrane	Na^+			$20 – 120 \times 10^{-3}$	
	LbL-CNT/AuNS/$CoWO_4$/CNT	*Glucose*	Amp.	1.3×10^{-6}	$0 – 0.3 \times 10^{-3}$	87
	PANi-Nafion-OPH/PVA hydrogel	*DFP*	Poten.	10×10^{-3}	$10 – 120 \times 10^{-3}$	88
	Au/rGO/Au-Pt NP/GOx/ Nafion	*Glucose*	Amp.	5×10^{-6}	$0 – 2.4 \times 10^{-3}$	92
	Urease/ZnO NW	*Urea*		0.5×10^{-3}	$5 – 25 \times 10^{-3}$	
	Uricase/ZnO NW	*Uric acid*	Piezo.	10×10^{-6}	$0.024 – 0.101 \times 10^{-3}$	89
	GOx/ZnO NW	*Glucose*		20×10^{-6}	$0.042 – 0.208 \times 10^{-3}$	
	LOx/ZnO NW	*Lactate*		0.1×10^{-3}	$0 – 20 \times 10^{-3}$	
	Au-ZnO/AOx	*Alcohol*	EIS Amp.	2.17×10^{-6}	$2.17 \times 10^{-6} – 43.4 \times 10^{-3}$	90
	MoS_2 nanosheet on flexible nanoporous membrane	*Cortisol*	EIS	2.76×10^{-9}	$27 \times 10^{-9} – 1.38 \times 10^{-6}$	84
	Textile-OECT/PEDOT:PSS ink	Ascorbic acid Adrenaline Dopamine	FET	101×10^{-6} 10×10^{-6} 1×10^{-6}	$0.1 – 10 \times 10^{-3}$ $10 – 100 \times 10^{-6}$ $1 – 10 \times 10^{-6}$	113
	PFI-PB-GOx	Glucose	Amp.	1×10^{-6}	$1 \times 10^{-6} – 1 \times 10^{-3}$	114
	C-PB ink/Chitosan-BSA-LOx C-PB ink-GOx	Lactate Glucose	Amp.	NR 50×10^{-6}	$4 – 20 \times 10^{-3}$ $2 – 10 \times 10^{-3}$	77
	MS-OECT	Cortisol	Amp.	NR	$0.01 – 10 \times 10^{-6}$	38
	Cl^- detection reagent	Chloride			$\sim 0 – 156 \times 10^{-3}$	
	D-Lactate assay kit	Lactate	Col.	200×10^{-6}	$\sim 1.5 – 100 \times 10^{-3}$	91
	Chromogenic reagents (GOx, HRP, trehalose, KI)	Glucose			$\sim 0 – 6.3 \times 10^{-3}$	
	AuND-ISE	Na^+	Poten.	0.8×10^{-6}	$0 – 40 \times 10^{-3}$	115
	BSA-LOx/SPEES/PES	Lactate	Amp.	NR	$0 – 28 \times 10^{-3}$	33
	Electrochemical fabric-CNT fabric substrate	Glucose Na^+ K^+ Ca^{2+}	Amp.	NR	$0 – 200 \times 10^{-6}$ $10 – 160 \times 10^{-3}$ $2 – 32 \times 10^{-3}$ $0.5 – 2.53 \times 10^{-3}$	116
	WSNF	Glucose	CV	500×10^{-9}	$500 \times 10^{-9} – 10 \times 10^{-3}$	117
	Ag chloranilate, pHEMA	Cl^-			$25 – 100 \times 10^{-3}$	
	Glucose colorimetric assay kit Dye-HRP-LOx	Glucose Lactate	Col.	NR	$25 – 100 \times 10^{-6}$ $5 – 20 \times 10^{-3}$	118

	CCY-Fe_2O_3-Anti-C_{mab}	Cortisol	CV	$1.38x10^{-17}$	$2.75x10^{-15}$ – $2.75 x10^{-6}$	119
Iontophoresis-based biosensors	Au/chitosan/CNT /PB /GOx Na^+ - ISE Cl^- - ISE	Glucose Na^+ Cl^-	Amp.	NR	$0 – 100x10^{-6}$ $10 – 80x10^{-3}$ $10 – 80x10^{-3}$	18
	Carbon ink/chitosan/BSA/AOx/ PB	Alcohol	Amp.	NR	$0 – 36x10^{-3}$	56
	PB ink/ agarose/ chitosan/ GOx	Glucose	Amp.	NR	$0 – 160x10^{-6}$	108
	PB ink/ agarose/ chitosan/ AOx	Alcohol			$0 – 40x10^{-3}$	
	Carbon ink/ CNT/ Nafion	Methyl xanthine	DPV	$3x10^{-6}$	$0 – 40x10^{-6}$	109
Reverse-iontophoresis based biosensors	Flex. subs.-graphene-Pt/GOx	Glucose	Amp.	$0.76x10^{-6}$	$8 – 25x10^{-6}$	106
	PB ink/ chitosan/ BSA/ GOx	Glucose	Amp.	$3x10^{-6}$	$10 – 100x10^{-6}$	98
	SPCE-PPy-Urease	Urea	Poten.	$8x10^{-6}$	$10x10^{-6}$ – $5x10^{-3}$	102

Abbreviations: DM-detection method, Amp-Amperometric, Poten-potentiometric, Piezo-piezoelectric, Col-colorimetric, Iont-iontophoresis, R.Iont-reverse iontophoresis, DPV-differential pulse voltammetry, pAu-porous Au, GOx-glucose oxidase, LOx-lactate oxidase, T-temperature, NR-not reported, FET-field-effect transistor, CNT-carbon nanotube, SWCNT-single-walled CNT, ISE-ion selective electrode, C-carbon, PB-Prussian Blue, LbL-layer by layer, DFP-diisopropyl fluorophosphate, PANi-polyaniline, OPH-organophosphate hydrolase, EIS-electrochemical impedance spectroscopy, AOx-alcohol oxidase, MS-molecular selective, OECT-organic electrochemical transistors, NW- nanowires, AuND- Au nanodendrites, SPEES-sulphonated polyesther ether sulphone, PES-polyether sulphone, PEDOT-poly(3,4-ethylenedioxythiophene), SPCE-screen printed carbon electrode, PPy-polypyrrole, PFI-perfluorosulfonated ionomer, WSNF-wrinkled, stretchable, nanohybrid fiber, CCY- conductive carbon yarn

2.3 Transdermal Biosensors

Transdermal monitoring most commonly targets the ISF residing in the dermis, although peripheral blood can also be transdermally sampled from the deeper layers of the skin. Transdermal blood sampling, however, may cause damage to nerve bundles and rupturing of blood vessels. In recent years, the transdermal analysis of the ISF environment has been used for the detection of metabolites (e.g. glucose,[100,120,121] lactic acid,[120] alcohol,[122] cortisol[123]) and biomarkers of various diseases, such as cancer.[124-129] Collecting and sampling ISF for real-time monitoring content demands advanced methods that are minimally invasive, painless, rapid, sensitive, and easy to use by patients. Current methods used for collection of blood for analysis cause discomfort and pain, especially for patients requiring testing on a daily basis such as diabetic patients, and this is affecting patient compliance.[82] In addition, those methods generate biohazard sharps waste, and can lead to infection via the punctured and disrupted skin. Research on developing an alternative approach for transdermal monitoring has attracted considerable attention. Microneedles (MNs) seem to be the most promising candidate with characteristics to address most of the problems faced by current methods. MNs are a miniaturized form of conventional hypodermic needles with few hundreds of microns in height.[11] Their size grants them the unique characteristic of reaching the interstitium eluding stimulation of dermal nerves or rupturing dermal blood vessels.[130] A variety of methods for microfabrication of microneedle arrays (MNAs) from various materials with different shape, size, morphological features and MN density has been demonstrated. Furthermore, combinatorial approaches of microscale MNAs with nanomaterials to capitalize on the advantages of both micro- and nanosystems emerged a decade ago and have been increasing steadily since then. MNAs have been primarily used in the pharmaceutical

field for drug and vaccine delivery across the skin.[131,132] The integration of MNAs with nano-sized materials such as carbon nanomaterials, quantum dots, and metallic, polymeric and magnetic nanoparticles have demonstrated great success for applications in enhanced drug delivery and imaging for diagnosis.[133-136] In parallel, there has been a surge in the studies of MNAs for transdermal biosensing and extraction of biological fluid for further analysis.[11,137] Table 2.3 summarizes recent works on ISF and biomarker extractions and sample analysis methods used, as well it compares various biosensors based on direct transdermal monitoring.

The application of MNAs in biosensing research is arguably more complex than skin delivery, and many parameters concerning MN development and biosensor design have to be taken into consideration. For example, the type of material from which MNAs are produced is of high importance for transdermal detection, as it will affect the biocompatibility, mechanical stability and long-term performance of the biosensor. Depending on the application area and the technological development, different material types have been used to fabricate MNAs. Since their emergence in the 1990s, high precision micro- and nanotechnological tools have enabled the micro and sub-micron sized MNA fabrication from Si, which was the first material applied towards transdermal drug delivery.[138-140] Its elastic modulus ranges from 50 to 180 GPa [141] and is higher than that of metals used in orthopedic implants.[130] For transdermal monitoring applications, next to biocompatibility, one of the main challenges in designing MNAs is to avoid fragility where individual MNs might break and end up inside the body, and can pose health concerns. The foreign body response to the transiently inserted MNA might be significantly different from the one observed when MNs break and potentially accumulate inside the skin tissue. To overcome this problem, various types of materials have been tested for the purpose of providing a

suitable mechanical strength while maintaining a favorable biocompatibility of MNAs. Additionally, the surface of MNs has to allow the incorporation of the functional groups required for the immobilization of the biological recognition element, responsible for providing selectivity to the analysis. Whilst most of the existing MNA transdermal biosensors are mainly based on microstructured materials, the recent progress in nanotechnology may provide new opportunities for addressing many of the barriers that the field is facing. Combinational approaches in which solid MNAs are coated with nanomaterials such as Pt nanoparticles,[142] Au nanorods [143] and MWCNT [144] have been recently proposed for the transdermal monitoring of metabolites and protein biomarkers. These reports have successfully demonstrated superior biosensing performance over the sensors not incorporating nanomaterials due to an increased surface area, versatile surface chemistry and good biocompatibility. However, the mechanical stability of these nanoparticles when MNAs are inserted into the skin remains challenging. Other combinational micro-/nanostructural approaches for MNA-based biosensing include hollow MNs filled with functional nanostructures [145,146] and hybrid nanocomposite MNs integrating nanoparticles within a polymer matrix.[147,148]

Here we will discuss sensing methodologies where ISF is harvested via MNAs and analyzed offline, and where *in vivo* monitoring is performed directly on skin using wearable MNAs, with a focus on the biosensor design. Recent advances on MNA fabrication techniques, materials, design and mechanical testing's have already been reviewed in detail and we refer the interested reader to this review.[130]

2.3.1 Microfluidic ISF Extraction and Subsequent Offline Analysis

Various wearable optical and electrochemical sensing devices have been developed by integrating hollow MNAs into microfluidic systems. These systems are designed to facilitate painless collection of transdermal fluid which is directed to microchannels or chambers where the analyte is selectively recognized by the bioreceptor, enabling final detection. This type of wearable devices can support different detection strategies such as affinity interactions where antibodies or DNA aptamers are immobilized at the inner lumen of the MNAs or along microchannels capturing the target analyte, or catalytic reactions where enzymes are used as the bioreceptor. As a particular case of a microfluidic device with integrated hollow MNAs Ranamukhaarachchi et al.[149] reported an optofluidic biosensor for vancomycin detection from artificial ISF, where MNs were used as microreactors. In this case, a peptide with affinity for vancomycin was immobilized at the inner lumen of MNs, enabling vancomycin detection upon a competitive step where vancomycin caused the displacement of a HRP-vancomycin conjugate previously bound to the immobilized peptide (Figure 2.5a). Requiring sub-nanoliter volumes, the enzyme reaction occurred in the 450 μm-MNA lumen. The subsequent optical detection of the product of the enzymatic reaction between the remaining HRP and 3,3',5,5'-tetramethylbenzidine substrate took place in the detection chamber of the optofluidic device that operated on the basis of total internal reflection via an optical waveguide (Figure 2.5b). Limitation of this device is that used displacement and/or labelled approaches are not suitable for monitoring purposes especially in wearable sensing.

Electrochemical biosensor devices have also been reported using similar ISF extraction systems based on MNAs integrated into microfluidic platforms for the detection of glucose and K^+ in an adjacent chamber where the electrochemical

biosensor is placed.[145,150-152] As a recent example, Strambini et al.[152] described a MNA-based electrochemical glucose sensing device composed of a densely packed array of hollow silicon dioxide MNs and an integrated chamber with an enzymatic glucose sensor at the backside of the MNA (Figure 2.5c and d). The SEM micrograph shown in Figure 2.5e illustrates the size comparison of the MNA with the tip of a conventional hypodermic needle. The working electrode was a carbon screen-printed electrode modified with GOx entrapped in a carboxymethyl-cellulose hydrophilic polymer. The size and density of the MNAs were selected to maximize their capillarity, affording ISF collection within a few seconds (1 µL/s). After filling the chamber with only 5 µL solution, accurate *in vitro* glucose measurements were carried out in artificial ISF. This device has unique features of acquiring small amount of ISF in very short time due to the size and density of hollow MNA. On the other hand, limitation of the devise is that it cannot be used in continuous long-term glucose monitoring with current design. Further modification such as microchamber for continuous flow of ISF or disposal of ISF should be investigated.

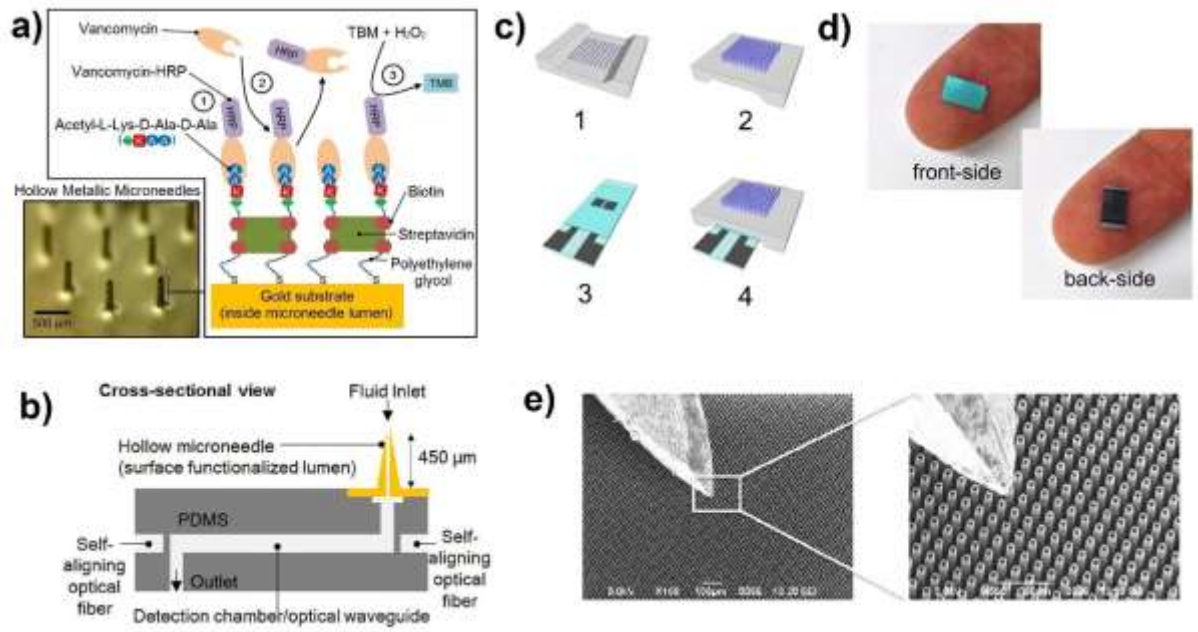

Figure 2.5: MNAs integrated into microfluidic systems. **a)** Illustration of the biosensing strategy that relies on a competitive assay, the analyte being vancomycin; **b)** cross-sectional schematic view of MN-based optofluidic biosensor, adapted from Ref. [149]. High density hollow silicon dioxide MNs for measurement of glucose in ISF; **c)** 1-front side and 2-back side of the MNA chip, 3- glucose biosensor, 4- glucose biosensor integrated with MNA chip; **d)** optical images of chips placed on fingertip; **e)** SEM of MNAs compared to the size of a typical insulin hypodermic needle, adapted with permission form Ref. [152] Copyright (2015) Elsevier.

Microfluidic devices based on collecting transdermal fluid for subsequent analysis have the potential to become an important component of point-of-care diagnostics. However, continuous monitoring would require constant flow of transdermal fluid through the system which actually could increase the complexity of the device to facilitate the required routes for the fluid to be directed, such as in the hollow MNA that rely on complex multi-step fabrication procedures.[153-155] To overcome these issues, alternative approaches have been suggested, including selective

biomarker capture (see Table 2.1) first, followed by subsequent analysis, and direct transdermal measurements. In the next parts, progress on these methodologies will be discussed.

2.3.2 Transdermal Biomarker Capture and Analysis via MNAs

Efficient selective biomarker capture and extraction from ISF using MNA modified with bioreceptors has been recently reported.[156-161] Typically, an antibody-modified MNA is first inserted into the skin to allow specific binding of the biomarker present in ISF. Then, the MNA is removed from the skin to proceed with further analysis. This approach is advantageous compared to MNA-based strategies that extract whole ISF because the biological complexity of ISF might introduce the requirement of additional sample pre-treatment steps.

Bhargav et al. reported the optimization of a MNA-based platform to efficiently capture a specific biomarker in the skin of live mice and subsequently quantify its levels via an indirect ELISA.[156] A COOH-PEG-HS compound was self-assembled on an Au-coated Si MNA followed by covalent coupling of ovalbumin (OVA). Following the *in vivo* anti-OVA IgG extraction (Figure 2.6a), ELISA results confirmed that the MNA capturing efficiency *in vivo* is lower than *in vitro* most likely due to the poor mass transfer in transdermal fluid (Figure 2.6b). The authors also found that ~20% of the OVA immobilized on the MNA was released into the skin upon application, which raises concerns for wearable device developers due to the immune response that might be triggered. In order to increase the amount of captured biomarker and thus improve diagnosis sensitivity, Kendall et al. recently optimized MN size and density (5000 – 30000 per cm^2) in a MNA patch to maximize influenza IgG antibodies capture from skin in less than one minute. Subsequently they quantified the amount of

captured antibodies via indirect ELISA (Figure 2.6c).[157] MNA penetration experiments and ELISA analysis were performed on murine skin which is substantially thinner than human skin (Figure 2.6d and e). There are few problems with using this approach. First, it is still not suitable for personal monitoring purposes and solely relies on working protocols to ensure consistency of the results. Second, OVA immobilized on the MNA was released into the skin upon application. This can give misleading results since very hard to determine OVA concentration removed from MNA surface. Future work should focus on *in vivo* application of MNA and eventually translating this technology to human skin.

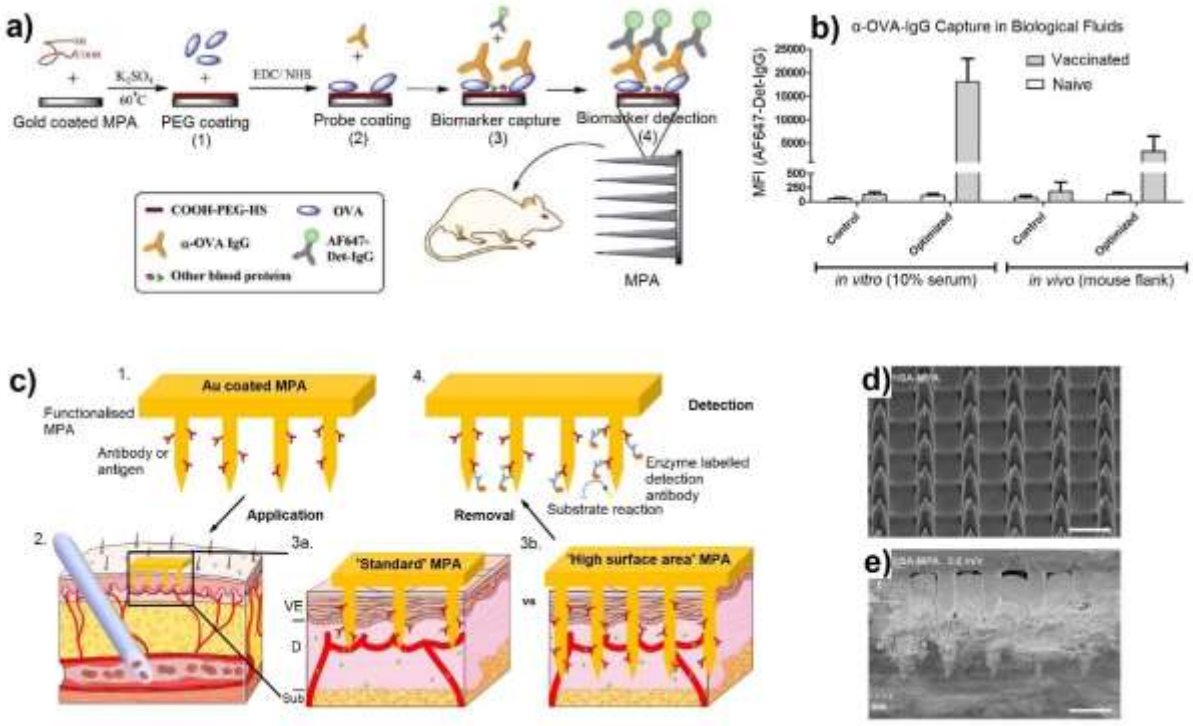

Figure 2.6: ISF analysis via affinity using receptor-modified MNAs. **a)** Schematic illustration of surface modification of MNAs and the detection strategy for the target biomarker, **b)** ELISA results illustrating *in vivo* and *in vitro* MNA application for the detection of α-OVA-IgG antibody, adapted with permission from Ref. [156] Copyright (2012) American Chemical Society. **c)** Schematic representation of selective protein capture and extraction via MNAs and comparison to a syringe needle, **d)** SEM image of MNA, and **e)**, cryoSEM of MNA penetration into mice skin, adapted with permission from Ref. [157] Copyright (2018) Elsevier.

In conclusion, direct extraction and subsequent analysis of biomarkers from transdermal fluid has the potential to lead to the development of point-of-care diagnostics and wearable devices for biomarker detection. And biomarker analysis from ISF is not only relevant for diagnostic purposes, but also for biomarker discovery research.[13,162] The main disadvantage of this method is the need for external analysis techniques, which is the additional step required to complete the analysis. However,

the complexity of ELISA-like methods could be overcome by the simplicity and high-throughput capabilities of biosensors.

2.3.3 Direct Transdermal Monitoring Using MNAs

Direct ISF analysis refers to the detection of a specific analyte in ISF without the need for sample extraction and external analysis. The measurements are performed when the MNA is applied on the skin. Most of the strategies reported for the direct ISF analysis rely on electrochemical detection, mainly using enzyme-based sensors as summarized in Table 2.3. Lee et al. reported an approach based on a non-enzymatic sensor developed using a Pt black-modified stainless steel MNA for continuous monitoring of transdermal glucose.[121] The MNA was fabricated by wet chemical etching of stainless steel using ferric chloride, followed by 90^{o} bend of the etched MNs (Figure 2.7a). A thin Au layer was electrodeposited on the stainless steel MNAs surface, passivated using a parylene coating, then the tip of the MNs was electroplated to form either a Pt black layer or an Ag/AgCl layer. The nanostructured Pt black-modified MN tips were then coated with a Nafion membrane to eliminate interference from other electroactive molecules. Deposited nanostructured Pt black drastically increased the active surface area of the glucose sensor by 444 times when compared to bare Pt, and served as a catalytic layer for glucose sensing. The sensor featuring the 650 µm-long MNs was attached on the back of a rabbit (Figure 2.7b), and allowed *in situ* glucose detection from ISF with a linear range from 2 to 36 mM and LOD of 50 µM. Results were compared with those obtained using a glucose analyzer for blood samples collected simultaneously to MNA analysis, and showed excellent correlation. The sensor was stable over the first three days of *in vivo* measurements but then failed to provide reliable results at day five, possibly due to

biofouling of the MNs. Most important feature of this work is illustration of how catalytic effect of nanomaterials can be successfully used for transdermal monitoring. This is especially important since enzyme activity will decrease by the time and nanomaterials can be solution for long-term continuous monitoring.

The Wang group has recently reported a similar approach combining a wearable bandage with a MNA-based electrochemical sensor for melanoma screening.[163] The target in this case was tyrosinase (TYR), which is involved in the synthesis of melanin and can lead to skin melanoma if overexpressed and accumulating in the skin.[164,165] The working principle of their wearable sensor is based on the oxidation of catechol, entrapped on an agar layer coating the MNA surface, to benzoquinone (Bq), in the presence of TYR. Bq is then reduced at a working potential of -0.25 V and the generated current is amperometrically measured. The MNA was designed to access TYR in the deeper parts of the dermis, the reticular dermis (Figure 2.7c). The sensor is composed of polymeric hollow MNs with 800 μm length and 425 μm diameter. The hollow structure of the MN was filled up with either carbon paste to prepare MN-based working and counter electrodes, or Ag/AgCl ink for the reference electrode. The working electrode was then coated with a catechol-agar solution. Furthermore, the MNA patch was integrated into a flexible printed electric board to support amperometric measurements. It was also equipped with a wireless electronic interface to facilitate data transfer. This wearable sensor device was firstly assessed on a phantom gel loaded with different TYR concentrations after which *ex vivo* testing was performed on pork skin (Figure 2.7d). This type of monitoring could minimize biopsies and thus decrease related delays in cancer diagnosis.

As mentioned above, the combination of MNA and nanomaterials hold great promise for achieving a superior biosensing performance. Particularly, in

electrochemical sensing, nanostructured electrodes have the potential to increase the electrical conductivity and the electroactive surface area, resulting in improved sensitivity and lower LOD. Recently, Bollella et al. have reported the first MNA-based biosensor for the continuous monitoring of lactate in ISF.[166] In a combinatorial approach, the authors engineered the initial gold MNA surface by first electrodepositing MWCNT, followed by the electropolymerization of a redox mediator (methylene blue) to finally immobilize the catalytic enzyme, LOx. The resulting micro-/nanostructured MNA constitutes a second-generation biosensor that was assessed for the detection of lactate *in vitro.* Continuous monitoring was demonstrated in both artificial ISF and human serum spiked with lactate. The authors reported a LOD of 2.4 µM and a sensitivity of 800 µA $cm^{-2}mM^{-1}$ in ISF, whereas in human serum the LOD was 3.2 µM and the sensitivity 180 µA $cm^{-2}mM^{-1}$. These results evidence that the biofouling effects have a strong impact in the biosensing performance, which may be further exacerbated in wearable settings for long-term applications.

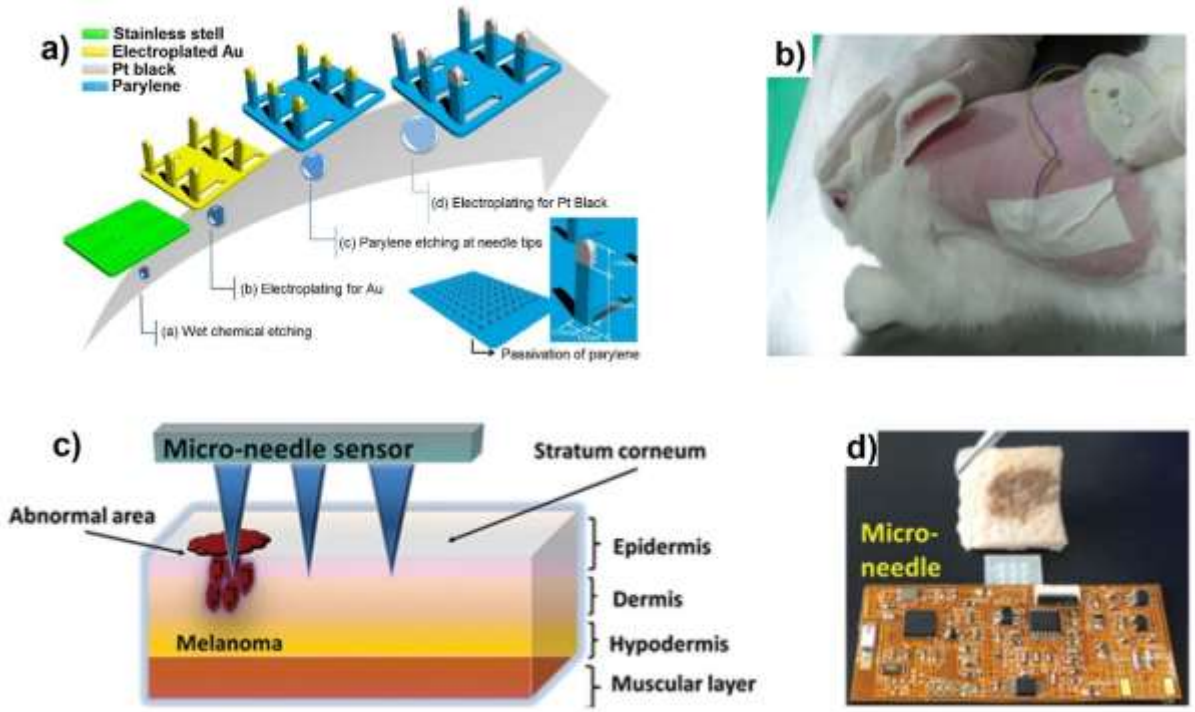

Figure 2.7: Examples of transdermal biosensors based on MNA. **a)** Schematic illustration of 3D MNA patch for non-enzymatic glucose sensing, **b)** testing of sensor after being applied to rabbit skin, adapted with permission from Ref. [121] Copyright (2016) Elsevier. **c)** Illustration of transdermal TYR melanoma biomarker detection using MN sensor, **d)** *ex vivo* screening of TYR biomarker in porcine skin model using MN sensor, adapted with permission from Ref. [163] Copyright (2018) Wiley.

Direct electrochemical ISF analysis of biomarkers using commercialization-ready MNA devices still faces quite a few challenges to be resolved before the long-awaited dream of patients and physicians can be realized. These challenges revolve around biocompatibility of the required componentry for sensing and the stability of the sensing layer in an *in vivo* environment over a time frame that is fit for a clinical purpose. Research towards solving of these challenges should be focused on fabrication of MNA from biocompatible polymers or uniform application of

biocompatible polymers coatings on MNA surface. Furthermore, special attention should be devoted to development of stable MNA surfaces for immobilization of biological recognition elements such as enzymes and applying protective layer on MNA surface in order to prevent delamination of sensing surface. During penetration of MNA through the skin, sensing surface like nanostructures and enzymes could be easily removed from the MNA surface due to the compression and friction between skin tissue and MNA. For these reason biocompatible and dissolvable protective polymeric coatings are necessary for stable and long-term application transdermal biosensors.

Table 2.3: List of reported transdermal monitoring biosensors.

	Materials	MN height	Target analyte	Sample	Sample analysis method	Ref.
ISF extraction and offline analysis	MNs/p-type S	350 µm	Glucose	Human	Commercial blood glucose test strip	167
	TSMA/Pt-C/BSA-GOx	300 µm	Glucose	Human	Electrochemical	150
	SSMA/SPE/GOx	325 µm	Glucose	Human	Electrochemical	151
	MeHA-MN-CL5 patch	800 µm	Glucose Cholesterol	Mouse	Commercial quantitation kits	168
	Eshell300-PC	1450 µm	K^+	NR	Electrochemical	145
	32 G Ultrafine Nano pen needles	NR	ISF proteins	Human	LC-MS/MS	13
	PEG-Au/MNA	110 µm 260 µm	NS1 protein	Mouse	ELISA	124
	PLA-HMDA	1000 µm	(TNF)-α IL-6, IL1-α	Mouse	ELISA	129
	Hydrogel PVP, Stainless steel MNs	250 -750 µm	Glucose, total protein content	Human	Commercial glucose assay kit and BCA protein assay kit	73
	Stainless steel	650 µm	Vancomycin, anti-polio IgG	Rat	HPLC-MS/MS analysis	169
	MN-PSS-AuNRs	650 µm	Rhodamine 6G	Rat	SERS	143
	BD 32 G Ultra-Fine Pen needles	1500 µm	Exosomes	Rat and Human	Exosomes isolation kit (Invitrogen) and TEM	162

	Materials	MN height	Target Analyte	Detection Limit (M)	Linear Range (M)	Ref.
Direct transdermal monitoring using MNAs	Au/Pt black-Nafion	650 µm	Glucose	$50x10^{-6}$	$50x10^{-6}$ - $36x10^{-3}$	121
	Nafion - Au/Pt black MNs	600 µm	Glucose	$23x10^{-6}$	1 - $40x10^{-3}$	170
	Pt/Stainless steel-EDOT/GOx	680 µm	Glucose	NR	2 - $24x10^{-3}$	171
	Pt/MWCNTs/MNs	380 µm	Glucose	NR	3 - $20x10^{-3}$	144
	PtNps/PANi/MEA/GOx PtNps/PANi/MEA/UOx PtNps/PANi/MEA/ChOx	600 µm	Glucose Uric acid Cholesterol	$260x10^{-6}$ $4x10^{-6}$ $440x10^{-6}$	2 – $12x10^{-3}$ 0.1 – $1.2x10^{-3}$ 1 – $12x10^{-3}$	142
	PEGDA	500 µm	Glucose Lactate	$1x10^{-6}$ $1x10^{-6}$	0 - $4x10^{-3}$ 0 - $1x10^{-3}$	120
	E200acryl-filled CP-PEI-LOx	1500 µm	Lactate	$0.42x10^{-3}$	0 - $8x10^{-3}$	172
	AuMN/AuMWCNT/MB	1000 µm	Lactate	$2.4x10^{-6}$	0.01 – $0.2x10^{-3}$	166
	LCP/MNs-Pt wire	800 µm	Alcohol	NR	0 - $80x10^{-3}$	122
	Au-ElectroNeedle	500 µm	p-Cresol	$1.8x10^{-6}$	$1x10^{-6}$ -$1x10^{-3}$	173
	AuMNA- P(GMA-co-VFc)	292 µm	Urea	$2.8x10^{-6}$	50 - $2500x10^{-3}$	174
	AuMN/pTCA-GOx	700 µm	Glucose	$19.4x10^{-6}$	0.05 – $20x10^{-3}$	175
	E200acryl-BMAE	1174 µm	Glucose Glutamate	$0.1x10^{-3}$ $3x10^{-6}$	0 -$14x10^{-3}$ 0 -$140x10^{-6}$	146
	E200acryl-CP/Catechol-agar	800 µm	Tyrosinase (TYR)	NR	0.1- 0.5 $mgml^{-1}$	163
	CP-OPH-Nafion/E200acryl	1500 µm	OP-nerve agent	$4x10^{-6}$	20 - $180x10^{-6}$	176
	PCL/PD/PEDOT/Hemin	700 µm	NO	$1x10^{-6}$	1 - $16x10^{-6}$	177
	Pt/REGO MNA	800 µm	H_2O_2	NR	0.1 – $8x10^{-3}$	148
	MNA-PLA/f-MWCNT	870 µm	Ascorbic acid	$180x10^{-6}$	0 – $1x10^{-3}$	147

Abbreviations; TSMA-tapered Si MNs, BSA- bovine serum albumin, GOx-glucose oxidase, SSMA-straight Si MNs, SPE-screen printed electrode, MeHA-methacrylated hyaluronic acid, CL5-UV exposure time for 5 min., PC-porous carbon, NR-not reported, LC-MS/MS- liquid chromatography mass spectrometry analysis, PEG-polyethylene glycol, PSS- poly-styrenesulfonate, AuNR- Au nanorods, SERS- surface enhanced Raman spectroscopy, PLA- polylactic acid, HMDA-hexamethylenediamine, (TNF)-α- human tumor necrosis factor, IL-6 interleukins and IL-1α- interleukins 1 α, PEGDA-poly(ethylene glycol) diacrylate, E200acryl- Eshell 200 acrylate based polymer, PANi-polyaniline, CP-carbon paste, PEI- polyethyleneimine, LOx-lactate oxidase, EDOT- PEDOT poly (3,4-ethylenedioxythiophene), LCP-liquid crystal polymer, BMAE-bio-component microneedle array electrode, OPH-organophosphorus hydrolase, OP-organophosphorus, PCL-polycaprolactone, PD-polydopamine, PLA-poly(lactic acid)

2.4 Subcutaneous Biosensors

Subcutaneously implanted biosensors can provide more accurate and reliable signals compared to less invasive sensing methods. The main characteristic of these devices is their integration with the local environment while providing full function. They can potentially sustain continuous, accurate monitoring of biomarkers in subcutaneous fluids, and deliver valuable information about the individual's health state, particularly important for chronic patients. These implanted systems have to meet the highest standards regarding biocompatibility, accuracy, lifetime, and of course, patient-acceptance. Subcutaneously implanted devices do not require very invasive surgery for placement, making them patient-compliant, but their long-term performance is still limited by a number of factors. The implantation triggers a host response when the object is inserted leading to a fibrous capsule forming around the device following an initial acute inflammation.[51] This may affect the accuracy and calibration of the device, and can potentially have life-threatening consequences if the sensor reading informs treatment decisions.

The most recent advances in nanotechnology have led to the development of novel nanomaterials that are emerging with the potential to underpin the implantable sensing field by allowing small, smart and energy efficient designs. Here we will review the latest advances in subcutaneously implanted biosensor design and fabrication.

Glucose sensing using implantable devices is certainly in a very advanced position compared to other body analytes. Research and development in this area is driven by the high prevalence of diabetes and the large associated market.[178] Implanted glucose sensor technology is nowadays solidly established in clinical practice and at the point of care. The technology has given diabetes sufferers a new level of autonomy and quality of life. There are seven FDA approved and commercially

available implantable glucose sensors, six of which are based on electrochemical enzymatic sensing.[179] The recently launched Eversense system (Senseonics) is based on non-enzymatic fluorescent methods. These devices are user-friendly and harness advanced communications to connect the sensor transmitter with portable smart devices for glucose concentration tracking. However, several limitations have been associated with implanted glucose sensors, including a short lifetime and sensor calibration issues. Typically, due to the host response mentioned above, these subcutaneous devices need to be replaced every three to seven days and recalibrated every 12 h.[180,181]

This host response may be moderated by employing biocompatible nanomaterials and/or engineered surface chemistries. Control over biofouling using PEG coating has been used to reduce tissue inflammation and extend the sensor lifetime.[182,183] For example, Hui et al. developed a DNA electrochemical biosensor based on PEGylated PANi nanofibers with demonstrated antifouling properties for the detection of a breast cancer marker, the BRCA-1 gene.[183] Zwitterionic systems have also been popular due to their ability to bind water molecules resulting in antifouling properties.[184,185] Nanostructured Pt-PANi electrodes were coated with ultrathin zwitterionic sulfobetaine methacrylate to minimize the biofouling impact on the performance of implantable biosensors. The engineered surface chemistry was demonstrated to reduce over 99% nonspecific protein adsorption and allowed maintained sensitivity at 94% for 15 days.[184] Alginate hydrogel encapsulation has also been broadly employed to improve implant biocompatibility and mitigate the host response. Abidian and Martin proposed a multifunctional coating for enhancing biocompatibility while preserving conductivity in implantable microelectrodes.[186] These electrodes were first coated with electrospun nanofibers, then covered with an alginate

hydrogel. Subsequently, a conductive polymer (PEDOT) was electropolymerized on the electrode side, which provided an increased conductivity. As an attempt to minimize local inflammation and diminish the fibrous capsule formation anti-inflammatory agents such as dexamethasone have been incorporated in hydrogel matrixes.[187,188] For instance, pH-sensitive molecularly imprinted polymer (MIP) nanospheres loaded with dexamethasone have been demonstrated to minimize the inflammation response of implanted biosensors for an extended period of time of over six weeks. Promotion of tissue vascularization by delivering vascular endothelial growth factors (VEGF) has also been proposed as a strategy for the attenuation of the host response. Sung et al. combined the release of both dexamethasone and VEGF in a sequential approach to control the immune response of hydrogel-coated SWCNT-based implantable biosensors.[54] *In vivo* studies showed that combined dexamethasone/VEGF delivery improves the vasculature around the implant and reduces inflammation. Also, sequential delivery was proven to be a more efficient strategy than simultaneous delivery, with an increased therapeutic index (vasculature/inflammation ratio) of over 30%. NO release can inhibit platelet activation and adhesion, motivating the development of a number of NO releasing platforms for implanted sensors.[189] For instance, S-nitrosothiols can act as NO donors and they have been incorporated in a number of implantable sensors. Soto et al. have recently reported the modification of a polyurethane membrane with nitrosothiol-doped silica nanoparticles for the long-term sensing of glucose. Results showed a stable, linear response to glucose at physiological levels *in vitro* for up to two weeks.[190] To date, no strategy has yet achieved suppression of the foreign body response and this certainly remains an obstacle for the further development of implanted devices. However, the combination of strategies to improve biocompatibility together with the release of

agents able to mitigate inflammation and improve vascularization promises to overcome long-term implantation issues.[188,191]

A common issue related to the mechanism of implanted GOx-based sensors with electrochemical transduction is the significant drift in the tissue oxygen. The formation of a cellular and protein fouling film alters local blood supply and limits the permeability of oxygen. Attempts to limit this phenomenon include the incorporation of nanostructural features to stimulate microvascularization [192] and the engineering of materials to balance oxygen and glucose transport.[193] Gough et al. have addressed the oxygen deficiency issue by regenerating *in situ* 50% of the oxygen consumed and establishing a glucose-sensing strategy based on differential oxygen detection.[194] The approach enabled the long-term monitoring of glucose by means of an electrochemical and telemetric sensor that remained implanted in pigs for more than one year. First, a two-step reaction was catalyzed by two enzymes immobilized in a PDMS membrane: GOx catalyzed the glucose reaction to gluconic acid; and catalase, subsequently regenerated the consumed oxygen. A second electrochemical non-enzymatic sensor, monitored the background oxygen current. The difference in the oxygen concentration between these two sensors is related to the glucose concentration. The sensor was tested in humans, remaining implanted for up to 180 days. The glucose reading displayed a 10 to 12 min delay between the actual blood concentration and that displayed by the implanted system, which was attributed to the glucose diffusion from capillaries through the interstitial space to the sensor surface.[195]

A range of optical methods such as fluorescence,[196] SERS [197,198] and surface plasmon resonance (SPR) [199] have been exploited as transducing mechanisms in a number of nanostructured implanted systems.[200] Although still at an early development stage, these optical approaches appear to be a less invasive alternative to

electrochemical methods and offer the advantage of a potentially longer life-span and less frequent calibration requirements.[201] Among implanted nanosensors with optical transduction, those based on non-enzymatic strategies have emerged as an alternative to overcome the limitations associated with the use of enzymes in glucose sensing. A range of fluorescent reporter probes have been employed for monitoring glucose levels, including anthracene acid [202] and oxygen-sensitive nanoparticles.[203] These probes are normally injected into subcutaneous tissue and their fluorescence is measured with a portable device outside of the body through the skin. However, their main drawback is that the injected probes are unlikely to remain in the specific site for long. To overcome this issue, fluorescent probes are normally embedded into microstructured hydrogels [204] or coupled with optical fibers using membranes such as cellulose,[205] thus prolonging their *in vivo* residence and also providing improved biocompatibility.[204]

Optical sensing based on affinity relies on the fluorescence change generated from the interaction of glucose with fluorescently-labelled glucose-binding moieties. The reversible affinity reaction between boronic acid and glucose has been studied for more than a century,[206] but it was not until 1994 that the first fluorescent probe based on boronic acid was realized.[207,208] The molecular combination of diboronic acid (saccharide binding) and anthracene (fluorophore) allowed their use in optical sensing of glucose via measurable changes in the fluorescence intensity.[209] However, the application *in vivo* of these glucose-binding moieties in implanted systems had not been exploited until their immobilization on solid supports (e.g. hydrogel matrices). The Takeuchi group established a fluorescent-based sensor by combining biocompatible injectable hydrogels microbeads with a fluorescent dye and boronic acid for glucose recognition (Figure 2.8d).[202,210] The hydrogel remained glucose responsive

for up to 140 days.[202] Zhang et al. developed a glucose-sensitive nanobiosensor based on the immobilization of a fluorescent poly(amido amine) dendrimer into a glucose-sensitive copolymer microgels based on phenylboronic acid. The co-polymer microgel morphology was demonstrated to be tunable, from sub-100 nm particles to flower-like nanostructures. This sensor showed better stability against photobleaching and lower toxicity compared to conventional fluorescent dyes and quantum dots. Furthermore, the sensor was used to measure transdermal glucose concentration wirelessly *in vivo*.[211] Implantable hydrogels and membrane-coupled optical fibers containing fluorescent probes have also been used for continuous non-enzymatic glucose monitoring. Fibers were co-polymerized with poly(acrylamide-co-poly(ethylene glycol) diacrylate) and phenylboronic acid. The complexation of the phenylboronic acid and cis-diol groups of glucose caused changes in the physical and optical properties of the hydrogel, being sensitive to glucose concentration.[212] ConA nano-formulations have also emerged in implantable glucose sensors. Typically, the sensing mechanism is based on the competition between glucose and a fluorescently labelled dextran for binding to ConA. Since glucose has higher affinity to ConA compared to dextran, it displaces donor-dye-bound dextran and disrupts the fluorescence energy transfer (FRET) between the donor dye and the acceptor dye that is covalently bound to ConA. In a report by McNichols et al. an optical fiber of 175 µm in diameter was inserted into a 210 µm diameter cellulose acetate membrane.[205] The space in between was filled with a fluorescent ConA-based assay suspension by aspiration, after which it was sealed with cyanoacrylate. The cellulose acetate membrane used to cover the optical fiber prevented leakage of fluorescent ConA-based assay suspension and at the same time allowed glucose diffusion. This system was implanted under the skin of a rat with the distal ends exposed on skin surface and

used for optical fiber connection. The presence of glucose leads to an increase in sensor fluorescence measured with optical fiber coupled spectrometer.

The enzymatic reaction of glucose in the presence of GOx can also be employed in implanted sensors to trigger a measurable optical response. For instance, oxygen consumption induces a change in the fluorescence intensity of metalloporphyrin-based hydrogels. McShane et al. have shown that alginate hydrogel microparticles responded in a linear fashion to physiologically relevant levels of glucose for up to two weeks.[204] Sun et al. have reported an ultrasensitive optical glucose sensor based on fluorescent polymer-dots (Pdots) and GOx that can be wirelessly monitored via a smartphone. The Pdots with a diameter varying between 18 to 25 nm containing oxygen-responsive palladium porphyrin complexes act as optical transducers that allowed to differentiate between euglycaemia and hyperglycemia (Figure 2.8a) Semiconductive Pdots were selected due to their distinctive properties of high luminescence, brightness and stability, and biocompatibility. The authors also reported that their palladium-based porphyrin complexes have 10 times longer lifetime compared to their platinum-based counterparts.[203]

Also, a wide variety of inorganic and hybrid nanomaterials such as noble metal nanoparticles, carbon nanomaterials and semiconductor quantum dots are currently emerging with the potential to overcome the current drawbacks such as short lifetime, long term accuracy and requirement for sensor calibration in implanted sensors.[213] Photoluminescent semiconductor quantum dots have been explored in cell imaging and are now being applied in the *in vivo* biosensing field. Indirect detection of glucose can be attained by a light-induced electron transfer from glucose via GOx and oxygen to a CdSe/ZnS QD electrode with the generated photocurrent being dependent on the

glucose concentration.[214] The ability of SWCNT to transmit signals in the near-infrared window, where biological components exhibit minimum absorption and auto-fluorescence, and respond to changes in the local environment can also be exploited for optical glucose detection.[215] The Strano group used this tunable emission in enzymatic and non-enzymatic approaches for the near-infrared fluorescence sensing of glucose.[216,217] They have also shown that SWCNT can remain functional for 300 days after subcutaneous implantation into mice in a biocompatible alginate gel matrix (Figure 2.8b-c).[218] This approach demonstrated to be successful for the detection of NO, being selective thanks to the specificity provided by the PEGylated DNA oligonucleotide sequence ($ds(AAAT)_7$) wrapped around the SWCNTs, and maintaining high *in vivo* stability, biocompatibility, and near-infrared fluorescence quantum yield. The authors reported a LOD of 1 μM for NO, and with this performance the sensor can be used as a potential indicator of pathological nitrosative and oxidative stress. These systems do not photobleach, show minimal fluorescent interference with biological media and a fast readout of the fluorescent signal during NO detection. One limitation of these fluorescent-based systems is that they exhibit a nonlinear response to glucose concentration.

Silicon-based nanomaterials have also been reported for *in vivo* biosensing. They offer numerous advantages including low toxicity, versatile surface chemistry, adjustable dimensions and low toxicity. Silica nanospheres have been shown to be biocompatible and have been used to identify cancerous lesions.[219] Silica nanoparticles were labelled with ^{124}I for positron emission tomography and functionalized with a peptide to target melanoma. Silica nanoparticles showed a preferential uptake and localization at the cancerous tissue. Porous silicon has also emerged as promising nanomaterial with exciting optical properties. Indeed, a number

of studies have demonstrated its biocompatibility [220] and *in vivo* biosensing capabilities.[221] Recently, Tong et al. demonstrated the stability and biocompatibility of implanted porous silicon optical rugate filter without compromising their optical functionality (Figure 2.8e-f).[222] The nanomaterial initially proved to be cytotoxic, possibly due to the generation of reactive oxygen species, regardless of its surface chemistry. However, incubating the developed porous silicon-based transducer for 10 days in the cell culture medium used during *in vitro* studies rendered the sensing device biocompatible *in vivo*.

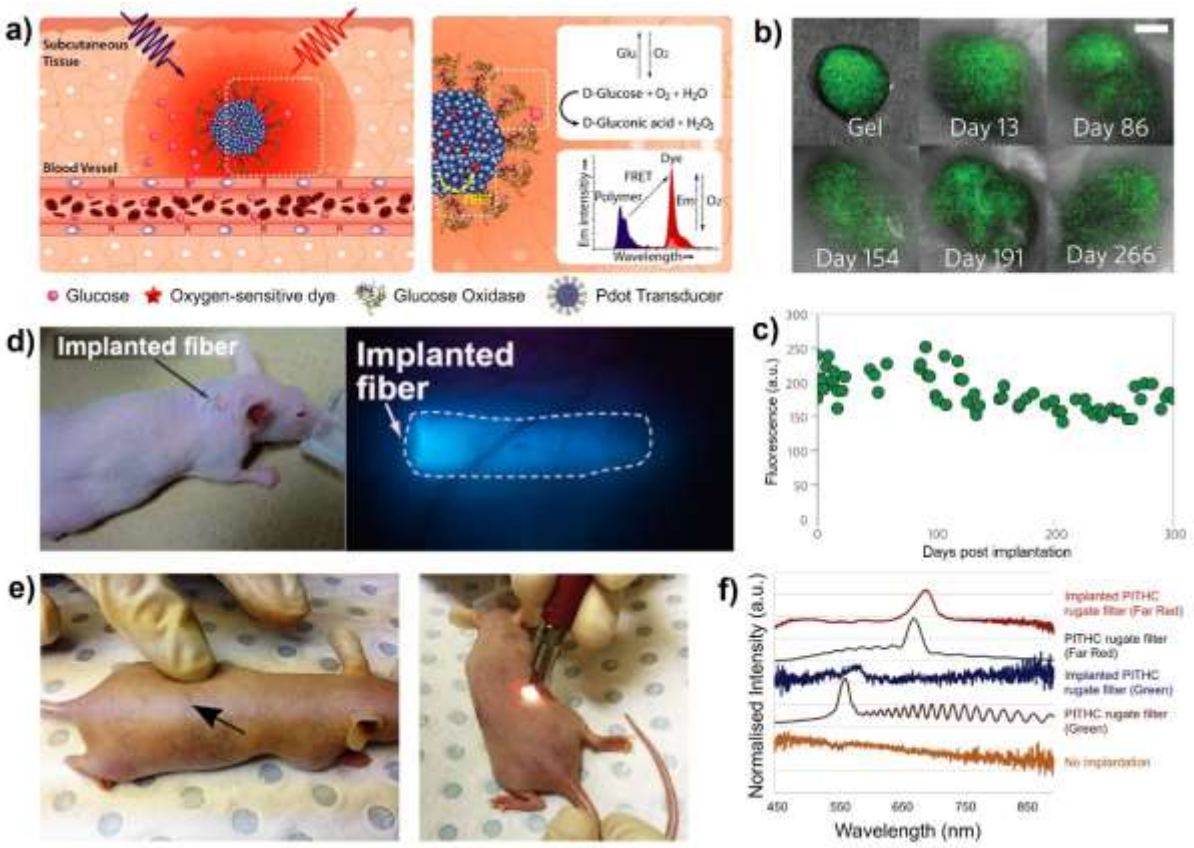

Figure 2.8: a) Schematic of the real-time optical monitoring of glucose levels using oxygen-responsive fluorescent Pdots, adapted with permission from Ref. [203] Copyright (2018) American Chemical Society. **b)** Images of alginate-SWNT gel prior subcutaneous implantation and after at several time points throughout a 300-day test period (scale bar, 4 mm), **c)** quantification of the SWNT fluorescence over a 300-day test, adapted with permission from Ref. [218] Copyright (203) Springer Nature. **d)** Optical image of the implantation in mouse ear of injectable hydrogel glucose sensor and fluorescent image of the mouse ear, adapted from Ref.,[202] **e)** optical images illustrating reading of the pSi rugate filter through the mouse skin, **f)** photonic peaks of pSi rugate film being read through the skin, adapted with permission from Ref. [222] Copyright (2017) Elsevier.

Photoacoustics has also been applied in the development of wearable devices. Photoacoustics can be seen as another optical technique, with the notable exception that the output are ultrasonic waves that occur as a response to a pulsating optical excitation. The method relies on the pressure variations caused by interaction between a laser beam and tissues through thermal expansion. The incident laser beam generates heat which results in variations in the acoustic signals, which can be measured by a piezoelectric transducer. This technology contributed to the early development of continuous glucose monitoring devices. Glucose can be selectively measured by targeting the molecule's absorption bands. These absorption bands range from UV to mid-infrared; therefore, a variety of incident optical excitation wavelengths may be used. Glucon Inc. (Boulder, CO) pioneered the use of this technology for continuous glucose monitoring and implemented it in their product Aprise. In 2007, they reported a pre-clinical study where they monitored 62 subjects.[223] The device presented a good correlation with blood sugar levels, but showed poor reproducibility and low specificity. Although the reported results were promising, the device never reached the market and has not been further investigated in the peer-reviewed literature. Some of its limitations may relate to the non-specific interferences caused by other substances, and its poor accuracy due to its sensitivity to environmental changes (e.g. temperature, pressure, humidity). Despite commercialization challenges, photoacoustics has continued to be subject of intensive investigations for the non-invasive monitoring of glucose with the aim to overcome some of these limitations.[224,225] For example, Kottmann et al. proposed the use of a small photoacoustic cell integrated with two lasers at fixed excitation wavelengths [224]. This method allows to correct the laser power variation by alternatively directing the lasers at the photoacoustic cell and a power meter, thus improving long-term drifting.

They also addressed the problem of varying humidity by introducing a N_2 flow into the chamber. However, this is not a feasible solution for a wearable device. Sim et al. proposed to obtain microscopic spatial information prior to the photoacoustic measurement to increase the reliability of the method.[225] The excitation laser was not only used to induce a photoacoustic signal but also to microscopically scan the skin and avoid physical and temporal homogeneities, such as sweat glands and secretion products. This method may enhance the accuracy and repeatability of glucose measurements, but increases measurement time. The combination of the dual-laser approach with the microscopic position scanning may overcome many of the limitations of the current systems.

2.5 Conclusions and Future Perspectives

Today, sophisticated yet affordable, user-friendly fitness trackers and smart watches are everyday widgets used by millions of people. While these devices are able to monitor a range of physical activity indicators (e.g. heart rate, sleep pattern, daily exercise), a next generation of personalized health and activity trackers is currently under development and promises to revolutionize the field. Next generation of wearable devices will provide real-time information about the user's physiological state at a molecular level, thus delivering relevant information to a wide variety of applications ranging from healthcare to sports management. This fast-developing technology comprises skin-interfaced biosensors integrated into wearable and implantable systems.

Over the past decade, investigations in material science, microfluidics, flexible electronics and communications have accelerated the development of this technology. In particular, the integration of nanostructured materials has contributed to some of

the most significant advances in the field. For example, the incorporation of nanomaterials such as CNT, metallic nanoparticles or semiconductor nanofilms greatly enhanced the biosensing performance of electrochemical and optical devices. However, there are several remaining challenges and opportunities for their effective integration into wearable devices. The long-term safety of nanomaterials continues to be under scrutiny. Therefore, long-term toxicity studies are critical to demonstrate the biocompatibility and biosafety of these nanostructured materials, especially for the more invasive applications here outlined. Because of the constant contact of wearable devices with the skin, physiological impact (i.e. coagulation issues, inflammation and foreign body response from the body) has to be studied *a priori* to avoid infection risks and detrimental sensor performance. Also, further effort has to be devoted to maintain the stability and accuracy of the wearable biosensors to be used in continuous long-term monitoring. These barriers are currently being addressed through novel use of nanomaterials, surface chemistry and device designs. Also, further effort has to be devoted to maintain the stability and accuracy of the wearable biosensors to be used in continuous long-term monitoring. Surface effects such as biofouling alters the interface between the biosensor and the bodily fluids, leading to reduced sensitivity and lifetime. Investigations to understand and control these effects, which are the main cause of performance deterioration, are still necessary. The challenge is currently being addressed through novel use of nanomaterials, surface chemistry and device designs. The use of highly biocompatible polymeric coatings has gained a prominent position as a strategy to lower biofouling and reduce immune responses. Polymeric matrices may also be used to entrap bioreceptors and thus minimize their intrinsic instability. Another strategy to improve stability and extend sensor lifetimes is the incorporation of anti-inflammatory drugs for enhanced tissue integration. The more

efficient use of nanomaterials into biosensor designs may see a further reduction of the size of these biosensors, which could potentially avoid, or at least reduce, foreign body responses.

Compared to transdermal or implantable systems, on-skin approaches, such as sweat biosensors, produce a minimal immune response and suffer reduced biofouling. But the low concentration of most clinically relevant analytes in sweat, currently limits their use to the detection of ions and a few small molecules (i.e. glucose, lactate). In order to expand the opportunities for on-skin biosensors to low concentration analytes such as hormones or proteins, more sensitive and selective techniques need to be developed. The incorporation of nanomaterials that increase surface area, amplify signals, and improve catalytic properties may be used in the device design to boost sensitivity. Also, a new generation of engineered bioreceptors (e.g. DNA aptamers, nanobodies) have emerged with the potential to increase sensitivity and specificity. Some have already been implemented in extraordinarily sensitive immunosensors, reaching up to sub-picomolar detection limits. However, their application in continuous sensing continues to be hindered by the difficulties to regenerate them. To date, demonstrations of continuous sensing are still monopolized by approaches that use enzymes as bioreceptors. To expand the continuous monitoring opportunities from catalytic to affinity-based biosensors, the regeneration of bioreceptors is a major challenge to overcome. Regenerable electrochemical aptamers, which have been demonstrated to reach suitable detection levels in blood, show potential for their implementation in wearable biosensors.

The collection of bodily fluids from the skin still brings many challenges. Sweat has attracted the greatest attention as an analytical biofluid for wearable devices, mainly because it is easily accessible via non-invasive techniques. However,

discontinuous availability and contamination from the skin surface have motivated the search for methodologies to induce sweat secretion. The well-established iontophoresis, although efficient, triggers skin irritations that make these devices non-user-friendly. Developing alternative sweat collection approaches that combine sweat stimulation with microfluidics are required to enable continuous monitoring. ISF has a substantial advantage over sweat as it may enable the detection of protein biomarkers that are not present in sweat, or are present at very low concentrations. Further research into the nature and composition of ISF towards understanding the correlation between the changing levels of a biomarker with medical conditions or sports performance is still necessary. Sampling of ISF via transdermal devices offers several advantages over subcutaneous devices, including minimal invasion, easy replacement and more efficient integration into devices. But subcutaneous devices could also be advantageous for long-term monitoring without external devices attached to the body. The lifetime requirements for the marketable success of each of these sensors is very different. On-skin sensors are amenable to short term use models (hours or days), whereas transdermal devices should remain functional for weeks and implanted for months, or even years.

We envisage that continuous monitoring of biomolecular profiles through wearable and implantable micro- and nanosystems will provide valuable information about our bodies for personalized and predictive healthcare in the near future. Great advances have been made in academic and industrial laboratories in the last few years. But for the successful translation of these systems from benchtop to commercialization, there are still many challenges to overcome. These challenges relate to safety, reliability, long-term performance, accuracy, device integration, and wearability. We expect micro- and nanotechnologies to be playing a central role in the

development of these devices, particularly in regards to miniaturization, robustness and stability. Microfluidics will contribute to fast, effective sample collection that provide reproducible and accurate sensor responses. Prototyped devices will require extensive validation via in vivo preclinical models and proven correlation with blood-based tests. Other than scientific requirements, these devices have to be simple and affordable, yet efficient and safe. The integration of biosensors with smartphones is expected to enable simple readouts and accelerate the development of these devices. The considerations here presented offer many opportunities for advancing the field. Overall, the achievements and challenges discussed throughout this review will assist the cross-disciplinary teams of researchers to enable wearable biosensing technology have a substantial impact in the diagnostics game.

2.6 References

(1) Bariya, M.; Nyein, H. Y. Y.; Javey, A. Wearable sweat sensors, *Nature Electronics* **2018**, *1*, 160-171.

(2) Heikenfeld, J.; Jajack, A.; Rogers, J.; Gutruf, P.; Tian, L.; Pan, T.; Li, R.; Khine, M.; Kim, J.; Wang, J.; Kim, J. Wearable sensors: modalities, challenges, and prospects, *Lab on a Chip* **2018**, *18*, 217-248.

(3) Yang, Y.; Gao, W. Wearable and flexible electronics for continuous molecular monitoring, *Chemical Society Reviews* **2018**, *48*, 1465-1491.

(4) Lou, Z.; Li, L.; Wang, L.; Shen, G. Recent Progress of Self-Powered Sensing Systems for Wearable Electronics, *Small* **2017**, *13*, 1701791.

(5) Heikenfeld, J.; Jajack, A.; Feldman, B.; Granger, S. W.; Gaitonde, S.; Begtrup, G.; Katchman, B. A. Accessing analytes in biofluids for peripheral biochemical monitoring, *Nature Biotechnology* **2019**, *37*, 407-419.

(6) Kim, J.; Campbell, A. S.; de Ávila, B. E.-F.; Wang, J. Wearable biosensors for healthcare monitoring, *Nature Biotechnology* **2019**, *37*, 389-406.

(7) Grayson, A. C. R.; Shawgo, R. S.; Johnson, A. M.; Flynn, N. T.; Yawen, L. I.; Cima, M. J.; R, L. A BioMEMS review: MEMS technology for physiologically integrated devices, *Proceedings of the IEEE* **2004**, *92*, 6-21.

(8) Liu, H.; Qing, H.; Li, Z.; Han, Y. L.; Lin, M.; Yang, H.; Li, A.; Lu, T. J.; Li, F.; Xu, F. Paper: A promising material for human-friendly functional wearable electronics, *Materials Science and Engineering: R: Reports* **2017**, *112*, 1-22.

(9) Mukhopadhyay, S. C. Wearable Sensors for Human Activity Monitoring: A Review, *IEEE Sensors Journal* **2015**, *15*, 1321-1330.

(10) Fenner, J.; Clark, R. A. F. In *Skin Tissue Engineering and Regenerative Medicine*, Iv, J. H. H., Ed.; Academic Press: Boston, 2016, pp 1-17.

(11) Ventrelli, L.; Marsilio Strambini, L.; Barillaro, G. Microneedles for Transdermal Biosensing: Current Picture and Future Direction, *Advanced Healthcare Materials* **2015**, *4*, 2606-2640.

(12) Kanitakis, J. Anatomy, histology and immunohistochemistry of normal human skin, *European Journal of Dermatology* **2002**, *12*, 390-399.

(13) Tran, B. Q.; Miller, P. R.; Taylor, R. M.; Boyd, G.; Mach, P. M.; Rosenzweig, C. N.; Baca, J. T.; Polsky, R.; Glaros, T. Proteomic Characterization of Dermal Interstitial Fluid Extracted Using a Novel Microneedle-Assisted Technique, *Journal of Proteome Research* **2018**, *17*, 479-485.

(14) Mikesh, L. M.; Aramadhaka, L. R.; Moskaluk, C.; Zigrino, P.; Mauch, C.; Fox, J. W. Proteomic anatomy of human skin, *Journal of Proteomics* **2013**, *84*, 190-200.

(15) Hendricks, A. J.; Vaughn, A. R.; Clark, A. K.; Yosipovitch, G.; Shi, V. Y. Sweat mechanisms and dysfunctions in atopic dermatitis, *Journal of Dermatological Science* **2018**, *89*, 105-111.

(16) Sonner, Z.; Wilder, E.; Heikenfeld, J.; Kasting, G.; Beyette, F.; Swaile, D.; Sherman, F.; Joyce, J.; Hagen, J.; Kelley-Loughnane, N.; Naik, R. The microfluidics of the eccrine sweat gland, including biomarker partitioning, transport, and biosensing implications, *Biomicrofluidics* **2015**, *9*, 031301.

(17) Gao, W.; Emaminejad, S.; Nyein, H. Y. Y.; Challa, S.; Chen, K.; Peck, A.; Fahad, H. M.; Ota, H.; Shiraki, H.; Kiriya, D.; Lien, D.-H.; Brooks, G. A.; Davis, R. W.; Javey, A. Fully integrated wearable sensor arrays for multiplexed in situ perspiration analysis, *Nature* **2016**, *529*, 509-514.

(18) Emaminejad, S.; Gao, W.; Wu, E.; Davies, Z. A.; Yin Yin Nyein, H.; Challa, S.; Ryan, S. P.; Fahad, H. M.; Chen, K.; Shahpar, Z.; Talebi, S.; Milla, C.; Javey, A.; Davis, R. W. Autonomous sweat extraction and analysis applied to cystic fibrosis and glucose

monitoring using a fully integrated wearable platform, *Proceedings of the National Academy of Sciences* **2017**, *114*, 4625-4630.

(19) Wiig, H.; Swartz, M. A. Interstitial fluid and lymph formation and transport: physiological regulation and roles in inflammation and cancer, *Physiological Reviews* **2012**, *92*, 1005-1060.

(20) Scallan J., H. V. H., Korthuis R.J. In *Capillary Fluid Exchange: Regulation, Functions, and Pathology*; Morgan & Claypool Life Sciences: San Rafael (CA), 2010.

(21) Koschinsky, T.; Jungheim, K.; Heinemann, L. Glucose Sensors and the Alternate Site Testing-Like Phenomenon: Relationship Between Rapid Blood Glucose Changes and Glucose Sensor Signals, *Journal of Diabetes Technology and Therapeutics* **2003**, *5*, 829-842.

(22) Anderson, N. L.; Anderson, N. G. The Human Plasma Proteome, *Molecular and Cellular Proteomics* **2002**, *1*, 845-867.

(23) Anderson, N. L. The clinical plasma proteome: a survey of clinical assays for proteins in plasma and serum, *Clinical Chemistry* **2010**, *56*, 177-185.

(24) Kupke, I. R.; Kather, B.; Zeugner, S. On the composition of capillary and venous blood serum, *Clinica Chimica Acta* **1981**, *112*, 177-185.

(25) Vermeer, B. J.; Reman, F. C.; van Gent, C. M. The determination of lipids and proteins in suction blister fluid, *Journal of Investigative Dermatology* **1979**, *73*, 303-305.

(26) Baker, L. B. Sweating Rate and Sweat Sodium Concentration in Athletes: A Review of Methodology and Intra/Interindividual Variability, *Sports Medicine (Auckland, N.Z.)* **2017**, *47*, 111-128.

(27) Baker, L. B.; Ungaro, C. T.; Barnes, K. A.; Nuccio, R. P.; Reimel, A. J.; Stofan, J. R. Validity and reliability of a field technique for sweat Na+ and K+ analysis during exercise in a hot-humid environment, *Physiological Reports* **2014**, *2*, e12007.

(28) Hall, S. K.; Stableforth, D. E.; Green, A. Sweat Sodium and Chloride Concentrations—Essential Criteria for the Diagnosis of Cystic Fibrosis in Adults, *Annals of Clinical Biochemistry* **1990**, *27*, 318-320.

(29) Montain, S. J.; Cheuvront, S. N.; Lukaski, H. C. Sweat mineral-element responses during 7 h of exercise-heat stress, *Int J Sport Nutr Exerc Metab* **2007**, *17*, 574-582.

(30) Takahama, U.; Ansai, T.; Hirota, S. In *Advances in Molecular Toxicology*, Fishbein, J. C.; Heilman, J. M., Eds.; Elsevier, 2013, pp 129-177.

(31) Hodges, R. E.; Hood, J.; Canham, J. E.; Sauberlich, H. E.; Baker, E. M. Clinical manifestations of ascorbic acid deficiency in man, *The American Journal of Clinical Nutrition* **1971**, *24*, 432-443.

(32) Moyer, J.; Wilson, D.; Finkelshtein, I.; Wong, B.; Potts, R. Correlation between sweat glucose and blood glucose in subjects with diabetes, *Journal of Diabetes Technology and Therapeutics* **2012**, *14*, 398-402.

(33) Anastasova, S.; Crewther, B.; Bembnowicz, P.; Curto, V.; Ip, H. M.; Rosa, B.; Yang, G. Z. A wearable multisensing patch for continuous sweat monitoring, *Biosensors and Bioelectronics* **2017**, *93*, 139-145.

(34) Huang, C. T.; Chen, M. L.; Huang, L. L.; Mao, I. F. Uric acid and urea in human sweat, *Chinese Journal Physiology* **2002**, *45*, 109-115.

(35) Mickelsen, O.; Keys, A. The composition of sweat, with special reference to vitamins, *Journal of Biological Chemistry* **1943**, *149*, 479-490.

(36) Windmiller, J. R.; Bandodkar, A. J.; Valdés-Ramírez, G.; Parkhomovsky, S.; Martinez, A. G.; Wang, J. Electrochemical sensing based on printable temporary transfer tattoos, *Chemical Communications* **2012**, *48*, 6794-6796.

(37) Griffing, G. T., Staros, E. B., Ed.; Medscape, 2014.

(38) Parlak, O.; Keene, S. T.; Marais, A.; Curto, V. F.; Salleo, A. Molecularly selective nanoporous membrane-based wearable organic electrochemical device for noninvasive cortisol sensing, *Science Advances* **2018**, *4*, eaar2904.

(39) Gonzalez-Quintela, A.; Alende, R.; Gude, F.; Campos, J.; Rey, J.; Meijide, L. M.; Fernandez-Merino, C.; Vidal, C. Serum levels of immunoglobulins (IgG, IgA, IgM) in a general adult population and their relationship with alcohol consumption, smoking and common metabolic abnormalities, *Clinical & Experimental Immunology* **2008**, *151*, 42-50.

(40) Katchman, B. A.; Zhu, M.; Blain Christen, J.; Anderson, K. S. Eccrine Sweat as a Biofluid for Profiling Immune Biomarkers, *Proteomics – Clinical Applications* **2018**, *12*, 1800010.

(41) Andreu-Perez, J.; Poon, C. C. Y.; Merrifield, R. D.; Wong, S. T. C.; Yang, G. Big Data for Health, *IEEE Journal of Biomedical and Health Informatics* **2015**, *19*, 1193-1208.

(42) Pyattaev, A.; Johnsson, K.; Andreev, S.; Koucheryavy, Y. Communication challenges in high-density deployments of wearable wireless devices, *IEEE Wireless Communications* **2015**, *22*, 12-18.

(43) Li, J.; Zhao, J.; Rogers, J. A. Materials and Designs for Power Supply Systems in Skin-Interfaced Electronics, *Accounts of Chemical Research* **2019**, *52*, 53-62.

(44) Gao, Y.; Yu, L.; Yeo, J. C.; Lim, C. T. Flexible Hybrid Sensors for Health Monitoring: Materials and Mechanisms to Render Wearability, *Advanced Materials* **2019**, *0*, 1902133.

(45) Arias, O.; Wurm, J.; Hoang, K.; Jin, Y. Privacy and Security in Internet of Things and Wearable Devices, *IEEE Transactions on Multi-Scale Computing Systems* **2015**, *1*, 99-109.

(46) Fang, L.; Liang, B.; Yang, G.; Hu, Y.; Zhu, Q.; Ye, X. A needle-type glucose biosensor based on PANI nanofibers and PU/E-PU membrane for long-term invasive continuous monitoring, *Biosensors and Bioelectronics* **2017**, *97*, 196-202.

(47) Wang, W.; Fan, X.; Xu, S.; Davis, J. J.; Luo, X. Low fouling label-free DNA sensor based on polyethylene glycols decorated with gold nanoparticles for the detection of breast cancer biomarkers, *Biosensors and Bioelectronics* **2015**, *71*, 51-56.

(48) Yang, W.; Xue, H.; Carr, L. R.; Wang, J.; Jiang, S. Zwitterionic poly(carboxybetaine) hydrogels for glucose biosensors in complex media, *Biosensors and Bioelectronics* **2011**, *26*, 2454-2459.

(49) Choleau, C.; Klein, J. C.; Reach, G.; Aussedat, B.; Demaria-Pesce, V.; Wilson, G. S.; Gifford, R.; Ward, W. K. Calibration of a subcutaneous amperometric glucose sensor implanted for 7 days in diabetic patients: Part 2. Superiority of the one-point calibration method, *Biosensors and Bioelectronics* **2002**, *17*, 647-654.

(50) Mahmoudi, Z.; Johansen, M. D.; Christiansen, J. S.; Hejlesen, O. Comparison Between One-Point Calibration and Two-Point Calibration Approaches in a Continuous Glucose Monitoring Algorithm, *Journal of Diabetes Technology and Therapeutics* **2014**, *8*, 709-719.

(51) Heo, Y. J.; Takeuchi, S. Towards Smart Tattoos: Implantable Biosensors for Continuous Glucose Monitoring, *Advanced Healthcare Materials* **2013**, *2*, 43-56.

(52) Wang, Y.; Papadimitrakopoulos, F.; Burgess, D. J. Polymeric “smart” coatings to prevent foreign body response to implantable biosensors, *Journal of Controlled Release* **2013**, *169*, 341-347.

(53) Roach, P.; Farrar, D.; Perry, C. C. Surface Tailoring for Controlled Protein Adsorption: Effect of Topography at the Nanometer Scale and Chemistry, *Journal of the American Chemical Society* **2006**, *128*, 3939-3945.

(54) Sung, J.; Barone, P. W.; Kong, H.; Strano, M. S. Sequential delivery of dexamethasone and VEGF to control local tissue response for carbon nanotube fluorescence based micro-capillary implantable sensors, *Biomaterials* **2009**, *30*, 622-631.

(55) Kumar, S.; Ahlawat, W.; Kumar, R.; Dilbaghi, N. Graphene, carbon nanotubes, zinc oxide and gold as elite nanomaterials for fabrication of biosensors for healthcare, *Biosensors and Bioelectronics* **2015**, *70*, 498-503.

(56) Kim, J.; Jeerapan, I.; Imani, S.; Cho, T. N.; Bandodkar, A.; Cinti, S.; Mercier, P. P.; Wang, J. Noninvasive Alcohol Monitoring Using a Wearable Tattoo-Based Iontophoretic-Biosensing System, *ACS Sensors* **2016**, *1*, 1011-1019.

(57) Biswas, A.; Bornhoeft, L. R.; Banerjee, S.; You, Y.-H.; McShane, M. J. Composite Hydrogels Containing Bioactive Microreactors for Optical Enzymatic Lactate Sensing, *ACS Sensors* **2017**, *2*, 1584-1588.

(58) Vaisocherova, H.; Brynda, E.; Homola, J. Functionalizable low-fouling coatings for label-free biosensing in complex biological media: advances and applications, *Analytical and Bioanalytical Chemistry* **2015**, *407*, 3927-3953.

(59) Bandodkar, A. J.; Wang, J. Non-invasive wearable electrochemical sensors: a review, *Trends in Biotechnology* **2014**, *32*, 363-371.

(60) Bankar, S. B.; Bule, M. V.; Singhal, R. S.; Ananthanarayan, L. Glucose oxidase — An overview, *Biotechnology Advances* **2009**, *27*, 489-501.

(61) Hoedemaekers, C. W.; Gunnewiek, J. M. K.; Prinsen, M. A.; Willems, J. L.; Van der Hoeven, J. G. Accuracy of bedside glucose measurement from three glucometers in critically ill patients, *Critical Care Medicine* **2008**, *36*, 3062-3066.

(62) Holliger, P.; Hudson, P. J. Engineered antibody fragments and the rise of single domains, *Nature Biotechnology* **2005**, *23*, 1126-1136.

(63) Goode, J. A.; Rushworth, J. V. H.; Millner, P. A. Biosensor Regeneration: A Review of Common Techniques and Outcomes, *Langmuir* **2015**, *31*, 6267-6276.

(64) Potyrailo, R. A.; Murray, A. J.; Nagraj, N.; Pris, A. D.; Ashe, J. M.; Todorovic, M. Towards Maintenance-Free Biosensors for Hundreds of Bind/Release Cycles, *Angewandte Chemie International Edition* **2014**, *54*, 2174-2178.

(65) Kandimalla, V. B.; Neeta, N. S.; Karanth, N. G.; Thakur, M. S.; Roshini, K. R.; Rani, B. E. A.; Pasha, A.; Karanth, N. G. K. Regeneration of ethyl parathion antibodies for repeated use in immunosensor: a study on dissociation of antigens from antibodies, *Biosensors and Bioelectronics* **2004**, *20*, 903-906.

(66) Mascini, M.; Tombelli, S. Biosensors for biomarkers in medical diagnostics, *Biomarkers* **2008**, *13*, 637-657.

(67) Zhu, C.; Yang, G.; Li, H.; Du, D.; Lin, Y. Electrochemical Sensors and Biosensors Based on Nanomaterials and Nanostructures, *Analytical Chemistry* **2015**, *87*, 230-249.

(68) Cash, K. J.; Clark, H. A. Nanosensors and nanomaterials for monitoring glucose in diabetes, *Trends in Molecular Medicine* **2010**, *16*, 584-593.

(69) Kausaite-Minkstimiene, A.; Ramanaviciene, A.; Kirlyte, J.; Ramanavicius, A. Comparative Study of Random and Oriented Antibody Immobilization Techniques on the Binding Capacity of Immunosensor, *Analytical Chemistry* **2010**, *82*, 6401-6408.

(70) Vareiro, M. M. L. M.; Liu, J.; Knoll, W.; Zak, K.; Williams, D.; Jenkins, A. T. A. Surface Plasmon Fluorescence Measurements of Human Chorionic Gonadotrophin: Role of Antibody Orientation in Obtaining Enhanced Sensitivity and Limit of Detection, *Analytical Chemistry* **2005**, *77*, 2426-2431.

(71) Huang, L.; Muyldermans, S.; Saerens, D. Nanobodies®: proficient tools in diagnostics, *Expert Review of Molecular Diagnostics* **2010**, *10*, 777-785.

(72) Cao, C.; Zhang, F.; Goldys, E. M.; Gao, F.; Liu, G. Advances in structure-switching aptasensing towards real time detection of cytokines, *TrAC Trends in Analytical Chemistry* **2018**, *102*, 379-396.

(73) Samant, P. P.; Prausnitz, M. R. Mechanisms of sampling interstitial fluid from skin using a microneedle patch, *Proceedings of the National Academy of Sciences* **2018**, *115*, 4583-4588.

(74) Modali, A.; Vanjari, S. R. K.; Dendukuri, D. Wearable Woven Electrochemical Biosensor Patch for Non-invasive Diagnostics, *Electroanalysis* **2016**, *28*, 1276-1282.

(75) Bandodkar, A. J.; Jeerapan, I.; Wang, J. Wearable Chemical Sensors: Present Challenges and Future Prospects, *ACS Sensors* **2016**, *1*, 464-482.

(76) Choi, J.; Kang, D.; Han, S.; Kim, S. B.; Rogers, J. A. Thin, Soft, Skin-Mounted Microfluidic Networks with Capillary Bursting Valves for Chrono-Sampling of Sweat, *Advanced Healthcare Materials* **2017**, *6*, 1601355.

(77) Martín, A.; Kim, J.; Kurniawan, J. F.; Sempionatto, J. R.; Moreto, J. R.; Tang, G.; Campbell, A. S.; Shin, A.; Lee, M. Y.; Liu, X.; Wang, J. Epidermal Microfluidic

Electrochemical Detection System: Enhanced Sweat Sampling and Metabolite Detection, *ACS Sensors* **2017**, *2*, 1860-1868.

(78) Zhang, D.; Liu, Q. Biosensors and bioelectronics on smartphone for portable biochemical detection, *Biosensors and Bioelectronics* **2016**, *75*, 273-284.

(79) Zarei, M. Portable biosensing devices for point-of-care diagnostics: Recent developments and applications, *TrAC Trends in Analytical Chemistry* **2017**, *91*, 26-41.

(80) Telting-Diaz, M.; Bakker, E. Effect of lipophilic ion-exchanger leaching on the detection limit of carrier-based ion-selective electrodes, *Analytical Chemistry* **2001**, *73*, 5582-5589.

(81) Gao, W.; Nyein, H. Y. Y.; Shahpar, Z.; Fahad, H. M.; Chen, K.; Emaminejad, S.; Gao, Y.; Tai, L.-C.; Ota, H.; Wu, E.; Bullock, J.; Zeng, Y.; Lien, D.-H.; Javey, A. Wearable Microsensor Array for Multiplexed Heavy Metal Monitoring of Body Fluids, *ACS Sensors* **2016**, *1*, 866-874.

(82) Lee, H.; Song, C.; Hong, Y. S.; Kim, M. S.; Cho, H. R.; Kang, T.; Shin, K.; Choi, S. H.; Hyeon, T.; Kim, D.-H. Wearable/disposable sweat-based glucose monitoring device with multistage transdermal drug delivery module, *Science Advances* **2017**, *3*, e1601314.

(83) Panneer Selvam, A.; Muthukumar, S.; Kamakoti, V.; Prasad, S. A wearable biochemical sensor for monitoring alcohol consumption lifestyle through Ethyl glucuronide (EtG) detection in human sweat, *Scientific Reports* **2016**, *6*, 23111.

(84) Kinnamon, D.; Ghanta, R.; Lin, K.-C.; Muthukumar, S.; Prasad, S. Portable biosensor for monitoring cortisol in low-volume perspired human sweat, *Scientific Reports* **2017**, *7*, 13312.

(85) McCaul, M.; Glennon, T.; Diamond, D. Challenges and opportunities in wearable technology for biochemical analysis in sweat, *Current Opinion in Electrochemistry* **2017**, *3*, 46-50.

(86) Liu, Q.; Liu, Y.; Wu, F.; Cao, X.; Li, Z.; Alharbi, M.; Abbas, A. N.; Amer, M. R.; Zhou, C. Highly Sensitive and Wearable In2O3 Nanoribbon Transistor Biosensors with Integrated On-Chip Gate for Glucose Monitoring in Body Fluids, *ACS Nano* **2018**, *12*, 1170-1178.

(87) Oh, S. Y.; Hong, S. Y.; Jeong, Y. R.; Yun, J.; Park, H.; Jin, S. W.; Lee, G.; Oh, J. H.; Lee, H.; Lee, S.-S.; Ha, J. S. Skin-Attachable, Stretchable Electrochemical Sweat Sensor for Glucose and pH Detection, *ACS Applied Materials & Interfaces* **2018**, *10*, 13729-13740.

(88) Mishra, R. K.; Barfidokht, A.; Karajic, A.; Sempionatto, J. R.; Wang, J.; Wang, J. Wearable potentiometric tattoo biosensor for on-body detection of G-type nerve agents simulants, *Sensors and Actuators B: Chemical* **2018**, *273*, 966-972.

(89) Han, W.; He, H.; Zhang, L.; Dong, C.; Zeng, H.; Dai, Y.; Xing, L.; Zhang, Y.; Xue, X. A Self-Powered Wearable Noninvasive Electronic-Skin for Perspiration Analysis Based on Piezo-Biosensing Unit Matrix of Enzyme/ZnO Nanoarrays, *ACS Applied Materials & Interfaces* **2017**, *9*, 29526-29537.

(90) Bhide, A.; Muthukumar, S.; Saini, A.; Prasad, S. Simultaneous lancet-free monitoring of alcohol and glucose from low-volumes of perspired human sweat, *Scientific Reports* **2018**, *8*, 6507.

(91) Koh, A.; Kang, D.; Xue, Y.; Lee, S.; Pielak, R. M.; Kim, J.; Hwang, T.; Min, S.; Banks, A.; Bastien, P.; Manco, M. C.; Wang, L.; Ammann, K. R.; Jang, K. I.; Won, P.; Han, S.; Ghaffari, R.; Paik, U.; Slepian, M. J.; Balooch, G., et al. A soft, wearable

microfluidic device for the capture, storage, and colorimetric sensing of sweat, *Science Translation Medicine* **2016**, *8*, 366ra165.

(92) Xuan, X.; Yoon, H. S.; Park, J. Y. A wearable electrochemical glucose sensor based on simple and low-cost fabrication supported micro-patterned reduced graphene oxide nanocomposite electrode on flexible substrate, *Biosensors and Bioelectronics* **2018**, *109*, 75-82.

(93) Choi, J.; Ghaffari, R.; Baker, L. B.; Rogers, J. A. Skin-interfaced systems for sweat collection and analytics, *Science Advances* **2018**, *4*, eaar3921.

(94) Lv, T.; Yao, Y.; Li, N.; Chen, T. Wearable fiber-shaped energy conversion and storage devices based on aligned carbon nanotubes, *Nano Today* **2016**, *11*, 644-660.

(95) Patterson, M. J.; Galloway, S. D.; Nimmo, M. A. Variations in regional sweat composition in normal human males, *Experimental Physiology* **2000**, *85*, 869-875.

(96) Syu, Y.-C.; Hsu, W.-E.; Lin, C.-T. Review—Field-Effect Transistor Biosensing: Devices and Clinical Applications, *ECS Journal of Solid State Science and Technology* **2018**, *7*, Q3196-Q3207.

(97) Sang, S.; Wang, Y.; Feng, Q.; Wei, Y.; Ji, J.; Zhang, W. Progress of new label-free techniques for biosensors: a review, *Critical Reviews in Biotechnology* **2016**, *36*, 465-481.

(98) Bandodkar, A. J.; Jia, W.; Yardimci, C.; Wang, X.; Ramirez, J.; Wang, J. Tattoo-based noninvasive glucose monitoring: a proof-of-concept study, *Analytical Chemistry* **2015**, *87*, 394-398.

(99) J., T. M.; L., K. H.; D., B. M.; Tamada, J. A.; O., P. R. Electroanalysis of Glucose in Transcutaneously Extracted Samples, *Electroanalysis* **2000**, *12*, 666-671.

(100) Chen, Y.; Lu, S.; Zhang, S.; Li, Y.; Qu, Z.; Chen, Y.; Lu, B.; Wang, X.; Feng, X. Skin-like biosensor system via electrochemical channels for noninvasive blood glucose monitoring, *Science Advances* **2017**, *3*, e1701629.

(101) Ching, T. S.; Connolly, P. Simultaneous transdermal extraction of glucose and lactate from human subjects by reverse iontophoresis, *International Journal of Nanomedicine* **2008**, *3*, 211-223.

(102) Varadharaj, E. K.; Jampana, N. Non-Invasive Potentiometric Sensor for Measurement of Blood Urea in Human Subjects Using Reverse Iontophoresis, *Journal of The Electrochemical Society* **2016**, *163*, B340-B347.

(103) Ebah, L. M.; Read, I.; Sayce, A.; Morgan, J.; Chaloner, C.; Brenchley, P.; Mitra, S. Reverse iontophoresis of urea in health and chronic kidney disease: a potential diagnostic and monitoring tool?, *European Journal of Clinical Investigation* **2012**, *42*, 840-847.

(104) Tierney, M. J.; Tamada, J. A.; Potts, R. O.; Eastman, R. C.; Pitzer, K.; Ackerman, N. R.; Fermi, S. J. The GlucoWatch biographer: a frequent automatic and noninvasive glucose monitor, *Annals of Medicine* **2000**, *32*, 632-641.

(105) Tierney, M. J.; Tamada, J. A.; Potts, R. O.; Jovanovic, L.; Garg, S. Clinical evaluation of the GlucoWatch biographer: a continual, non-invasive glucose monitor for patients with diabetes, *Biosensors and Bioelectronics* **2001**, *16*, 621-629.

(106) Lipani, L.; Dupont, B. G. R.; Doungmene, F.; Marken, F.; Tyrrell, R. M.; Guy, R. H.; Ilie, A. Non-invasive, transdermal, path-selective and specific glucose monitoring via a graphene-based platform, *Nature Nanotechnology* **2018**, *13*, 504-511.

(107) Mayer, M.; Baeumner, A. J. A Megatrend Challenging Analytical Chemistry: Biosensor and Chemosensor Concepts Ready for the Internet of Things, *Chemical Reviews* **2019**, *119*, 7996-8027.

(108) Kim, J.; Sempionatto, J. R.; Imani, S.; Hartel, M. C.; Barfidokht, A.; Tang, G.; Campbell, A. S.; Mercier, P. P.; Wang, J. Simultaneous Monitoring of Sweat and Interstitial Fluid Using a Single Wearable Biosensor Platform, *Advanced Science* **2018**, *5*, 1800880.

(109) Tai, L.-C.; Gao, W.; Chao, M.; Bariya, M.; Ngo, Q. P.; Shahpar, Z.; Nyein, H. Y. Y.; Park, H.; Sun, J.; Jung, Y.; Wu, E.; Fahad, H. M.; Lien, D.-H.; Ota, H.; Cho, G.; Javey, A. Methylxanthine Drug Monitoring with Wearable Sweat Sensors, *Advanced Materials* **2018**, *30*, 1707442.

(110) Leboulanger, B.; Guy, R. H.; Delgado-Charro, M. B. Reverse iontophoresis for non-invasive transdermal monitoring, *Physiological Measurement* **2004**, *25*, R35-R50.

(111) McCormick, C.; Heath, D.; Connolly, P. Towards blood free measurement of glucose and potassium in humans using reverse iontophoresis, *Sensors and Actuators B: Chemical* **2012**, *166-167*, 593-600.

(112) Sieg, A.; Guy, R. H.; Delgado-Charro, M. B. Simultaneous extraction of urea and glucose by reverse iontophoresis in vivo, *Pharmaceutical Research* **2004**, *21*, 1805-1810.

(113) Gualandi, I.; Marzocchi, M.; Achilli, A.; Cavedale, D.; Bonfiglio, A.; Fraboni, B. Textile Organic Electrochemical Transistors as a Platform for Wearable Biosensors, *Scientific Reports* **2016**, *6*, 33637.

(114) Karpova, E. V.; Shcherbacheva, E. V.; Galushin, A. A.; Vokhmyanina, D. V.; Karyakina, E. E.; Karyakin, A. A. Noninvasive Diabetes Monitoring through Continuous Analysis of Sweat Using Flow-Through Glucose Biosensor, *Analytical Chemistry* **2019**, *91*, 3778-3783.

(115) Wang, S.; Wu, Y.; Gu, Y.; Li, T.; Luo, H.; Li, L. H.; Bai, Y.; Li, L.; Liu, L.; Cao, Y.; Ding, H.; Zhang, T. Wearable Sweatband Sensor Platform Based on Gold

Nanodendrite Array as Efficient Solid Contact of Ion-Selective Electrode, *Analytical Chemistry* **2017**, *89*, 10224-10231.

(116) Wang, L.; Wang, L.; Zhang, Y.; Pan, J.; Li, S.; Sun, X.; Zhang, B.; Peng, H. Weaving Sensing Fibers into Electrochemical Fabric for Real-Time Health Monitoring, *Advanced Functional Materials* **2018**, *28*, 1804456.

(117) Toi, P. T.; Trung, T. Q.; Dang, T. M. L.; Bae, C. W.; Lee, N.-E. Highly Electrocatalytic, Durable, and Stretchable Nanohybrid Fiber for On-body Sweat Glucose Detection, *ACS Applied Materials & Interfaces* **2019**.

(118) Choi, J.; Bandodkar, A. J.; Reeder, J. T.; Ray, T. R.; Turnquist, A.; Kim, S. B.; Nyberg, N.; Hourlier-Fargette, A.; Model, J. B.; Aranyosi, A. J.; Xu, S.; Ghaffari, R.; Rogers, J. A. Soft, Skin-Integrated Multifunctional Microfluidic Systems for Accurate Colorimetric Analysis of Sweat Biomarkers and Temperature, *ACS Sensors* **2019**, *4*, 379-388.

(119) Sekar, M.; Pandiaraj, M.; Bhansali, S.; Ponpandian, N.; Viswanathan, C. Carbon fiber based electrochemical sensor for sweat cortisol measurement, *Scientific Reports* **2019**, *9*, 403.

(120) Caliò, A.; Dardano, P.; Di Palma, V.; Bevilacqua, M. F.; Di Matteo, A.; Iuele, H.; De Stefano, L. Polymeric microneedles based enzymatic electrodes for electrochemical biosensing of glucose and lactic acid, *Sensors and Actuators B: Chemical* **2016**, *236*, 343-349.

(121) Lee, S. J.; Yoon, H. S.; Xuan, X.; Park, J. Y.; Paik, S.-J.; Allen, M. G. A patch type non-enzymatic biosensor based on 3D SUS micro-needle electrode array for minimally invasive continuous glucose monitoring, *Sensors and Actuators B: Chemical* **2016**, *222*, 1144-1151.

(122) Mohan, A. M. V.; Windmiller, J. R.; Mishra, R. K.; Wang, J. Continuous minimally-invasive alcohol monitoring using microneedle sensor arrays, *Biosensors and Bioelectronics* **2017**, *91*, 574-579.

(123) Venugopal, M.; Arya, S. K.; Chornokur, G.; Bhansali, S. A realtime and continuous assessment of cortisol in ISF using electrochemical impedance spectroscopy, *Sensors and Actuators A: Physical* **2011**, *172*, 154-160.

(124) Muller, D. A.; Corrie, S. R.; Coffey, J.; Young, P. R.; Kendall, M. A. Surface modified microprojection arrays for the selective extraction of the dengue virus NS1 protein as a marker for disease, *Analytical Chemistry* **2012**, *84*, 3262-3268.

(125) Munnikes, R. J.; Muis, C.; Boersma, M.; Heijmans-Antonissen, C.; Zijlstra, F. J.; Huygen, F. J. Intermediate stage complex regional pain syndrome type 1 is unrelated to proinflammatory cytokines, *Mediators of Inflammation* **2005**, *2005*, 366-372.

(126) Kool, J.; Reubsaet, L.; Wesseldijk, F.; Maravilha, R. T.; Pinkse, M. W.; D'Santos, C. S.; van Hilten, J. J.; Zijlstra, F. J.; Heck, A. J. Suction blister fluid as potential body fluid for biomarker proteins, *Proteomics* **2007**, *7*, 3638-3650.

(127) Zhang, J.; Hao, N.; Liu, W.; Lu, M.; Sun, L.; Chen, N.; Wu, M.; Zhao, X.; Xing, B.; Sun, W.; He, F. In-depth proteomic analysis of tissue interstitial fluid for hepatocellular carcinoma serum biomarker discovery, *British Journal Of Cancer* **2017**, *117*, 1676-1684.

(128) Bobko, A. A.; Eubank, T. D.; Driesschaert, B.; Dhimitruka, I.; Evans, J.; Mohammad, R.; Tchekneva, E. E.; Dikov, M. M.; Khramtsov, V. V. Interstitial Inorganic Phosphate as a Tumor Microenvironment Marker for Tumor Progression, *Scientific Reports* **2017**, *7*, 41233.

(129) Ng, K. W.; Lau, W. M.; Williams, A. C. Towards pain-free diagnosis of skin diseases through multiplexed microneedles: biomarker extraction and detection using

a highly sensitive blotting method, *Drug Delivery and Translational Research* **2015**, *5*, 387-396.

(130) Larrañeta, E.; Lutton, R. E. M.; Woolfson, A. D.; Donnelly, R. F. Microneedle arrays as transdermal and intradermal drug delivery systems: Materials science, manufacture and commercial development, *Materials Science and Engineering: R: Reports* **2016**, *104*, 1-32.

(131) Alkilani, A. Z.; McCrudden, M. T. C.; Donnelly, R. F. Transdermal Drug Delivery: Innovative Pharmaceutical Developments Based on Disruption of the Barrier Properties of the stratum corneum, *Pharmaceutics* **2015**, *7*, 438-470.

(132) Quinn, H. L.; Kearney, M. C.; Courtenay, A. J.; McCrudden, M. T.; Donnelly, R. F. The role of microneedles for drug and vaccine delivery, *Expert Opinion on Drug Delivery* **2014**, *11*, 1769-1780.

(133) Yang, H.-W.; Ye, L.; Guo, X. D.; Yang, C.; Compans, R. W.; Prausnitz, M. R. Ebola Vaccination Using a DNA Vaccine Coated on PLGA-PLL/γPGA Nanoparticles Administered Using a Microneedle Patch, *Advanced Healthcare Materials* **2017**, *6*, 1600750.

(134) Seeni, R. Z.; Yu, X.; Chang, H.; Chen, P.; Liu, L.; Xu, C. Iron Oxide Nanoparticle-Powered Micro-Optical Coherence Tomography for in Situ Imaging the Penetration and Swelling of Polymeric Microneedles in the Skin, *ACS Applied Materials & Interfaces* **2017**, *9*, 20340-20347.

(135) Justin, R.; Román, S.; Chen, D.; Tao, K.; Geng, X.; Grant, R. T.; MacNeil, S.; Sun, K.; Chen, B. Biodegradable and conductive chitosan–graphene quantum dot nanocomposite microneedles for delivery of both small and large molecular weight therapeutics, *RSC Advances* **2015**, *5*, 51934-51946.

(136) Xu, B.; Cao, Q.; Zhang, Y.; Yu, W.; Zhu, J.; Liu, D.; Jiang, G. Microneedles Integrated with ZnO Quantum-Dot-Capped Mesoporous Bioactive Glasses for Glucose-Mediated Insulin Delivery, *ACS Biomaterials Science & Engineering* **2018**, *4*, 2473-2483.

(137) Larraneta, E.; McCrudden, M. T.; Courtenay, A. J.; Donnelly, R. F. Microneedles: A New Frontier in Nanomedicine Delivery, *Pharmaceutical Research* **2016**, *33*, 1055-1073.

(138) Henry, S.; McAllister, D. V.; Allen, M. G.; Prausnitz, M. R. Microfabricated microneedles: a novel approach to transdermal drug delivery, *Journal of Pharmaceutical Sciences* **1998**, *87*, 922-925.

(139) Gardeniers, H. J. G. E.; Luttge, R.; Berenschot, E. J. W.; Boer, M. J. d.; Yeshurun, S. Y.; Hefetz, M.; Oever, R. v. t.; Berg, A. v. d. Silicon micromachined hollow microneedles for transdermal liquid transport, *Journal of Microelectromechanical Systems* **2003**, *12*, 855-862.

(140) Indermun, S.; Luttge, R.; Choonara, Y. E.; Kumar, P.; du Toit, L. C.; Modi, G.; Pillay, V. Current advances in the fabrication of microneedles for transdermal delivery, *Journal of Controlled Release* **2014**, *185*, 130-138.

(141) Hopcroft, M. A.; Nix, W. D.; Kenny, T. W. What is the Young's Modulus of Silicon?, *Journal of Microelectromechanical Systems* **2010**, *19*, 229-238.

(142) Gao, J.; Huang, W.; Chen, Z.; Yi, C.; Jiang, L. Simultaneous detection of glucose, uric acid and cholesterol using flexible microneedle electrode array-based biosensor and multi-channel portable electrochemical analyzer, *Sensors and Actuators B: Chemical* **2019**, *287*, 102-110.

(143) Kolluru, C.; Gupta, R.; Jiang, Q.; Williams, M.; Gholami Derami, H.; Cao, S.; Noel, R. K.; Singamaneni, S.; Prausnitz, M. R. Plasmonic Paper Microneedle Patch for On-Patch Detection of Molecules in Dermal Interstitial Fluid, *ACS Sensors* **2019**.

(144) Yoon, Y.; Lee, G. S.; Yoo, K.; Lee, J. B. Fabrication of a microneedle/CNT hierarchical micro/nano surface electrochemical sensor and its in-vitro glucose sensing characterization, *Sensors* **2013**, *13*, 16672-16681.

(145) Miller, P. R.; Xiao, X.; Brener, I.; Burckel, D. B.; Narayan, R.; Polsky, R. Microneedle-Based Transdermal Sensor for On-Chip Potentiometric Determination of K+, *Advanced Healthcare Materials* **2014**, *3*, 876-881.

(146) Windmiller, J. R.; Valdés-Ramírez, G.; Zhou, N.; Zhou, M.; Miller, P. R.; Jin, C.; Brozik, S. M.; Polsky, R.; Katz, E.; Narayan, R.; Wang, J. Bicomponent Microneedle Array Biosensor for Minimally-Invasive Glutamate Monitoring, *Electroanalysis* **2011**, *23*, 2302-2309.

(147) Skaria, E.; Patel, B. A.; Flint, M. S.; Ng, K. W. Poly(lactic acid)/Carbon Nanotube Composite Microneedle Arrays for Dermal Biosensing, *Analytical Chemistry* **2019**, *91*, 4436-4443.

(148) Jin, Q.; Chen, H.-J.; Li, X.; Huang, X.; Wu, Q.; He, G.; Hang, T.; Yang, C.; Jiang, Z.; Li, E.; Zhang, A.; Lin, Z.; Liu, F.; Xie, X. Reduced Graphene Oxide Nanohybrid–Assembled Microneedles as Mini-Invasive Electrodes for Real-Time Transdermal Biosensing, *Small* **2019**, *15*, 1804298.

(149) Ranamukhaarachchi, S. A.; Padeste, C.; Dübner, M.; Häfeli, U. O.; Stoeber, B.; Cadarso, V. J. Integrated hollow microneedle-optofluidic biosensor for therapeutic drug monitoring in sub-nanoliter volumes, *Scientific Reports* **2016**, *6*, 29075.

(150) Jina, A.; Tierney, M. J.; Tamada, J. A.; McGill, S.; Desai, S.; Chua, B.; Chang, A.; Christiansen, M. Design, development, and evaluation of a novel microneedle

array-based continuous glucose monitor, *Journal of Diabetes Science and Technology* **2014**, *8*, 483-487.

(151) Chua, B.; Desai, S. P.; Tierney, M. J.; Tamada, J. A.; Jina, A. N. Effect of microneedles shape on skin penetration and minimally invasive continuous glucose monitoring in vivo, *Sensors and Actuators A: Physical* **2013**, *203*, 373-381.

(152) Strambini, L. M.; Longo, A.; Scarano, S.; Prescimone, T.; Palchetti, I.; Minunni, M.; Giannessi, D.; Barillaro, G. Self-powered microneedle-based biosensors for pain-free high-accuracy measurement of glycaemia in interstitial fluid, *Biosensors and Bioelectronics* **2015**, *66*, 162-168.

(153) McConville, A.; Hegarty, C.; Davis, J. Mini-Review: Assessing the Potential Impact of Microneedle Technologies on Home Healthcare Applications, *Medicines* **2018**, *5*.

(154) Puneet, K.; Kevin, L.; Joel, A. S.; Shekhar, B. Sharpening of hollow silicon microneedles to reduce skin penetration force, *Journal of Micromechanics and Microengineering* **2010**, *20*, 045011.

(155) Kochhar, J. S.; Quek, T. C.; Soon, W. J.; Choi, J.; Zou, S.; Kang, L. Effect of microneedle geometry and supporting substrate on microneedle array penetration into skin, *Journal of Pharmaceutical Sciences* **2013**, *102*, 4100-4108.

(156) Bhargav, A.; Muller, D. A.; Kendall, M. A.; Corrie, S. R. Surface modifications of microprojection arrays for improved biomarker capture in the skin of live mice, *ACS Applied Materials & Interfaces* **2012**, *4*, 2483-2489.

(157) Coffey, J. W.; Corrie, S. R.; Kendall, M. A. F. Rapid and selective sampling of IgG from skin in less than 1 min using a high surface area wearable immunoassay patch, *Biomaterials* **2018**, *170*, 49-57.

(158) Coffey, J. W.; Meliga, S. C.; Corrie, S. R.; Kendall, M. A. F. Dynamic application of microprojection arrays to skin induces circulating protein extravasation for enhanced biomarker capture and detection, *Biomaterials* **2016**, *84*, 130-143.

(159) Yeow, B.; Coffey, J. W.; Muller, D. A.; Grondahl, L.; Kendall, M. A.; Corrie, S. R. Surface modification and characterization of polycarbonate microdevices for capture of circulating biomarkers, both in vitro and in vivo, *Analytical Chemistry* **2013**, *85*, 10196-10204.

(160) Coffey, J. W.; Corrie, S. R.; Kendall, M. A. Early circulating biomarker detection using a wearable microprojection array skin patch, *Biomaterials* **2013**, *34*, 9572-9583.

(161) Lee, K. T.; Muller, D. A.; Coffey, J. W.; Robinson, K. J.; McCarthy, J. S.; Kendall, M. A.; Corrie, S. R. Capture of the circulating Plasmodium falciparum biomarker HRP2 in a multiplexed format, via a wearable skin patch, *Analytical Chemistry* **2014**, *86*, 10474-10483.

(162) Miller, P. R.; Taylor, R. M.; Tran, B. Q.; Boyd, G.; Glaros, T.; Chavez, V. H.; Krishnakumar, R.; Sinha, A.; Poorey, K.; Williams, K. P.; Branda, S. S.; Baca, J. T.; Polsky, R. Extraction and biomolecular analysis of dermal interstitial fluid collected with hollow microneedles, *Communications Biology* **2018**, *1*, 173.

(163) Ciui, B.; Martin, A.; Mishra, R. K.; Brunetti, B.; Nakagawa, T.; Dawkins, T. J.; Lyu, M.; Cristea, C.; Sandulescu, R.; Wang, J. Wearable Wireless Tyrosinase Bandage and Microneedle Sensors: Toward Melanoma Screening, *Advanced Healthcare Materials* **2018**, *7*, e1701264.

(164) Boyle, J. L.; Haupt, H. M.; Stern, J. B.; Multhaupt, H. A. Tyrosinase expression in malignant melanoma, desmoplastic melanoma, and peripheral nerve tumors, *Archives of Pathology & Laboratory Medicine* **2002**, *126*, 816-822.

(165) Yan, X.; Li, H.; Zheng, W.; Su, X. Visual and fluorescent detection of tyrosinase activity by using a dual-emission ratiometric fluorescence probe, *Analytical Chemistry* **2015**, *87*, 8904-8909.

(166) Bollella, P.; Sharma, S.; Cass, A. E. G.; Antiochia, R. Microneedle-based biosensor for minimally-invasive lactate detection, *Biosensors and Bioelectronics* **2019**, *123*, 152-159.

(167) Mukerjee, E. V.; Collins, S. D.; Isseroff, R. R.; Smith, R. L. Microneedle array for transdermal biological fluid extraction and in situ analysis, *Sensors and Actuators A: Physical* **2004**, *114*, 267-275.

(168) Chang, H.; Zheng, M.; Yu, X.; Than, A.; Seeni, R. Z.; Kang, R.; Tian, J.; Khanh, D. P.; Liu, L.; Chen, P.; Xu, C. A Swellable Microneedle Patch to Rapidly Extract Skin Interstitial Fluid for Timely Metabolic Analysis, *Advanced Materials* **2017**, *29*, 1702243.

(169) Kolluru, C.; Williams, M.; Yeh, J. S.; Noel, R. K.; Knaack, J.; Prausnitz, M. R. Monitoring drug pharmacokinetics and immunologic biomarkers in dermal interstitial fluid using a microneedle patch, *Biomedical Microdevices* **2019**, *21*, 14.

(170) Chinnadayyala, S. R.; Park, I.; Cho, S. Nonenzymatic determination of glucose at near neutral pH values based on the use of nafion and platinum black coated microneedle electrode array, *Mikrochimica Acta* **2018**, *185*, 250.

(171) Invernale, M. A.; Tang, B. C.; York, R. L.; Le, L.; Hou, D. Y.; Anderson, D. G. Microneedle Electrodes Toward an Amperometric Glucose-Sensing Smart Patch, *Advanced Healthcare Materials* **2014**, *3*, 338-342.

(172) Windmiller, J. R.; Zhou, N.; Chuang, M.-C.; Valdes-Ramirez, G.; Santhosh, P.; Miller, P. R.; Narayan, R.; Wang, J. Microneedle array-based carbon paste amperometric sensors and biosensors, *Analyst* **2011**, *136*, 1846-1851.

(173) Harper, J. C.; Brozik, S. M.; Flemming, J. H.; McClain, J. L.; Polsky, R.; Raj, D.; Ten Eyck, G. A.; Wheeler, D. R.; Achyuthan, K. E. Fabrication and Testing of a Microneedles Sensor Array for p-Cresol Detection with Potential Biofuel Applications, *ACS Applied Materials & Interfaces* **2009**, *1*, 1591-1598.

(174) Senel, M.; Dervisevic, M.; Voelcker, N. H. Gold microneedles fabricated by casting of gold ink used for urea sensing, *Materials Letters* **2019**, *243*, 50-53.

(175) Kim, K. B.; Lee, W.-C.; Cho, C.-H.; Park, D.-S.; Cho, S. J.; Shim, Y.-B. Continuous glucose monitoring using a microneedle array sensor coupled with a wireless signal transmitter, *Sensors and Actuators B: Chemical* **2019**, *281*, 14-21.

(176) Mishra, R. K.; Vinu Mohan, A. M.; Soto, F.; Chrostowski, R.; Wang, J. A microneedle biosensor for minimally-invasive transdermal detection of nerve agents, *Analyst* **2017**, *142*, 918-924.

(177) Keum, D. H.; Jung, H. S.; Wang, T.; Shin, M. H.; Kim, Y. E.; Kim, K. H.; Ahn, G. O.; Hahn, S. K. Microneedle Biosensor for Real-Time Electrical Detection of Nitric Oxide for In Situ Cancer Diagnosis During Endomicroscopy, *Advanced Healthcare Materials* **2015**, *4*, 1153-1158.

(178) Veiseh, O.; Tang, B. C.; Whitehead, K. A.; Anderson, D. G.; Langer, R. Managing diabetes with nanomedicine: challenges and opportunities, *Nature Reviews Drug Discovery* **2014**, *14*, 45-57.

(179) Bobrowski, T.; Schuhmann, W. Long-term implantable glucose biosensors, *Current Opinion in Electrochemistry* **2018**, *10*, 112-119.

(180) Bailey, T. S.; Ahmann, A.; Brazg, R.; Christiansen, M.; Garg, S.; Watkins, E.; Welsh, J. B.; Lee, S. W. Accuracy and Acceptability of the 6-Day Enlite Continuous Subcutaneous Glucose Sensor, *Journal of Diabetes Technology and Therapeutics* **2014**, *16*, 277-283.

(181) Christiansen, M. P.; Garg, S. K.; Brazg, R.; Bode, B. W.; Bailey, T. S.; Slover, R. H.; Sullivan, A.; Huang, S.; Shin, J.; Lee, S. W.; Kaufman, F. R. Accuracy of a Fourth-Generation Subcutaneous Continuous Glucose Sensor, *Journal of Diabetes Technology and Therapeutics* **2017**, *19*, 446-456.

(182) Locke, A. K.; Cummins, B. M.; Abraham, A. A.; Coté, G. L. PEGylation of Concanavalin A to Improve Its Stability for an In Vivo Glucose Sensing Assay, *Analytical Chemistry* **2014**, *86*, 9091-9097.

(183) Hui, N.; Sun, X.; Niu, S.; Luo, X. PEGylated Polyaniline Nanofibers: Antifouling and Conducting Biomaterial for Electrochemical DNA Sensing, *ACS Applied Materials & Interfaces* **2017**, *9*, 2914-2923.

(184) Chou, Y.-N.; Sun, F.; Hung, H.-C.; Jain, P.; Sinclair, A.; Zhang, P.; Bai, T.; Chang, Y.; Wen, T.-C.; Yu, Q.; Jiang, S. Ultra-low fouling and high antibody loading zwitterionic hydrogel coatings for sensing and detection in complex media, *Acta Biomaterialia* **2016**, *40*, 31-37.

(185) Xie, X.; Doloff, J. C.; Yesilyurt, V.; Sadraei, A.; McGarrigle, J. J.; Omami, M.; Veiseh, O.; Farah, S.; Isa, D.; Ghani, S.; Joshi, I.; Vegas, A.; Li, J.; Wang, W.; Bader, A.; Tam, H. H.; Tao, J.; Chen, H.-j.; Yang, B.; Williamson, K. A., et al. Reduction of measurement noise in a continuous glucose monitor by coating the sensor with a zwitterionic polymer, *Nature Biomedical Engineering* **2018**, *2*, 894-906.

(186) Abidian, M. R.; Martin, D. C. Multifunctional Nanobiomaterials for Neural Interfaces, *Advanced Functional Materials* **2009**, *19*, 573-585.

(187) Wang, C.; Javadi, A.; Ghaffari, M.; Gong, S. A pH-sensitive molecularly imprinted nanospheres/hydrogel composite as a coating for implantable biosensors, *Biomaterials* **2010**, *31*, 4944-4951.

(188) Kastellorizios, M.; Papadimitrakopoulos, F.; Burgess, D. J. Prevention of foreign body reaction in a pre-clinical large animal model, *Journal of Controlled Release* **2015**, *202*, 101-107.

(189) Cha, K. H.; Wang, X.; Meyerhoff, M. E. Nitric oxide release for improving performance of implantable chemical sensors – A review, *Applied Materials Today* **2017**, *9*, 589-597.

(190) Soto, R. J.; Schofield, J. B.; Walter, S. E.; Malone-Povolny, M. J.; Schoenfisch, M. H. Design Considerations for Silica-Particle-Doped Nitric-Oxide-Releasing Polyurethane Glucose Biosensor Membranes, *ACS Sensors* **2017**, *2*, 140-150.

(191) Gu, B.; Papadimitrakopoulos, F.; Burgess, D. J. PLGA microsphere/PVA hydrogel coatings suppress the foreign body reaction for 6 months, *Journal of Controlled Release* **2018**, *289*, 35-43.

(192) Sieminski, A. L.; Gooch, K. J. Biomaterial–microvasculature interactions, *Biomaterials* **2000**, *21*, 2233-2241.

(193) Chen, D.; Wang, C.; Chen, W.; Chen, Y.; Zhang, J. X. J. PVDF-Nafion nanomembranes coated microneedles for in vivo transcutaneous implantable glucose sensing, *Biosensors and Bioelectronics* **2015**, *74*, 1047-1052.

(194) Gough, D. A.; Kumosa, L. S.; Routh, T. L.; Lin, J. T.; Lucisano, J. Y. Function of an Implanted Tissue Glucose Sensor for More than 1 Year in Animals, *Science Translation Medicine* **2010**, *2*, 42ra53.

(195) Lucisano, J. Y.; Routh, T. L.; Lin, J. T.; Gough, D. A. Glucose Monitoring in Individuals With Diabetes Using a Long-Term Implanted Sensor/Telemetry System and Model, *IEEE Transactions on Biomedical Engineering* **2017**, *64*, 1982-1993.

(196) Barone, P. W.; Parker, R. S.; Strano, M. S. In Vivo Fluorescence Detection of Glucose Using a Single-Walled Carbon Nanotube Optical Sensor: Design,

Fluorophore Properties, Advantages, and Disadvantages, *Analytical Chemistry* **2005**, *77*, 7556-7562.

(197) Stuart, D. A.; Yuen, J. M.; Shah, N.; Lyandres, O.; Yonzon, C. R.; Glucksberg, M. R.; Walsh, J. T.; Van Duyne, R. P. In Vivo Glucose Measurement by Surface-Enhanced Raman Spectroscopy, *Analytical Chemistry* **2006**, *78*, 7211-7215.

(198) Yuen, J. M.; Shah, N. C.; Walsh, J. T.; Glucksberg, M. R.; Van Duyne, R. P. Transcutaneous Glucose Sensing by Surface-Enhanced Spatially Offset Raman Spectroscopy in a Rat Model, *Analytical Chemistry* **2010**, *82*, 8382-8385.

(199) Johari, P.; Pandey, H.; Jornet, J. M. In *Optical Diagnostics and Sensing XVIII: Toward Point-of-Care Diagnostics*; International Society for Optics and Photonics, 2018, p 105011C.

(200) Steiner, M.-S.; Duerkop, A.; Wolfbeis, O. S. Optical methods for sensing glucose, *Chemical Society Reviews* **2011**, *40*, 4805-4839.

(201) Ruckh, T. T.; Clark, H. A. Implantable Nanosensors: Toward Continuous Physiologic Monitoring, *Analytical Chemistry* **2014**, *86*, 1314-1323.

(202) Heo, Y. J.; Shibata, H.; Okitsu, T.; Kawanishi, T.; Takeuchi, S. Long-term in vivo glucose monitoring using fluorescent hydrogel fibers, *Proceedings of the National Academy of Sciences* **2011**, *108*, 13399-13403.

(203) Sun, K.; Yang, Y.; Zhou, H.; Yin, S.; Qin, W.; Yu, J.; Chiu, D. T.; Yuan, Z.; Zhang, X.; Wu, C. Ultrabright Polymer-Dot Transducer Enabled Wireless Glucose Monitoring via a Smartphone, *ACS Nano* **2018**, *12*, 5176-5184.

(204) Bornhoeft, R. L.; Biswas, A.; McShane, J. M. Composite Hydrogels with Engineered Microdomains for Optical Glucose Sensing at Low Oxygen Conditions, *Biosensors* **2017**, *7*, 8.

(205) Ballerstadt, R.; Evans, C.; Gowda, A.; McNichols, R. Fiber-Coupled Fluorescence Affinity Sensor for 3-Day in Vivo Glucose Sensing, *Journal of Diabetes Science and Technology* **2007**, *1*, 384-393.

(206) Lowry, T. M. Optical rotatory power, *Journal of Chemical Technology and Biotechnology* **1935**, *54*, 477-483.

(207) James, T. D.; Sandanayake, K. R. A. S.; Iguchi, R.; Shinkai, S. Novel Saccharide-Photoinduced Electron Transfer Sensors Based on the Interaction of Boronic Acid and Amine, *Journal of the American Chemical Society* **1995**, *117*, 8982-8987.

(208) James, T. D.; Sandanayake, K. R. A. S.; Shinkai, S. A Glucose-Selective Molecular Fluorescence Sensor, *Angewandte Chemie International Edition in English* **1994**, *33*, 2207-2209.

(209) James, T. D.; Samankumara Sandanayake, K. R. A.; Shinkai, S. Chiral discrimination of monosaccharides using a fluorescent molecular sensor, *Nature* **1995**, *374*, 345-347.

(210) Shibata, H.; Heo, Y. J.; Okitsu, T.; Matsunaga, Y.; Kawanishi, T.; Takeuchi, S. Injectable hydrogel microbeads for fluorescence-based in vivo continuous glucose monitoring, *Proceedings of the National Academy of Sciences* **2010**, *107*, 17894-17898.

(211) Zhang, X.; Gao, C.; Lü, S.; Duan, H.; Jing, N.; Dong, D.; Shi, C.; Liu, M. Anti-photobleaching flower-like microgels as optical nanobiosensors with high selectivity at physiological conditions for continuous glucose monitoring, *Journal of Materials Chemistry B* **2014**, *2*, 5452-5460.

(212) Yetisen, A. K.; Jiang, N.; Fallahi, A.; Montelongo, Y.; Ruiz-Esparza, G. U.; Tamayol, A.; Zhang, Y. S.; Mahmood, I.; Yang, S.-A.; Kim, K. S.; Butt, H.;

Khademhosseini, A.; Yun, S.-H. Glucose-Sensitive Hydrogel Optical Fibers Functionalized with Phenylboronic Acid, *Advanced Materials* **2017**, *29*, 1606380.

(213) Rong, G.; Corrie, S. R.; Clark, H. A. In Vivo Biosensing: Progress and Perspectives, *ACS Sensors* **2017**, *2*, 327-338.

(214) Tanne, J.; Schäfer, D.; Khalid, W.; Parak, W. J.; Lisdat, F. Light-Controlled Bioelectrochemical Sensor Based on CdSe/ZnS Quantum Dots, *Analytical Chemistry* **2011**, *83*, 7778-7785.

(215) Barone, P. W.; Baik, S.; Heller, D. A.; Strano, M. S. Near-infrared optical sensors based on single-walled carbon nanotubes, *Nature Materials* **2004**, *4*, 86-92.

(216) Barone, P. W.; Strano, M. S. Single Walled Carbon Nanotubes as Reporters for the Optical Detection of Glucose, *Journal of Diabetes Science and Technology* **2009**, *3*, 242-252.

(217) Yum, K.; McNicholas, T. P.; Mu, B.; Strano, M. S. Single-Walled Carbon Nanotube-Based Near-Infrared Optical Glucose Sensors toward In Vivo Continuous Glucose Monitoring, *Journal of Diabetes Science and Technology* **2013**, *7*, 72-87.

(218) Iverson, N. M.; Barone, P. W.; Shandell, M.; Trudel, L. J.; Sen, S.; Sen, F.; Ivanov, V.; Atolia, E.; Farias, E.; McNicholas, T. P.; Reuel, N.; Parry, N. M. A.; Wogan, G. N.; Strano, M. S. In vivo biosensing via tissue-localizable near-infrared-fluorescent single-walled carbon nanotubes, *Nature Nanotechnology* **2013**, *8*, 873-880.

(219) Phillips, E.; Penate-Medina, O.; Zanzonico, P. B.; Carvajal, R. D.; Mohan, P.; Ye, Y.; Humm, J.; Gönen, M.; Kalaigian, H.; Schöder, H.; Strauss, H. W.; Larson, S. M.; Wiesner, U.; Bradbury, M. S. Clinical translation of an ultrasmall inorganic optical-PET imaging nanoparticle probe, *Science Translation Medicine* **2014**, *6*, 260ra149.

(220) Low, S. P.; Voelcker, N. H.; Canham, L. T.; Williams, K. A. The biocompatibility of porous silicon in tissues of the eye, *Biomaterials* **2009**, *30*, 2873-2880.

(221) Gupta, B.; Mai, K.; Lowe, S. B.; Wakefield, D.; Di Girolamo, N.; Gaus, K.; Reece, P. J.; Gooding, J. J. Ultrasensitive and Specific Measurement of Protease Activity Using Functionalized Photonic Crystals, *Analytical Chemistry* **2015**, *87*, 9946-9953.

(222) Tong, W. Y.; Sweetman, M. J.; Marzouk, E. R.; Fraser, C.; Kuchel, T.; Voelcker, N. H. Towards a subcutaneous optical biosensor based on thermally hydrocarbonised porous silicon, *Biomaterials* **2016**, *74*, 217-230.

(223) Weiss, R.; Yegorchikov, Y.; Shusterman, A.; Raz, I. Noninvasive continuous glucose monitoring using photoacoustic technology-results from the first 62 subjects, *Diabetes Technology and Therapeutics* **2007**, *9*, 68-74.

(224) Kottmann, J.; Rey, J. M.; Sigrist, M. W. Mid-Infrared Photoacoustic Detection of Glucose in Human Skin: Towards Non-Invasive Diagnostics, *Sensors* **2016**, *16*.

(225) Sim, J. Y.; Ahn, C.-G.; Jeong, E.-J.; Kim, B. K. In vivo Microscopic Photoacoustic Spectroscopy for Non-Invasive Glucose Monitoring Invulnerable to Skin Secretion Products, *Scientific Reports* **2018**, *8*, 1059.

Chapter 3: Noninvasive Epidermal Glucose Monitoring in Sweat Using a Wearable Micropillar-Based Biosensing Patch

3.1 Introduction

Sweat is the skin fluid easiest to access which makes it an attractive biofluid for health assessments based on noninvasive monitoring devices. It is secreted by eccrine glands after neurotransmitter stimulation, mainly acetylcholine, which results in the release of Ca^{2+} followed by the flow of Na^{+} and Cl^{-} ions with water into the lumen and thus sweat generation.[1] Apart from Na^{+} and Cl^{-}, secreted sweat also contains different metabolites, peptides, proteins, and hormones [2,3] such as K^{+},[4,5] cortisol,[6] lactate,[7] and glucose,[8] which are useful biomarkers for diagnosis and health monitoring. Recently, wearable sensors for sweat analysis have received considerable attention due to their ability for non-invasive monitoring of specific analytes and their wide application in healthcare, fitness, and environmental monitoring.[9]

Despite the major advantages and many reported studies focusing on wearable sweat analysis, several key challenges have to be addressed. These include low sweat rates, changes in sweat composition, production rate during physical activity, evaporation of sweat sample, sample transfer, and contamination from skin. Other major challenges are relate to the biosensor design and its interaction with the skin. Complex phenomena occur at the biosensor-skin interface, and the biosensing platform should aim to protect the sensitive microenvironment of the working electrode.[1] For example, the loss of recognition elements from the electrode surface due to the friction between the skin and the sensing platform can result in impaired sensor response and inaccurate results. Different microfluidic devices have been developed to address the issues of sweat evaporation and low sweat rates,[2,9] but avoiding the damage of the working electrode microenvironment still remains a challenge. In order to address this challenge, in this study, a micropillar-based sensing

patch was developed with the ability to protect the sensing layer while being in contact with only sweat, and not the skin.

This chapter focuses on developing and optimizing a glucose sensing patch utilizing high-density micropillar array (MPA) for noninvasive monitoring of glucose levels in human sweat. The proposed glucose-sensing patch is composed of a three-electrode system, namely reference, counter, and working electrodes, all prepared using the micropillar arrays that have a density of 65,500 pillars/cm^2. The sensing patch exhibited excellent analytical performance with a linear range between 50 µM to 1.4 mM, detection limit of 26 µM, and sensitivity of 4.7 µA/mM. The sensor's performance is sufficient for the analysis of glucose in healthy individuals with glucose levels ranging from 36 to 60 µM, and in diabetic patients which can show glucose levels significantly higher than 60 µM.[1] Moreover, the glucose-sensing patch was tested in human sweat where glucose was successfully measured during 3 h period. The changes in glucose levels measured from human sweat correlate well with the changes in blood glucose levels obtained using a commercial glucometer.

3.2 Experimental Section

3.2.1 Materials

D-(+)-glucose, glucose oxidase (GOx) from Aspergillus Niger, chitosan low molecular weight, pyrrole, gold chloride ($HAuCl_4$), acetic acid, glutaraldehyde, potassium hexacyanoferrate (III) ($K_3Fe(CN)_6$), potassium hexacyanoferrate (II) trihydrate ($K_4[FeCN_6]\cdot 3H_2O$), uric acid, ascorbic acid, lactate, dopamine hydrochloride, iron (III) chloride ($FeCl_3$), potassium chloride (KCl), sodium chloride (NaCl), sodium sulfate (Na_2SO_4), calcium carbonate ($CaCO_3$), magnesium chloride ($MgCl_2$), sodium bicarbonate ($NaHCO_3$), sodium dihydrogen phosphate (NaH_2PO_4), and ammonium

hydroxide (NH_4OH) were purchased from Sigma Aldrich Chemical Co. Hydrochloric acid (HCl) and sulfuric acid (H_2SO_4) were purchased from J.T. Baker. All chemicals were of analytical grade and were used without further purification. Aqueous solutions were prepared using Milli Q water (18.2 MΩ·cm at 25 ^oC).

3.2.2 Fabrication and Modification of Micropillar Array-based Glucose Sensing Patch

Micropillars were fabricated by UV-photolithography and deep reactive ion etching (DRIE) (Plasmalab 100 ICP380) of p-type crystalline Si (Figure 3.1a). Prior to the pre-patterning of the Si wafer using a chromium mask and a positive photoresist (AZ® 4562, MicroChemicals), the Si wafer was treated with hexamethyldisilazane (HMDS, MicroChemicals) as chemical adhesion promoter to increase hydrophobicity and adhesion of the subsequent AZ® 4562 film. HMDS was spin-coated on the Si wafer with a maximum speed of 3000 rpm for 30 s. Later on, a similar process was repeated using AZ® 4562 positive photoresist which was soft-baked at 110°C for 90 s. In the next step, Si wafer was exposed to 150 mJ/cm^2 dose of ultraviolet radiation under a patterned mask which consists of an array of circles of 12 µm diameter and 40 µm lattice constant in hexagonal arrangement. In the last step, the exposed photoresist was developed for 30 s using AZ® 400K (MicroChemicals) developer solution consisting of 3:2 developer/water ratio after which the developed wafers were rinsed with dH_2O and dried under N_2 gas. Once photolithography was finalized, Si wafers were etched via DRIE using a Bosch process which alternates etching with SF_6 and passivation with C_4F_8 cycles to obtain cylindrical microstructures. In total, the Bosch process consisting of 90 cycles was performed during which helium pressure was set at 10 Torr and table temperature was set at 15℃. At the end, the remaining

photoresist was removed by rinsing the Si wafer with isopropanol, ethanol, and dH_2O ready to use for the patch fabrication.

The wearable glucose-sensing patch is designed as a three-electrode system composed of counter (C), reference (R), and working (W) electrodes all made of MPA. The Si-MPA substrate was attached to a 3D printed holder (Figure 3.1b) made in the Objet Eden 260V 3D printing system using Full Cure 720 (FC720) high-resolution printing material. Before attachment of Si-MPA substrate, the 3D printed holder was cleaned with aqueous 20% (w/v) NaOH solution in order to remove remaining printing residues of supporting material used during the printing process. The electrodes were cleaned with O_2 plasma (180 W) (IoN Wave 10 Plasma Asher) for 1 min and then a conformal Au conductive layer was deposited on the electrode surface using an AC/DC sputtering system (Intlvac Nanochrome AC/DC). The deposition process was composed of two consequent steps; deposition of 15 nm of Cr (AC, 300W) which served as an adhesion layer, and then deposition of 200 nm Au layer (DC, 100V). Both processes were performed under vacuum at 1.95 mTorr and with sample rotation at 100 rpm. The resulting electrodes (Figure 3.1b), referred as Au-Si-MPA, were undertaken a sticky tape test in order to assess the adhesion of the Au layer to the MPA. This fabrication process was employed in the production of all three electrodes, and each electrode is as shown in Figure 3.1d. Prior to assembling electrodes into a single three-electrode patch, R electrode was coated with AgCl ink and dried at 60^o for 30-40 min and W electrode was modified as described below for the immobilization of GOx.

Modification of the W electrode (Figure 3.1c) involved the electrodeposition of Prussian Blue (PB) on the Au-Si-MPA electrode surface. The electrodeposition process was performed in a solution composed of 2.5 mM $FeCl_3$, 2.5 mM $K_3Fe(CN)_6$,

0.1 M KCl, and 0.1 M HCl using cyclic voltammetry (CV) by scanning the applied potential between -0.50 and 0.65 V at 50 mV/s. Then the electrode was rinsed with distilled water (dH_2O) and dried at room temperature. Later on, the surface of the Au-Si-MPA electrode was modified with a chitosan-Au nanoparticles (Ch-AuNP) nanocomposite, which was prepared following the procedure reported by Dervisevic et al.[10] Briefly, the nanocomposite was prepared using chitosan, pyrrole, and $HAuCl_4$ solutions in v/v ratio of 5:1:1, respectively. First, 1% chitosan solution prepared in 1% of acetic acid was mixed with pyrrole and then 1% (w/v) $HAuCl_4$ solution. During the mixing, the appearance of a dark reddish-brown color was observed due to the formation of AuNPs. Ch-AuNP mixture was vortexed and sonicated for 30 min in order to disperse AuNPs and then drop-casted onto the electrode surface and dried for 15 min at 60^oC. Next, the electrode was immersed in 2.5% glutaraldehyde solution for 45 min after which it was rinsed with dH_2O. Then, it was incubated into 20 mg/mL GOx solution prepared in 10 mM PBS and kept overnight at 4^oC. Prior to use, the electrode was again thoroughly rinsed with 10 mM PBS. The wearable patch was prepared by integrating the W, C, and R electrodes in a three-electrode system supported by a bandage, as shown in Figure 3.1c and 3.1e.

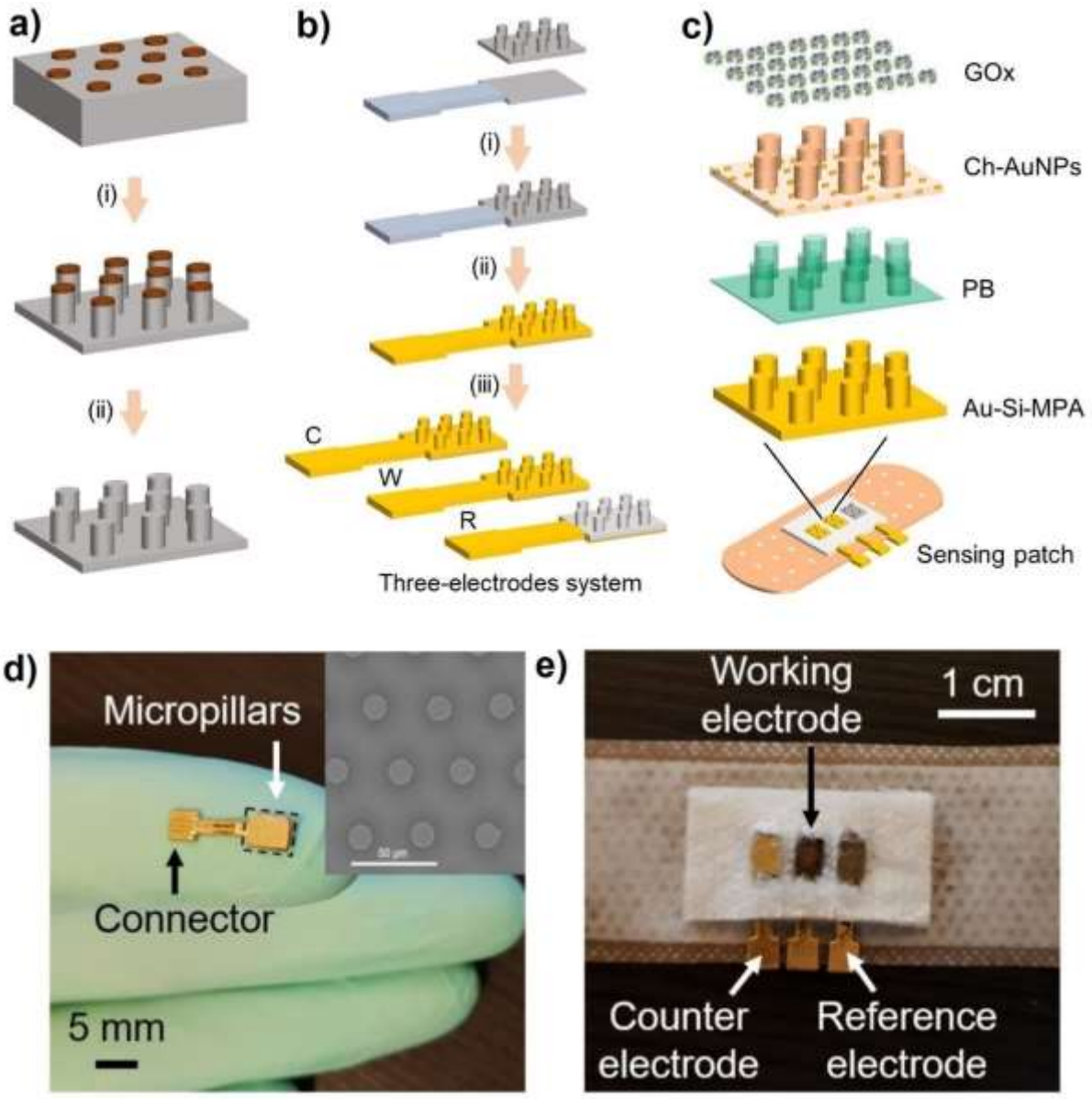

Figure 3.1: Schematic illustration of **(a)** Si-MPA fabrication process; i) pre-patterning of the Si wafer using a chromium mask and a positive photoresist and ii) deep reactive ion etching of Si, **(b)** Au-Si-MPA electrode fabrication process; i) attaching MPA to 3D printed holder, ii) deposition of Au layer on electrode surface, iii) three-electrode system patch, and **(c)** surface modification procedure of Au-Si-MPA electrode. Photograph of **d)** single Au-Si-MPA electrode (inset: SEM micrographs of MPA) and **e)** three-electrode system wearable patch.

3.2.3 Electrochemical Analysis using MPA Sensing Patch

Electrochemical measurements were performed using a CHI 650E (CH Instruments, USA) electrochemical analyzer. Electrochemical characterization was conducted using CV and electrochemical impedance spectroscopy (EIS) methods recorded in a solution containing 5 mM $K_4[Fe(CN)_6]/K_3[Fe(CN)_6]$ (1:1 ratio) in 0.1 M KCl. The analytical performance of the MPA sensing patch was studied via the amperometry method recorded in both 0.1 M PBS and artificial sweat composed of KCl, NaCl, $CaCO_3$, $MgCl_2$, $NaHCO_3$, NaH_2PO_4, Na_2SO_4 and NH_4OH. Monitoring of glucose levels from human sweat was conducted according to the National Health and Medical Research Council (NHMRC) guidelines under the approval of the Monash University Human Research Ethics Committee (project ID: 26495). Glucose levels in blood were measured using commercial glucometer and test strips (Accu-Chek Active, Roche), whereas glucose levels in sweat were measured using our MPA sensing patch, at different time intervals. Glucose levels were monitored 30 min before finishing an 8-hour fasting period, and after 30, 60, 90, and 120 min of having a meal composed of carbohydrate, protein, and fat. Prior to all measurements, the individual was subjected to moderate physical exercise for approximately 15 min in order to increase perspiration.

3.3 Results and Discussion

3.3.1 Characterization of MPA Sensing Patch

Morphological characterization of Au-Si-MPA electrodes and Ch-AuNPs was performed by means of field-emission gun scanning electron microscope (FEG-SEM) (FEI NovaNano SEM 430). Figure 3.2 shows SEM micrographs of side view (Figure 3.2a), cross-section (Figure 3.2b), and top view (Figure 3.2c) of Au-Si-MPA electrode. MPA has a hexagonal arrangement, composed of micropillars with 12 μm diameter, ~22 μm height, and 40 μm center-to-center distance between two adjacent pillars. Figures 3.2d and 3.2e show SEM micrographs of Ch and Ch-AuNPs, respectively, coated MPA. Ch produced a smooth surface as expected from the literature.[11] Conversely, in situ chemical synthesis of Ch-AuNPs resulted in a significant change of film morphology with visibly increased roughness and porosity of the film.

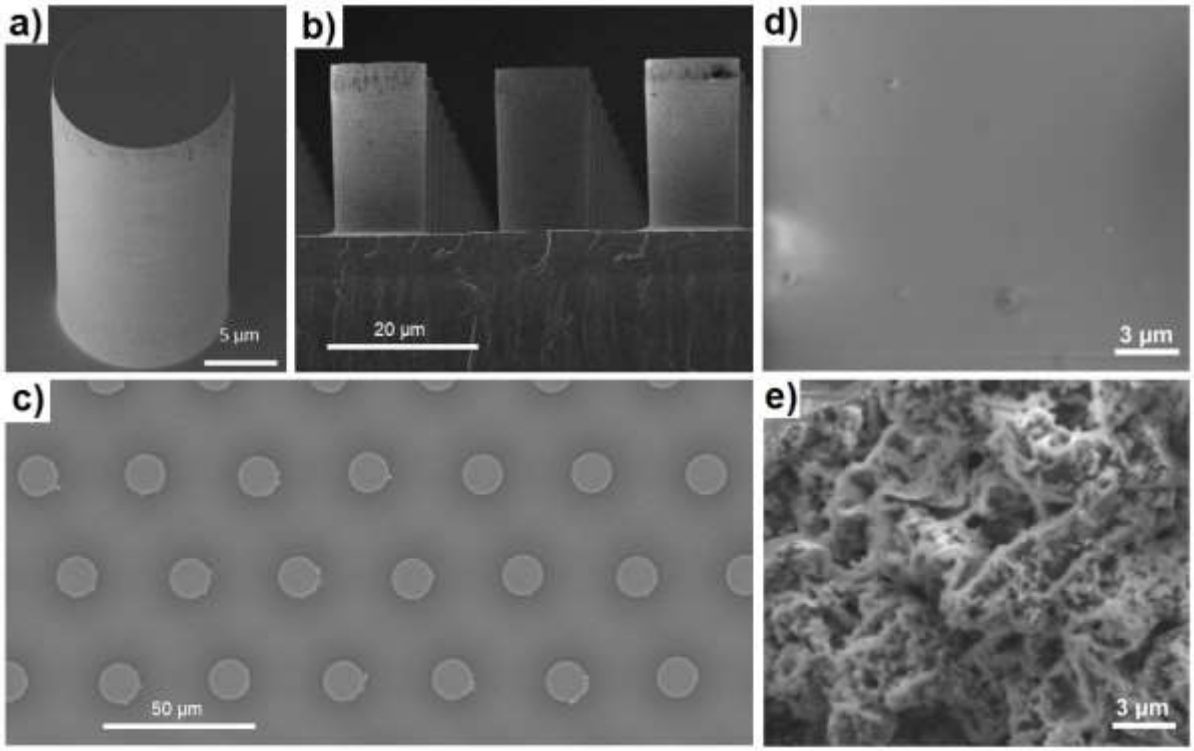

Figure 3.2: SEM micrographs of MPA **a)** side view, **b)** cross section, **c)** top view, and of **d)** Ch and **e)** Ch-AuNP nanocomposite on top of MPA.

Prior to chemical modification, the surface of Au-Si-MPA was electrochemically cleaned by scanning CV in 0.5 M H_2SO_4 solution. This step is commonly applied in cleaning process of Au surfaces; however, it can also be used to determine the active surface area.[12] The active surface area was quantified by dividing the charge of the reduction peak of the Au-coated electrodes by the charge per microscopic unit area of Au which is 390 ± 10 µC/cm^2.[13,14] Figure 3.3a shows the comparison between CV plots of a MPA-based electrode and a planar Au-Si electrode that does not contain any MPA structures, recorded in H_2SO_4 solution. The oxidation of Au layer and the reduction of oxidized Au can be observed at 1.0 – 1.2 V and 0.7 V, respectively. MPA-based electrodes show higher reduction peak when compared to the planar electrodes and that is attributed to the increased Au surface area provided by the presence of the

vertical MPA. The active surface area of both types of electrodes with geometric area of 0.15 cm^2 is determined by the aforementioned approach, obtaining 0.97 ± 0.60 cm^2 and 0.8 ± 0.4 cm^2 for Au-Si-MPA and planar Au-Si electrodes, respectively.

Further electrochemical characterization was performed in order to monitor the surface modification of the Au-Si-MPA electrode. The stepwise functionalization process comprised PB deposition, drop-casting of the Ch-AuNP nanocomposite, and immobilization of GOx. Figure 3.3b displays a typical CV obtained during the electrochemical deposition of the PB layer on the Au-Si-MPA electrode surface. During electrodeposition of PB, the oxidation and reduction peaks centered at 0.15 and 0.10 V, respectively, increased with the number of sweeping scans in the potential between -0.50 and 0.65 V at 50 mV/s scan rate. The continuous increase in the current indicates the accumulation of PB on the Au-coated MPA.[15] Additionally, Figure 3.3c shows a comparison of the CV characteristics between planar Au-Si and Au-Si-MPA electrodes, as well as the step-by-step modification of the Au-Si-MPA electrode surface. CV recorded in 5 mM $K_4[Fe(CN)_6]/K_3[Fe(CN)_6]$ (1:1 ratio) in 0.1 M KCl solution illustrates the variation of redox peaks after each modification step. The oxidation peak intensity of bare planar Au-Si and Au-Si-MPA electrodes was 0.39 ± 0.2 mA and 0.68 ± 0.3 mA, respectively. This increase in current intensity can be attributed to the larger active surface area of Au-Si-MPA electrode. Modification of MPA surface with Ch resulted in decreased current peak to 0.29 ± 0.24 mA which is expected since Ch is a nonconductive material,[11] whereas the incorporation of electrically conductive AuNPs resulted in the increase of the redox peak current to 0.56 ± 0.28 mA. After the immobilization of GOx on the Au-Si-MPA electrode surface, the current peak intensity decreased to 0.35 ± 0.21 mA due to the insulation effect of the enzyme immobilized on the surface. These results were comparable to those

found by EIS analysis. EIS measurements were recorded over a frequency range between 1 Hz and 10 kHz in 5 mM $K_4[Fe(CN)_6]/K_3[Fe(CN)_6]$ (1:1 ratio) in 0.1 M KCl solution. Figure 3.3d represents the Nyquist plots corresponding to the EIS measurements obtained using planar Au-Si and MPA electrodes, and MPA electrode modified with Ch, Ch-AuNP, and GOx (MPA/PB/Ch-AuNP/GOx). According to the EIS results, the charge transfer resistance (Rct) was 40 ± 8 kΩ and 25 ± 5 kΩ for planar Au-Si and Au-Si-MPA electrodes, respectively. After the modification of Au-Si-MPA electrode with Ch, the Rct increased to 100 ± 21 kΩ, the incorporation of AuNP decreased the Rct to 59 ± 13 kΩ, and after the immobilization of GOx, the Rct increased to 164 ± 26 kΩ. EIS results are in good agreement with CV results showing that the Ch-AuNP nanocomposite has a smaller Rct which is representative of a more effective charge transfer resistance and thus a favorable property for electrochemical biosensors.

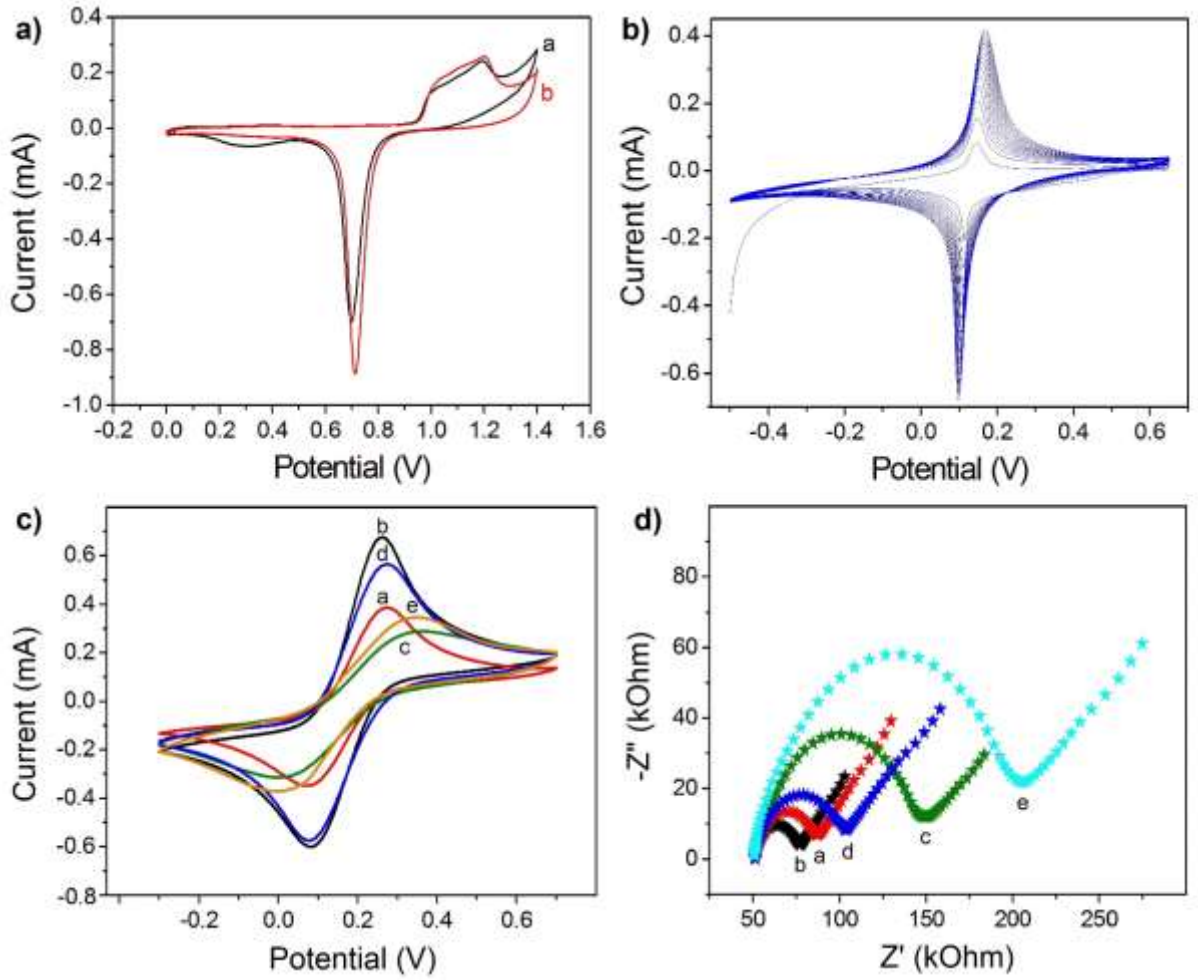

Figure 3.3: CV plots **a)** of planar Au-Si (a) and MPA (b) electrodes recorded in 0.5 M H_2SO_4 solution, and **b)** recorded during deposition of PB on MPA electrode surface. **c)** CV and **d)** EIS of planar Au-Si (a), MPA (b), MPA/Ch (c), MPA/PB/Ch-AuNP (d), and MPA/PB/Ch-AuNP/GOx (e) recorded in 5 mM of $K_4Fe(CN)_6/K_3Fe(CN)_6$ (1:1 ratio) in 0.1 M KCl.

3.3.2 In Vitro Characterization of MPA Sensing patch

The detection of glucose is based on the electrocatalytic reduction of H_2O_2, generated from the reaction between GOx and glucose through the reaction sequence illustrated in Figure 3.4a, at the PB-modified surface. Increase in glucose concentration in PBS solution increases the current change recorded by amperometry. Figure 3.4b illustrates the amperometric response of the MPA sensing patch to consecutive additions of different concentrations of glucose recorded in 0.1 M PBS under an applied potential of -0.15 V. The biosensor exhibits a highly linear response to glucose within the 50 µM to 1.35 mM range, with the regression equation of I = 8.34 [glucose] – 0.1033 (correlation coefficient of 0.9989), as represented in Figure 3.4c. From this analysis, the sensitivity was found to be 8.34 µA/mM and the limit of detection 22 µM. The selectivity of the MPA glucose patch against other potential interfering species was tested. Figure 3.5a shows the amperometric plot of MPA sensing patch in the presence of 100 µM of glucose, ascorbic acid, uric acid, lactate, and dopamine, from where no significant effect on the current change was observed (inset of Figure 3.5a), demonstrating that the patch can be used in matrices containing commonly interfering species.

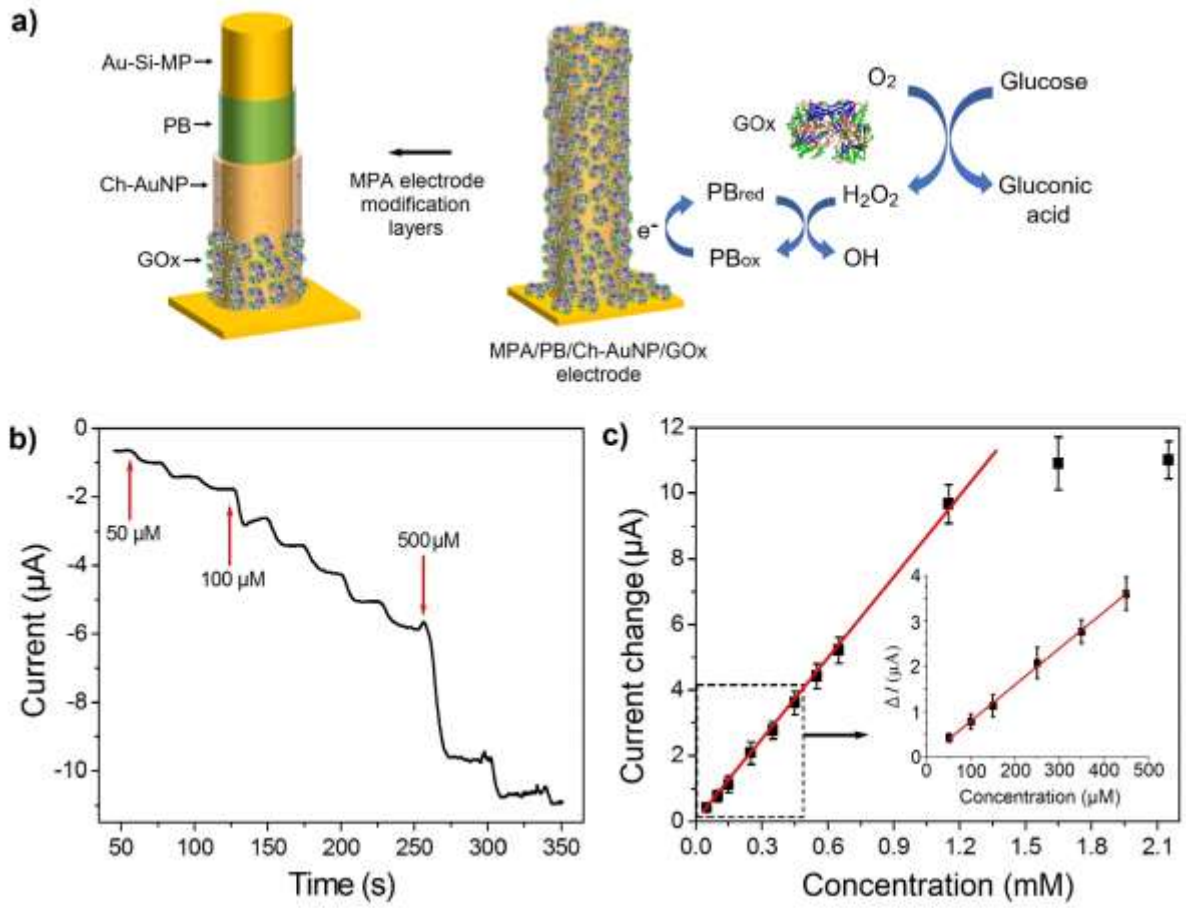

Figure 3.4: a) Schematic illustration of MPA electrode modification layers and of glucose detection mechanism via MPA sensing patch. **b)** Amperometric response of MPA sensing patch to the consecutive additions of glucose (50 µM, 100 µM, 500 µM) recorded in 0.1 M PBS at applied potential of -0.15 V. **c)** Calibration curve derived from the amperometric measurements shown in b (inset of c: zoom in of the calibration curve at lower glucose concentrations ranging from 50 to 450 µM) (SD of n=3).

Preventing loss of, and damage in, the biological recognition layer of skin-interfaced wearable sensors is a challenge due to the mechanical stress caused by friction. Herein, we propose a solution to this challenge where micropillar surfaces are part of the sensing layer with the majority of the enzyme immobilized at the bottom and sidewalls of the pillars and being protected from mechanical stress. A study was performed in order to investigate the effect of the MPA presence in the sensing electrode architecture on the sensor`s current response where MPA-based and planar Au-Si electrodes were attached on the skin for 4 h during which they were exposed to friction and reused for several times. Although, both MPA-based and planar Au-Si electrodes had insignificantly different responses when not exposed to friction as shown in Figure 3.5b(i) & 3.5b(iii), only MPA-based electrode was not significantly affected by the friction (Figure 3.5b(ii)) even after being used for five times in 4 h. On the other hand, the planar Au-Si electrode had lost almost 50% of its initial response after being worn for 1 h, and after 4 h response of planar Au-Si electrode decreased by approximately 95%. During the experiments, delamination of nanocomposite film form planar electrode surface was observed. These results demonstrate that a micropillar type of microstructure greatly enhanced the stability of the sensing layer by preventing its exposure to skin-caused friction and thus damage helping to maintain a stable sensor response. The use of micropillars not only provided an alternative solution to the existing strategies implemented for preventing enzyme loss that mainly involve masking the sensing layer with a semi-permeable thin layer that allows the penetration of sweat with small molecules such as glucose, but also provided a higher surface area for enzyme immobilization contributing to the sensor`s sensitivity and dynamic range.

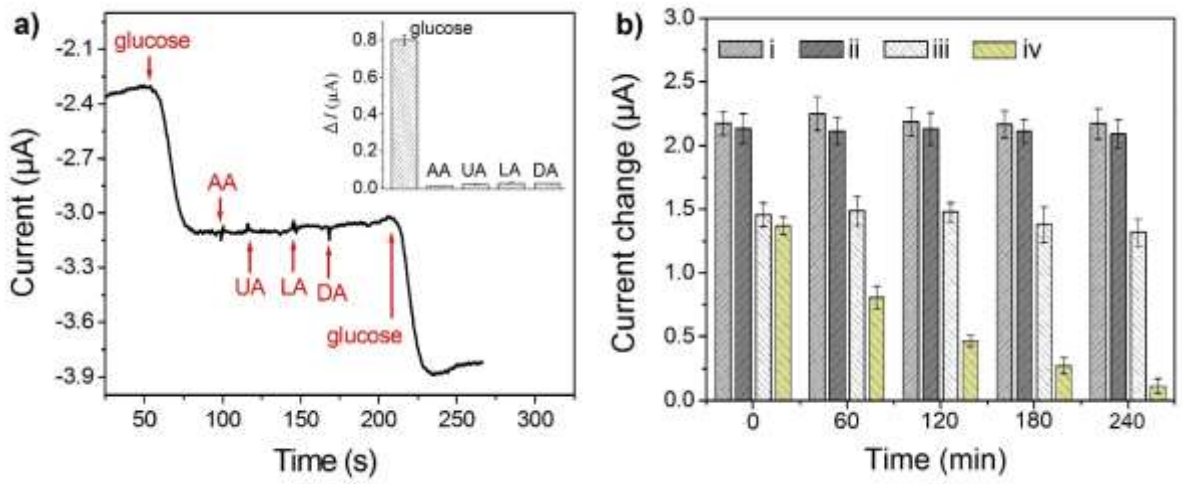

Figure 3.5: a) Interference study of MPA patch at applied potential of -0.15 V using 100 µM of glucose, ascorbic acid (AA), uric acid (UA), lactate (LA), and dopamine (DA) (inset of d: histogram showing current change obtained due to the addition of different interfering species (SD of n=3)). **b)** Study of loss of enzyme from electrode surface when exposed to mechanical friction; MPA-based electrode not exposed (i) and exposed to (ii) mechanical friction and planar Au-Si electrode not exposed (iii) and exposed to mechanical friction (iv) (SD of n=3).

3.3.3 Glucose Monitoring in Human Sweat

In order to better understand the potential of MPA sensing patch, real application scenarios were established to determine the glucose concentration in sweat of human subjects before, during, and after meal consumption. First, the electrochemical performance of the MPA patch was tested in simulated real sample using artificial sweat. Amperometric measurements were performed in artificial sweat composed of an aqueous mixture of KCl, NaCl, $CaCO_3$, $MgCl_2$, $NaHCO_3$, NaH_2PO_4, Na_2SO_4 and NH_4OH.[9,16] Figure 3.6a shows an amperometric plot representing the current response of the MPA sensing patch to increasing glucose concentrations in

artificial sweat, recorded under an applied potential of -0.15 V. The MPA patch exhibited excellent analytical performance in monitoring glucose in artificial sweat, showing a linear response from 50 µM to 1.4 mM with the linear regression equation of I = 4.7142 [glucose] – 0.1084 and correlation coefficient of 0.9994, detection limit of 26 µM, and sensitivity of 4.7 µA/mM (Figure 3.6b). Despite good correlation in glucose levels between blood and sweat,[17] monitoring of glucose in sweat imposes an additional challenge, as its concentration is ~100 times lower than that found in the blood.[18] Therefore, sweat sensing technology requires highly sensitive sensors with a working range in µM concentrations. The analytical performance of our wearable MPA patch is sufficient for the analysis of glucose in healthy individuals, who have glucose levels in the range of 3.6 to 6 mM in blood, and 36 to 60 µM in sweat.[1] For diabetic patients who suffer hyperglycemic episodes, their blood glucose levels can reach 7.8 mM and higher,[19] or 78 µM in sweat. After illustrating the performance of MPA sensing patch in artificial sweat, the detection of glucose in real human sweat was performed. These measurements were performed before and after meal consumption, which was expected to trigger a conspicuous increase in blood glucose levels.[8] In order to clearly see the change in the glucose levels after meal consumption, the human subject fasted for ~8 h. Measurements were performed 30 min before the meal, immediately after the meal, and every 30 min during 2 h time after the meal. Glucose levels were measured from both sweat (using MPA sensing patch) and blood (using commercially available glucometer).

Figure 3.6c shows the current response of MPA sensing patch recorded from sweat at different time intervals. The lowest glucose level of ~0.022 mM was observed during the fasting period and no significant change was observed immediately after the meal consumption. 30 min later, the concentration increased sharply to ~0.083

mM and at 60, 90, and 120 min after the meal consumption, the concentration decreased to 0.054, 0.045, and 0.042 mM, respectively, as shown in Figure 3.6d. Inset of Figure 3.6c shows the amperometric response of MPA sensing patch during the glucose measurements in human sweat. The comparison between sweat glucose and blood glucose levels measured with MPA sensing patch and glucometer, respectively, is shown in Figure 3.6d. These results indicate that there is a lag time between the changes observed in the and in the sweat glucose levels. This lag time is related to the time it takes for glucose to diffuse from blood vessels through the capillary walls to the ISF, which is approximately 15 to 20 min. [8,20] Then, glucose may be excreted to the skin surface via sweat glands. Overall, the results presented in Figure 3.6 demonstrate that MPA sensing patch is a highly promising platform to be used as a wearable patch (Figure 3.6e and 3.6f) for noninvasive epidermal glucose monitoring using sweat.

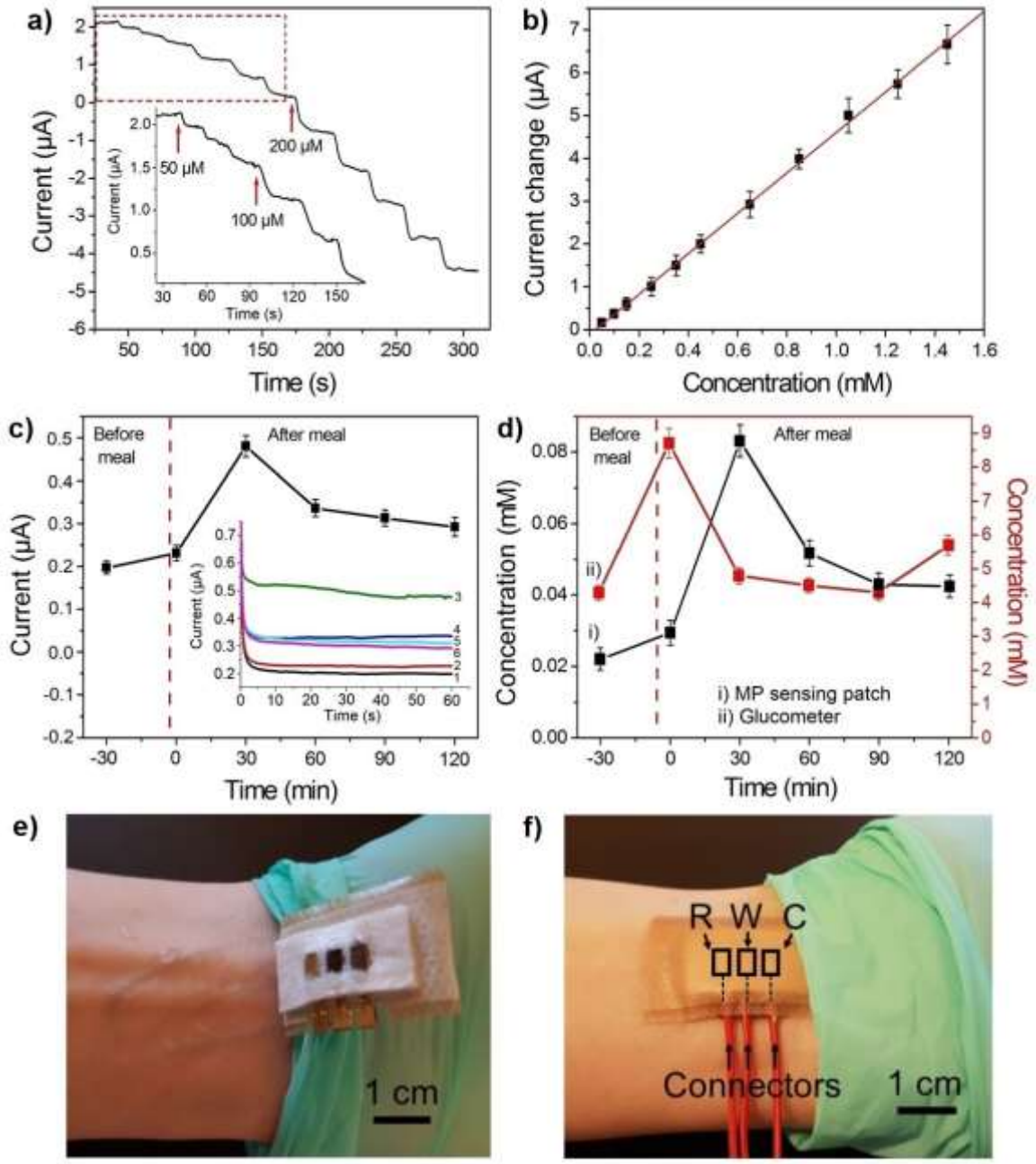

Figure 3.6: a) Amperometric response of MPA sensing patch on the consecutive additions of glucose in artificial sweat at an applied potential of -0.15 V (inset of a: zoom in of amperometric response of MPA patch to 50 μM and 100 μM glucose). **b)** Calibration curve of MPA patch in artificial sweat (SD of n=3). **c)** Current plot of MPA patch response to the glucose from human sweat at different time intervals (inset of c: amperometric curves of MPA patch recorded in human sweat (SD of n=3)). **d)** Comparison of glucose concentration measured in human sweat using MPA patch and in blood using commercially available glucometer at different time intervals (SD of n=3). **e)** and **f)** photographs of glucose sensing patch applied on the skin.

3.4 Conclusions

A wearable sensing patch for glucose monitoring from human sweat was developed using a MPA sensing patch composed of reference, counter, and working electrodes. This approach enabled noninvasive monitoring of glucose in sweat with high sensitivity of 4.7 µA/mM, low detection limit of 26 µM, and wide linear range of 50 µM to 1.4 mM. The glucose-sensing patch was tested using human sweat where glucose levels were successfully measured before and after meal consumption. Furthermore, measured glucose levels from sweat correlated very well with blood glucose levels measured using a commercial glucometer and also showed the lag time, of ~30 min., required for the blood glucose to reach the sweat. The developed MPA wearable sensing patch did not just provide excellent analytical performance, but also provided physical protection to the immobilized glucose oxidase enzyme from leaking from the electrode surface due to the induced friction between skin and the sensors surface. Also, MPA provided easy flow of the sweat towards the inner parts of the electrode creating an efficient sensing environment and thus enhancing the analytical performance. This study provided an alternative solution to the challenges faced by wearable technology regarding the damage of the sensor microenvironment induced by friction between skin and sensor’s surface.

3.5 References

(1) Dervisevic, M.; Alba, M.; Prieto-Simon, B.; Voelcker, N. H. Skin in the diagnostics game: Wearable biosensor nano- and microsystems for medical diagnostics, *Nano Today* **2020**, *30*, 100828.

(2) Sonner, Z.; Wilder, E.; Heikenfeld, J.; Kasting, G.; Beyette, F.; Swaile, D.; Sherman, F.; Joyce, J.; Hagen, J.; Kelley-Loughnane, N.; Naik, R. The microfluidics of the eccrine sweat gland, including biomarker partitioning, transport, and biosensing implications, *Biomicrofluidics* **2015**, *9*, 031301.

(3) Jadoon, S.; Karim, S.; Akram, M. R.; Kalsoom Khan, A.; Zia, M. A.; Siddiqi, A. R.; Murtaza, G. Recent developments in sweat analysis and its applications, *International Journal of Analytical Chemistry* **2015**, *2015*, 164974-164974.

(4) Baker, L. B.; Ungaro, C. T.; Barnes, K. A.; Nuccio, R. P.; Reimel, A. J.; Stofan, J. R. Validity and reliability of a field technique for sweat Na+ and K+ analysis during exercise in a hot-humid environment, *Physiological Reports* **2014**, *2*, e12007.

(5) Sato, K.; Kang, W. H.; Saga, K.; Sato, K. T. Biology of sweat glands and their disorders. I. Normal sweat gland function, *Journal of the American Academy of Dermatology* **1989**, *20*, 537-563.

(6) Parlak, O.; Keene, S. T.; Marais, A.; Curto, V. F.; Salleo, A. Molecularly selective nanoporous membrane-based wearable organic electrochemical device for noninvasive cortisol sensing, *Science Advances* **2018**, *4*, eaar2904.

(7) Jia, W.; Bandodkar, A. J.; Valdés-Ramírez, G.; Windmiller, J. R.; Yang, Z.; Ramírez, J.; Chan, G.; Wang, J. Electrochemical Tattoo Biosensors for Real-Time Noninvasive Lactate Monitoring in Human Perspiration, *Analytical Chemistry* **2013**, *85*, 6553-6560.

(8) Bandodkar, A. J.; Jia, W.; Yardımcı, C.; Wang, X.; Ramirez, J.; Wang, J. Tattoo-Based Noninvasive Glucose Monitoring: A Proof-of-Concept Study, *Analytical Chemistry* **2015**, *87*, 394-398.

(9) Martín, A.; Kim, J.; Kurniawan, J. F.; Sempionatto, J. R.; Moreto, J. R.; Tang, G.; Campbell, A. S.; Shin, A.; Lee, M. Y.; Liu, X.; Wang, J. Epidermal Microfluidic Electrochemical Detection System: Enhanced Sweat Sampling and Metabolite Detection, *ACS Sensors* **2017**, *2*, 1860-1868.

(10) Dervisevic, M.; Dervisevic, E.; Çevik, E.; Şenel, M. Novel electrochemical xanthine biosensor based on chitosan–polypyrrole–gold nanoparticles hybrid bio-nanocomposite platform, *Journal of Food and Drug Analysis* **2017**, *25*, 510-519.

(11) Senel, M.; Dervisevic, M.; Esser, L.; Dervisevic, E.; Dyson, J.; Easton, C. D.; Cadarso, V. J.; Voelcker, N. H. Enhanced electrochemical sensing performance by in situ electrocopolymerization of pyrrole and thiophene-grafted chitosan, *International Journal of Biological Macromolecules* **2020**, *143*, 582-593.

(12) Xiao, X.; Si, P.; Magner, E. An overview of dealloyed nanoporous gold in bioelectrochemistry, *Bioelectrochemistry* **2016**, *109*, 117-126.

(13) Trasatti, S.; Petrii, O. A. Real surface area measurements in electrochemistry, *Journal of Electroanalytical Chemistry* **1992**, *327*, 353-376.

(14) Dervisevic, M.; Shi, Q.; Alba, M.; Prieto-Simon, B.; Cheng, W.; Voelcker, N. H. Enzyme-like electrocatalysis from 2D gold nanograss-nanocube assemblies, *Journal of Colloid and Interface Science* **2020**, *575*, 24-34.

(15) Li, N. B.; Park, J. H.; Park, K.; Kwon, S. J.; Shin, H.; Kwak, J. Characterization and electrocatalytic properties of Prussian blue electrochemically deposited on nano-Au/PAMAM dendrimer-modified gold electrode, *Biosensors and Bioelectronics* **2008**, *23*, 1519-1526.

(16) Harvey, C. J.; LeBouf, R. F.; Stefaniak, A. B. Formulation and stability of a novel artificial human sweat under conditions of storage and use, *Toxicology in Vitro* **2010**, *24*, 1790-1796.

(17) Moyer, J.; Wilson, D.; Finkelshtein, I.; Wong, B.; Potts, R. Correlation Between Sweat Glucose and Blood Glucose in Subjects with Diabetes, *Diabetes Technology and Therapeutics* **2012**, *14*, 398-402.

(18) Kim, J.; Campbell, A. S.; Wang, J. Wearable non-invasive epidermal glucose sensors: A review, *Talanta* **2018**, *177*, 163-170.

(19) Clement, S.; Braithwaite, S. S.; Magee, M. F.; Ahmann, A.; Smith, E. P.; Schafer, R. G.; Hirsch, I. B. Management of Diabetes and Hyperglycemia in Hospitals, *Diabetes Care* **2004**, *27*, 553.

(20) Cengiz, E.; Tamborlane, W. V. A tale of two compartments: interstitial versus blood glucose monitoring, *Diabetes Technology and Therapeutics* **2009**, *11 Suppl 1*, S11-S16.

Chapter 4: Transdermal Electrochemical Monitoring of Glucose via High-density Silicon Microneedle Array Patch

Declaration

This chapter was published as Dervisevic, M.; Alba, M.; Yan, L.; Senel, M.; Gengenbach, R.T.; Prieto-Simon, B.; Voelcker, N.H. Transdermal Electrochemical Monitoring of Glucose via High-density Silicon Microneedle Array Patch. *Advanced Functional Materials, **2021**, 2009850.*

4.1 Introduction

Transdermal wearable biosensors have received a growing worldwide attention since they promise to bring us one step closer to implementing personalized and precision medicine through continuous monitoring of health conditions.[1,2] The skin, as the largest organ of a human body, has multiple essential roles like maintaining the homeostasis, protecting the underlying organs against injuries, preventing the loss of excessive amount of fluid, sensing the external stimuli, etc.[3] The skin is composed of three main layers, starting with the epidermis, which is the outermost layer with a thickness that varies depending on the part of the body (e.g. forearm thickness is 36 to 61 µm);[4] continuing with dermis, with a thickness ranging between 500 to 2000 µm; and finally, the hypodermis. The lower part of the dermis and hypodermis contain nerve bundles and blood vessels, while the epidermis lacks both.[3] The interstitial space is the area surrounding parenchymal cells, vascular and lymphatic capillaries and it is filled with interstitial fluid (ISF). ISF carries nutrients from blood vessels to the cells, and also waste components from cells to the lymph vessels. It is, therefore, a composition of serum and cellular materials such as ions, proteins, and metabolites.[5,6] Due to the similarity of ISF constituents to the ones found in blood serum and plasma, ISF can be used to monitor important biomarkers for disease diagnostics and management, including glucose. The similarity in composition between ISF and blood

serum and plasma has been demonstrated in several studies.[7,8] This is particularly the case for low molecular weight species (e.g., Na^+, K^+, glucose) where the fast diffusion of small and polar molecules through capillary walls is driven by the increased pressure in blood capillary compared to ISF.[6] Specifically for glucose at equilibrium, data comparison between commercial glucometers sampling ISF and blood indicates nearly identical concentrations.[8] For larger molecules, a filtering effect may occur. Regardless, 93% of the proteins found in ISF are also found in both plasma and serum.[7]

Recent research activities in wearable biosensors have focused on addressing epidermal sensing from perspiration because sweat is the easiest accessible body fluid and it is rich in different metabolites and electrolytes.[9-12] However, this type of biosensors faces various limitations such as low and inconsistent sweat production rates, sample evaporation, contamination with exogenous compounds such as cosmetics, etc.[2,5] For this reason, transdermal monitoring via individual microneedles (MN) or microneedle arrays (MNA) that target ISF or peripheral blood may overcome some of the challenges presented by sweat biosensors.[1,13-16] MN are the downsized form of conventional hypodermic needles, which can be fabricated from a variety of materials with different sizes, shapes, and array densities.[17] MN are minimally invasive compared to hypodermic needles, enabling painless needle insertion into the skin and providing a large surface area of interaction.[18-20] Their tunable dimensions and shapes, including length, sharpness, and density, facilitate the design of MNs that target different depths of epidermal and dermal layers without stimulation of dermal nerves thus not causing pain or discomfort.[21] Several MN designs have been employed for continuous glucose monitoring, including solid, hollow and porous MNA.[22] Hollow and porous MNA may enhance fluid collection, but the manufacturing

process and the integration with fluid collectors can be complicated. Solid MNA, however, are easier and cheaper to fabricate. They can be used in direct contact with bodily fluids, exploiting their large surface area. This is particularly beneficial when MNA act as sensing transducers. Indeed, MNA coated with conductive layers can be used as efficient electrodes for continuous glucose monitoring using electrochemical methods. Up to date, different types of materials have been used for MN-based electrochemical glucose biosensors such as stainless steel coated with Pt,[23] porous Au,[24] 3D-printed E200acryl,[25] conductive polymer,[26] etc. Silicon is a desirable material used for MN fabrication due to its biocompatibility, high rigidity and mechanical strength that increases skin penetration and prevents MN to break and accumulate inside the skin causing an immune response or other related health problems.[21] The elastic modulus of Si ranges from 50 to 180 GPa,[27] which is more than enough to withstand the force needed to pierce the skin.

The present work demonstrates the application of a MNA patch for the transdermal monitoring of glucose. Glucose is an important biomarker, and the monitoring of its levels is the gold standard in the management of diabetes. Typically, diabetic patients use a finger-prick test that measures the levels of blood glucose to help them regulate the insulin intake. The normal physiological blood glucose level ranges from 3.6 to 6.0 mM. Persistent irregularities in these levels can cause damage to large and small blood vessels, and subsequently, cardiovascular, nephrotic, ocular, neurotic, and pulmonary system disorders.[28,29] The pain and discomfort faced during long-term repetitive (up to ten times a day for type 1 diabetes sufferers) finger-prick tests can deter the patients from being tested on a regular basis. In addition, the lack of care with the sterilization process can cause infection.[30] Research on alternative technologies to avoid the aforementioned problems and provide patients with more

convenient user-friendly glucose monitoring is ongoing. Sampling of ISF instead of blood has emerged as powerful minimally invasive method, given that glucose concentration in ISF reflects the exact concentration found in blood, with minimal lag time (5-15 min).[6,31,32]

In this chapter, for the first time, we report a MNA sensing patch containing high-density Si MN and its application to the electrochemical transdermal monitoring of glucose. This MNA system provides a large surface area to interface transdermal ISF without reaching nerve terminations. The glucose sensing patch combines in a 3D-printed holder a three-electrode system consisting of a reference, a working and a counter electrode, all made of Si MNAs (Figure 4.1a-f). The surface of the Si MNA was initially coated with a thin layer of gold (Au-Si-MNA) and subsequently modified to conjugate dendrimers containing a redox mediator (ferrocene-cored poly(amidoamine) dendrimer, Fc-PAMAM) and the catalytic bioreceptor glucose oxidase (GOx), as illustrated in Figure 4.1g. Skin penetration tests were performed to test the ability of MNA to pierce the skin and reach the ISF-rich layers. Glucose detection and quantification analysis were first carried out using amperometric measurements *in vitro*, which demonstrated the high sensitivity and selectivity of the MNA system, along with good stability and a linear current response. Furthermore, the *in vivo* application of the glucose sensing patch using mice, as proof of concept, demonstrated the ability of the biosensor to detect an increase in ISF glucose concentration initiated by external injection of a glucose bolus. The results obtained from monitoring ISF glucose levels in mice showed a very good correlation with the blood glucose values recorded with a commercial glucometer. The developments herein described will contribute to the advancement of minimally invasive transdermal

devices, which promise to improve the management of diabetes and the patients' quality of life.

4.2 Experimental Section

4.2.1 Materials and Instrumentations

Glucose oxidase from Aspergillus Niger, D-(+)-glucose, potassium hexacyanoferrate (III), potassium hexacyanoferrate (II) trihydrate, 1-ethyl-3-[3-dimethylaminopropyl] carbodiimide hydrochloride (EDC), N-hydroxysuccinimide (NHS), 2-(N-morpholino) ethanesulfonic acid hydrate (MES), 3-mercaptopropionic acid, 2-mercaptoethanol, uric acid, ascorbic acid, 4-(2-hydroxyethyl)-1-piperazineethanesulfonic acid (HEPES), KCl, $MgSO_4$, NaCl, $CaCl_2$, NaOH, sodium salt, sucrose, hydrogen peroxide (H_2O_2), rhodamine-labeled dextran dye, and glutaraldehyde were purchased from Sigma Aldrich Chemical Co. Disodium hydrogen phosphate and sodium dihydrogen phosphate monohydrate were purchased from Merck. Hydrochloric acid and sulfuric acid were purchased from J.T. Baker, and ammonia solution was obtained from AJAX. All chemicals were of analytical grade and were used without further purification. Aqueous solutions were prepared using Milli Q water (18.2 MΩ cm at 25 °C). Ferrocene-cored poly(amidoamine) dendrimers were synthesized as previously reported.[47]

Electrochemical measurements were carried out using an electrochemical analyzer CHI 650E (CH Instruments, USA). The Objet Eden 260V 3D printing system, O_2 plasma IoN Wave 10 Plasma Asher (PVA TePla), and AC/DC sputtering instrument Intlvac Nanochrome were used in patch fabrication process. A field-emission gun scanning electron microscope (FEG-SEM) (FEI NovaNano SEM 430) was used for morphological analysis of MN. Confocal imaging was carried out by Nikon A1Rsi.

XPS analysis was performed using either an AXIS Ultra DLD or an AXIS Nova spectrometer (Kratos Analytical Inc., Manchester, UK) with a monochromated Al Kα source at a power of 180 W (15 kV × 12 mA), a hemispherical analyzer operating in the fixed analyzer transmission mode, and the standard aperture (analysis area: 0.3 mm × 0.7 mm). The total pressure in the main vacuum chamber during analysis was typically between 10^{-9} and 10^{-8} mbar. Data processing was performed using CasaXPS processing software version 2.3.15 (Casa Software Ltd., Teignmouth, UK). All elements present were identified from survey spectra. The atomic concentrations of the detected elements were calculated using integral peak intensities and the sensitivity factors supplied by the manufacturer. Binding energies were referenced to the C 1s peak at 285 eV (aliphatic hydrocarbon).

4.2.2 MNA Fabrication and Preparation of MNA Glucose Sensing Patch

MNA were fabricated by UV-photolithography and DRIE (Plasmalab 100 ICP380) of mono-crystalline <100> Si wafers. First, AZ 40XT photoresist (MicroChemicals) was spin coated onto the Si wafer and baked according to manufacturer instructions. The Si wafer was pre-patterned via UV exposure using a chromium mask. The photoresist was developed in AZ 726 MIF (MicroChemicals) after which clear hexagonal arrangement of patterns 60 µm in diameter and 110 µm separation could be observed. The DRIE etching process consisted of three steps. First, the pre-patterned Si wafer was etched via controlled pseudo-Bosch anisotropic etching mixing SF6 and C4F8 gases. A standard Bosch anisotropic process was subsequently performed until the desired height was obtained. Finally, in order to sharpen the tip and remove the remaining resist, a second pseudo-Bosch anisotropic

etching was performed. The resulting Si-MNA arrays had length of approximately 250 µm, a base diameter of ~50 µm and a sharp tip with ~2 µm diameter.

The glucose sensing patch is designed as a three-electrode system, where each electrode is made of MNA. The Si-MNA substrate sits in a holder made by 3D printing technology (Figure 4.1a), using the Objet Eden 260V 3D printing system and Full Cure 720 (FC720) high-resolution, rigid and translucent printing material. After the fabrication, the 3D printed holder was immersed in 20% NaOH solution in order to remove the remaining printing residues. If not completely removed, this supporting material will decrease the adhesion of Au and subsequently have a negative effect on the biosensor performance. Next, the Si-MNA substrate was attached to the 3D printed holder using fast curing adhesive glue (Figure 4.1b). In the next step, a thin film of Au was deposited using an AC/DC sputter coater (Figure 4.1c). Prior the Au deposition, Si-MNA electrode were cleaned with O2 plasma (180 W) using an IoN Wave 10 Plasma Asher for 1 min after which it was placed in the AC/DC sputtering instrument (Intlvac Nanochrome AC/DC) containing Cr and Au targets powered by dual AC and DC power supplies for Cr and Au, respectively. First, 15 nm of Cr was deposited using dual AC with power of 300 W, which served as an adhesive layer for the subsequent Au layer. 150 nm of Au was deposited using DC with target voltage of 100 V. During the deposition of both Cr and Au layers, the chamber vacuum and the sample rotation were kept at constant 1.95 mTorr pressure and 100 rpm, respectively. The resulting Au-coated electrodes are referred as Au-Si-MNA. After the sputtering process, a sticky tape test was performed on Au-Si-MNA electrode in order to assess the adhesion of the Au layer. An insulating ink was applied on some parts of the Au-coated 3D holder (Figure 4.1d) in order to confine the source of the electrochemical signal only to the MNA region. The aforementioned electrode preparation procedure was used for the

fabrication of the working and counter electrodes. The procedure for the reference electrode involves one extra step which is drop-casting an AgCl ink on the Au-Si-MNA surface and drying it at 60 °C for 30 min. Finally, the Au-Si-MNA electrodes were assembled into a single three-electrode glucose sensing patch (Figure 4.1e) suitable for the electrochemical measurements as well as in vivo application (Figure 4.1f).

Prior to functionalization of the working electrode, the Au-Si-MNA surface was thoroughly rinsed with ethanol and acetone in order to remove any remaining impurities and/or organic contaminants from the electrode surface. Next, the Au-Si-MNA was immersed in preheated base Piranha solution prepared using 20% ammonia solution, distilled water (dH_2O), and 35% H_2O_2 for 1 min at 80 °C, and then thoroughly rinsed with dH_2O.[48] Surface functionalization (Figure 4.1g) was performed by incubating the Au-Si-MNA electrode in 2 mM 3-mercaptopropionic acid overnight, allowing self-assembling of thiol groups on the Au surface. Further on, the electrode was thoroughly rinsed with dH_2O and the backfilling of any exposed Au surface was achieved by immersing the electrode into 2 mM 2-mercaptoethanol solution for 30 min. In the next step, the electrode was incubated for 45 min in a mixture of 1:1 10 mg mL^{-1} EDC and 15 mg mL^{-1} NHS solution, both prepared in 10 mM MES buffer pH 5. The Au-Si-MNA electrode was then immersed in 10 mM Fc-PAMAM solution prepared in 10 mM PBS, for 4 h. Subsequently, the electrode was thoroughly rinsed with dH_2O and incubated in 2.5% glutaraldehyde for 45 min. In the final step, the functionalized Au-Si-MNA/Fc-PAMAM electrode was immersed in 15 mg mL^{-1} GOx solution prepared in 10 mM PBS and left overnight at 5 °C. Finally, before proceeding with electrochemical measurements, the Au-Si-MNA/Fc-PAMAM/GOx electrode was once again rinsed with dH_2O to remove unbound GOx. When not in use, Au-Si-MNA/Fc-PAMAM/GOx electrodes were stored in 10 mM PBS at 5 °C.

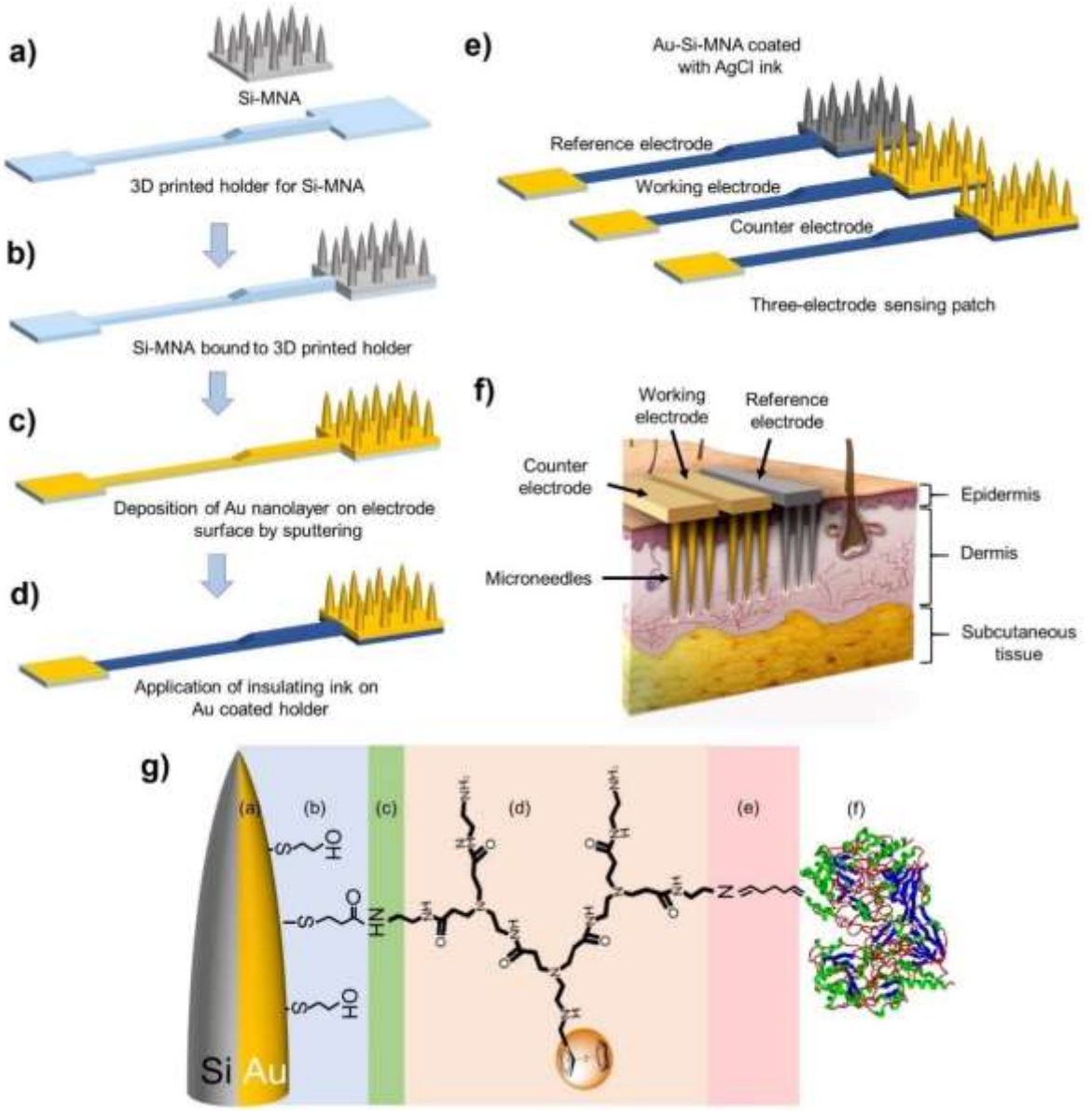

Figure 4.1: Schematic illustration of Au-Si-MNA electrode preparation. **a)** Si-MNA and 3D printed holder, **b)** Si-MNA substrate attached to the 3D printed holder, **c)** sputter deposition of a thin film of Au, **d)** insulating ink application, and **e)** three-electrode sensing patch with Au-Si-MNA as working (W) and counter (C) electrodes and reference (R) electrode with Au-Si-MNA coated with AgCl ink. **f)** Schematic of the three-electrode MNA patch penetrating the skin and interfacing the epidermis and dermis. **g)** Schematic illustration of modification of W electrode; (a) Au layer, (b) self-assembled monolayer of 3-mercaptopropionic acid and 3-mercaptoethanol, (c) EDC/NHS activation, (d) Fc-PAMAM immobilization, (e) glutaraldehyde, and (f) glucose oxidase enzyme immobilization.

4.2.3 *In Vivo* Testing of the MNA Glucose Sensing Patch

In vivo testing of the three-electrode system glucose sensing patch was performed on mice anesthetized through inhalation of 1.2% isoflurane in 2 L min^{-1} O_2. Hair on the dorsal side of the mice was shaved off using hair removal cream (Nair) and the shaved area was thoroughly cleaned with dH_2O. Later, the MNA sensing glucose patch (Figure 4.1e) was applied onto the dorsal side of the mouse skin by thumb pressure and then the electrochemical signal was recorded. *In vivo* electrochemical measurements were performed by recording the amperometric signal under 0.35 V applied potential before and after intramuscular injection of 120 µL of 30 wt% glucose solution. In parallel, the glucose level in mouse blood was measured using a commercial glucometer (CareSens N). The blood glucose level values obtained from both glucose patch and glucometer were compared. The experimental protocol was approved by the Animal Ethics Committee of Monash University, which was conducted in accordance with the guidelines of the National Health and Medical Research Council (NHMRC) of Australia.

4.3 Results and Discussion

4.3.1 Morphological Characterization of MNA and Skin Penetration Test

The three-electrode system for transdermal glucose monitoring was constructed by using silicon MN. We aimed to produce high density MNA patches (9500 needles cm-2) consisting of high aspect ratio, sharp-tipped, vertical projections that enable access to ISF from the epidermis and superficial dermis. Si-MNA were fabricated from crystalline silicon wafers by combining UV-photolithography and deep reactive ion etching (DRIE). Silicon was selected as base substrate material due to its versatility for microfabrication, convenient mechanical properties and favorable biocompatibility. Despite its excellent semiconducting properties, the electronic properties of silicon are not suitable for its application as electrochemical transducer. Not only does the intrinsic bandgap hinder the electron transfer, but the native silicon oxide layer acts as an electrical insulator. Therefore, in order to improve their transducing behavior, Si-MNA were coated with a thin film of sputtered gold of a thickness of 150 nm. Morphological characterization of Au-Si-MNA was carried out by means of scanning electron microscopy (SEM). Figure 4.2a-d show SEM micrographs of Au-coated Si needles with detailed morphological features. Micrographs of top (Figure 4.2a) and tilted (Figure 4.2b) views show well-ordered MNA in hexagonal arrangement with a density of ~9500 microneedles cm^{-2}, where the space between two adjacent cone centers is ~110 µm. A cross section image of MNA (Figure 4.2c) reveals a height of ~250 µm, with a base diameter of ~50 µm. At increased magnification, the sharpness of individual needle tips of ~2 µm diameter was apparent (Figure 4.2d). The sharpness of the presented MNs is ideal for the painless penetration of the skin whereas the shape, size and density of the MNA are all suitable for the

analysis of epidermis and dermis layers without puncturing blood vessels or damaging nerve bundles.[33] This MNA was used for the preparation of the three-electrode system glucose sensing patch. Furthermore, to demonstrate that MN can successfully and uniformly penetrate the skin, the MNA was applied to porcine skin by finger pressing. To check the effectiveness of skin penetration, before applying to porcine skin, the MNA was spin-coated with rhodamine-labeled dextran dye (Figure 4.2e) and left to dry for 24 h. As shown in Figure 4.2f, the MNA generated uniform pores on the surface of the porcine skin in an arrangement that matches those of the original MNA patch.

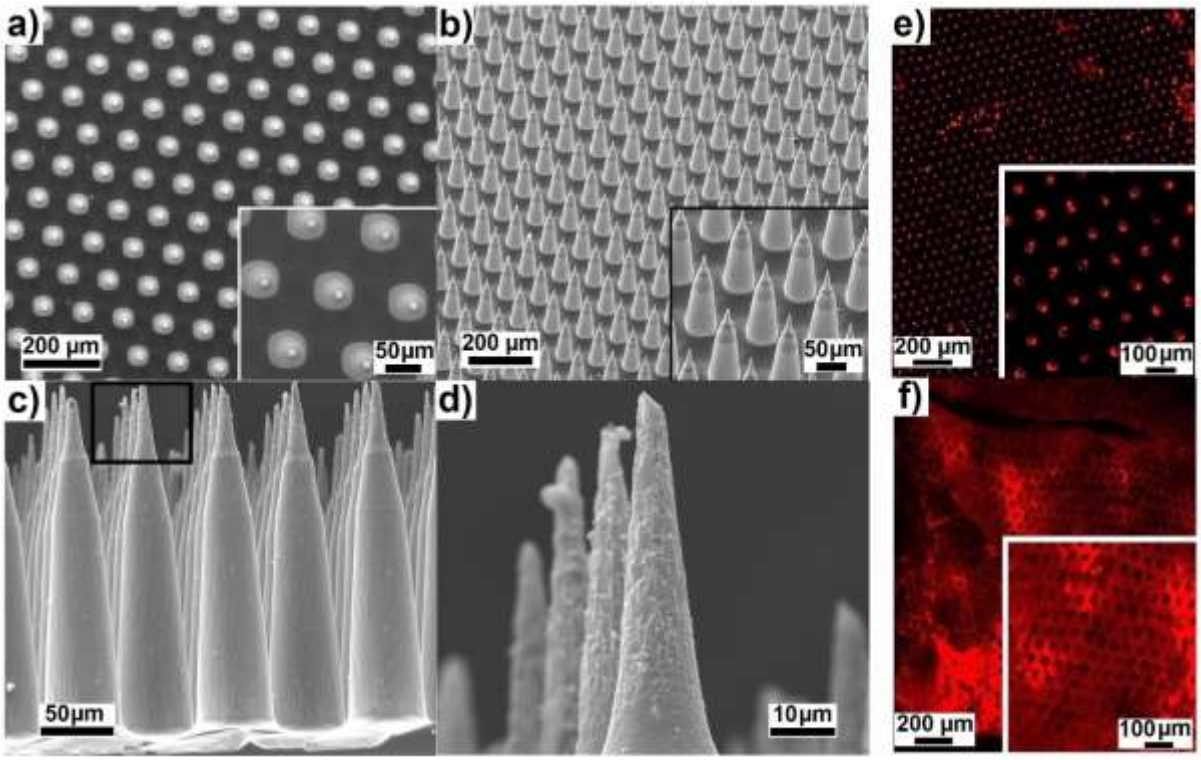

Figure 4.2: SEM micrographs of Au-Si-MNA; **a)** top view, **b)** tilted view, **c)** cross section, and **d)** magnified tip area (black square) of MNs shown in C. Confocal microscopy images of **e)** MNA after coating with rhodamine-labeled dextran dye and **f)** porcine skin after MNA application.

4.3.2 Electrochemical Characterization of MNA Glucose Sensing Patch

The electrochemical characterization of the gold coated MNA glucose sensing patch was performed using cyclic voltammetry (CV) and electrochemical impedance spectroscopy (EIS). The first CV in 0.5 M H_2SO_4 solution was carried out using Au-Si-MNA and flat Au-Si as working electrodes. This step is commonly performed as an electrochemical cleaning of the Au surface but is also used for surface characterization and determination of surface area.[34] Figure 4.3a shows the obtained CVs, where the oxidation peaks of the deposited Au layer can be observed between 0.93 V and 1.20 V, and the reduction peaks between 0.7 V and 0.9 V potential range. The charge of the reduction peaks can be used to calculate the active surface area of the electrodes, assuming that 390 μC cm^{-2} is required for Au reduction.[34,35] The inset for Figure 4.3a compares the active surface area of the Au-Si-MNA and flat Au-Si electrodes for a geometric area of 0.22 cm^2. The former has an active area of 0.97 cm^2, about 3 times that of the latter (0.33 cm^2).

Further electrochemical characterization was carried out to monitor the surface modifications of Au-Si-MNA working electrode with Fc-PAMAM and GOx as the biological recognition element. The functionalization of MNA towards glucose sensing includes the formation of a self-assembled monolayer (SAM) of 3-mercaptopropionic acid to generate a carboxylic acid-terminated surface. Upon activation of –COOH groups, the $–NH_2$-terminated Fc-PAMAM was covalently bound to the surface. Then, GOx was attached to the surface using glutaraldehyde as the crosslinking molecule. Figure 4.3b shows the CVs corresponding to each electrode modification step starting with bare Au-Si-MNA electrode where no oxidation-reduction peaks were observed. After the immobilization of Fc-PAMAM on the Au-Si-MNA and flat Au-Si electrodes, an

oxidation and a reduction peak appeared at 0.45 V and 0.35 V, respectively, as a result of the redox activity of the Fc core of the dendrimers. A difference in the intensity of the redox peaks of Au-Si-MNA and flat Au-Si electrodes both modified with Fc-PAMAM was observed. The Au-Si-MNA electrode exhibited a current peak intensity ~3 times higher than that of the flat Au-Si electrode. This is consistent with the larger surface area exhibited by the MNA (see Figure 4.3a) that results in more available sites for Fc-PAMAM immobilization. The intensity of Fc current peaks drastically decreased when GOx enzyme was immobilized onto Fc-PAMAM, as expected and as a result of the shielding effect of GOx on the Fc molecules. Figure S4.1 illustrates the CVs obtained at different scan rates ranging from 10 mV s^{-1} to 500 mVs^{-1} using the Au-Si-MNA/Fc-PAMAM working electrode. As the scan rate increased, oxidation-reduction peaks of Fc also increased, indicating a quasi-reversible process. The inset for the Figure S4.1 depicts the anodic and cathodic peak currents versus the square root of the scan rate where the linear increase of both peak currents supports the diffusion-controlled electron transfer property of the Au-Si-MNA/Fc-PAMAM electrode. Further characterization was performed by means of EIS recorded in a redox probe $K_4Fe(CN)_6/K_3Fe(CN)_6$ (5 mM, 1:1 ratio) in 0.1 M KCl. Figure 4.3c shows the Nyquist plots obtained using bare Au-Si-MNA (a), flat Au-Si (b), and Au-Si-MNA modified with Fc-PAMAM (c), and GOx (d), as working electrode. The EIS data were fitted using a Randles electrical equivalent circuit model (see inset of Figure 4.3c) composed of Rc representing resistance of all connections and electrolytes, capacitance (C), the charge transfer resist (Rct), and Zw, the Warburg impedance. According to the results plotted in Figure 4.3c, the charge transfer resistance (Rct) was 19±1.6 Ω and 345±13 Ω when using a bare Au-Si-MNA and a flat Au-Si, respectively, as working electrodes. After the immobilization of Fc-PAMAM, Rct increased to 1220±87 Ω and after GOx

immobilization, the Rct increased to 6170±350 Ω. Both EIS and CV results confirm successful immobilization of Fc-PAMAM and GOx enzyme on the Au nanolayer surface.

X-ray photoelectron spectroscopy (XPS) was employed to further characterize the stepwise surface modifications of the Au-coated electrodes. The results are summarized in Table S4.1. Gold was detected at every step, with a clear trend of decreasing Au/C ratio in each step of the functionalization process; this is consistent with the modification of the electrodes, indicating the presence of an organic layer of increasing thickness on the gold surfaces. The modification of pre-cleaned gold surface with –COOH terminated alkanethiols after formation of SAMs was confirmed by the S/C ratio, which increased from 0.027 to 0.093. Additionally, we observed a significant increase in the O/C ratio after SAM modification (from 0.186 to 0.362). The analysis of the C 1s high-resolution spectrum of SAM modified Au-coated electrodes confirmed a main peak centered at ~285 eV (component C1), which was assigned to the aliphatic carbons of the alkyl chains (Figure 4.3d). The formation of a SAM was further evidenced by the peak observed at ~289 eV (C4), which was assigned to the carboxyl group of the SAM, with the corresponding ratio of C4/C increasing from 0.038 to 0.125.[36] The immobilization of the Fc-PAMAM was confirmed by the increase in the N/C ratio (from 0.021 to 0.182) and by the presence of Fe (Fe/C ratio of 0.070). A significant change in the C 1s spectrum can be observed after the attachment of the Fc-PAMAM dendrimer to the EDC/NHS activated Au-SAM surface. The main peak at 285.0 eV (C1) was attributed to aliphatic carbon atoms of the alkyl chains in the SAM and the PAMAM. The higher binding energy peak centered at ~288 eV (C3) can be ascribed to the amide groups of the PAMAM dendrimers and the newly formed bond between the –COOH terminated SAM and the $–NH_2$ functional PAMAM (C3/C ratio

increased from 0.048 to 0.100).[36] The peak at 286.5 eV (C2 component) was mostly attributed to the carbon singly bonded to an amide nitrogen (−CH_2−NH−C=O) and represented by the C2/C ratio, which increased from 0.114 to 0.285.[37] The attachment of GOx was evident from the decrease in the Au/C, S/C and Fe/C ratios. The O/C and N/C ratios remained comparable before and after GOx immobilization; this can be explained by the similarity of chemical structures of the Fc-PAMAM dendrimer and the glucose oxidase for XPS – except for the presence of Fe.[38] After GOx immobilization, the main peak at ~285 eV was still assigned to aliphatic carbon, present in the SAM, PAMAM and GOx. A significant increase in the higher energy peaks was observed, which is consistent with the presence of amide bonds in the immobilized biomolecule: a peak at ~286.5 eV was attributed to C–N and C–O based bonds (C2/C increased from 0.285 to 0.337), while the peak at ~288 eV was due to N-C=O bonds of peptide moieties of the enzyme (with C3/C increasing from 0.100 to 0.124).[36,38]

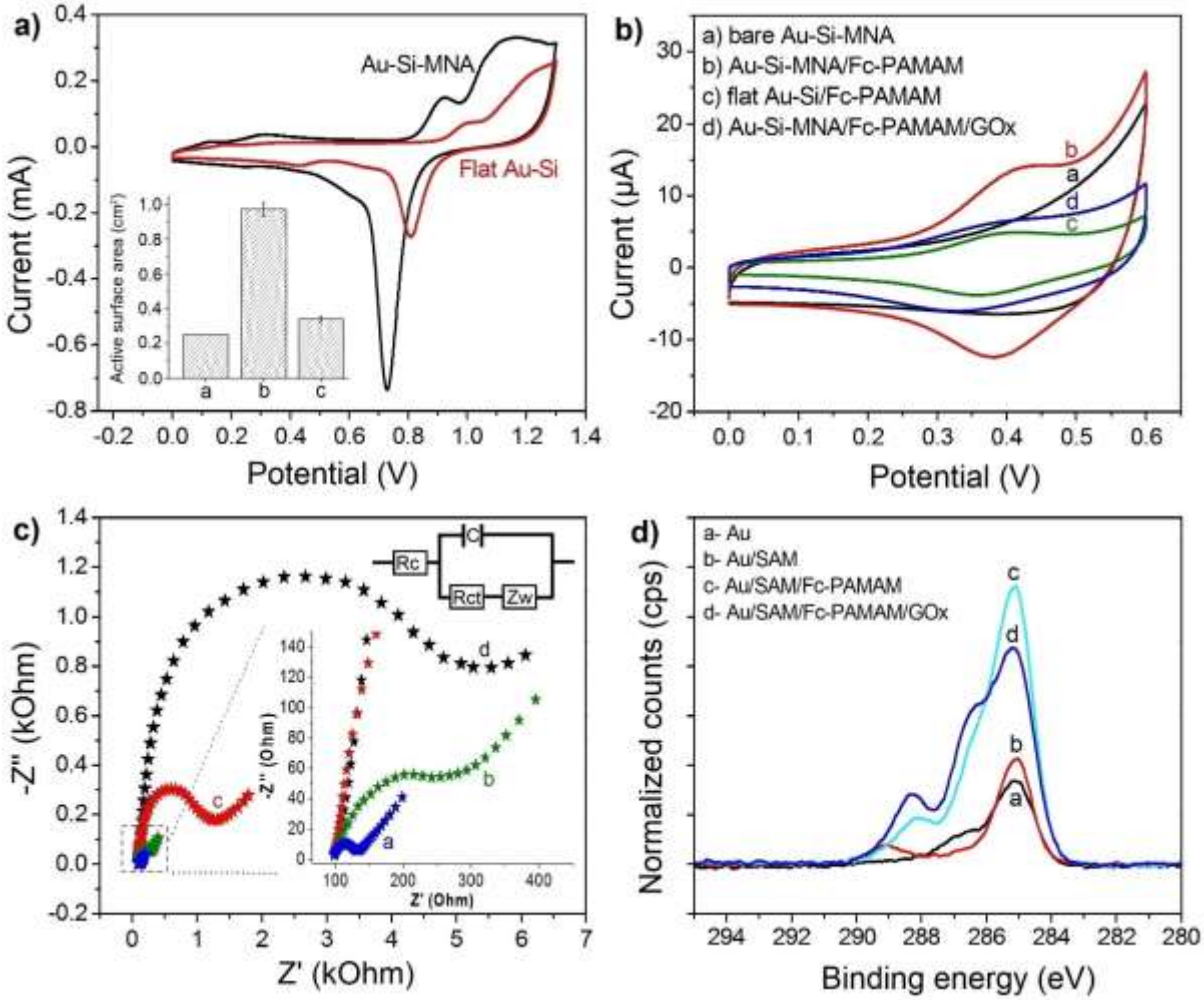

Figure 4.3: Electrochemical characterization of Au-Si-MNA electrode. **a)** CV plots of Au-Si-MNA (a) and flat Au-Si (b) electrodes recorded in 0.5 M aqueous H_2SO_4 solution (inset: histogram showing comparison of (a) measured surface area, and calculated active surface area of (b) Au-Si-MNA, and (c) Flat Au-Si electrodes. (SD, n=3)), **b)** CV plots of Au-Si-MNA, Au-Si-MNA and flat Au-Si modified with Fc-PAMAM, and Au-Si-MNA/Fc-PAMAM/GOx electrodes recorded in 0.1 M PBS (pH 7.4), **c)** impedance spectra of Au-Si-MNA (a), flat Au-Si (b), Au-Si-MNA/Fc-PAMAM (c), and Au-Si-MNA/Fc-PAMAM/GOx (d) (insets: zoom in of impedance spectra of Au-Si-MNA (a) and flat Au-Si (b) and Randles equivalent circuit used from impedance data fitting). **d)** XPS high resolution spectra of the C 1s obtained after each functionalization step: pre-cleaned gold (a); SAM modification (b); immobilization of Fc-PAMAM (C); and immobilization of GOx (d).

4.3.3 Biosensor Optimization and Glucose Detection

The optimization of the electrochemical performance of the MNA glucose patch was performed by measuring the amperometric response to 2 mM glucose, with an applied potential of 0.35 V, in buffered solutions of different pH and testing various temperature conditions. The current response to glucose is represented as a relative response (%) with 100% being the maximum obtained response. We first investigated the effect of the pH of the measuring solution on the response of the MNA patch to 2 mM glucose in buffer solutions with pH values ranging from 6.2 to 8.2 (0.1 M PBS). Free GOx enzyme operates under a relatively broad pH range (pH 4 to 7) and its optimum working pH is 5.5,[39] yet after enzyme immobilization its optimum pH can change.[40] According to the results represented in Figure S4.2, there was no significant response to glucose at pH 6.2. With the increase of pH, response to glucose also increased reaching its maximum at pH 7.4. A further increase in pH resulted in decreasing sensor performance. Therefore, the optimum working pH for the MNA glucose sensing patch was found to be 7.4, which is also seen for various reported glucose biosensors.[41-44] The effect of temperature on the performance of the MNA glucose sensing patch was investigated in order to determine whether the transducer or the MNA are temperature sensitive. Sensing was carried out in 0.1 M PBS (pH 7.4) with 2 mM glucose over the range of 25 °C to 55 °C. The recorded amperometric response of the biosensor to glucose, represented in Figure S4.3, slightly increased from 25 °C to 35 °C, with a maximum at 35 °C. At higher temperatures, the response drastically decreased with the increase in temperature, which can be due to the denaturation of GOx enzyme. Thus, the optimum working temperature for the MNA glucose sensing patch was 35 °C. These results are especially important since the skin temperature of the arm and trunk varies between 32.5 and 35.5 °C, and 34 to

36.3 °C, respectively.[45] Furthermore, the reusability of the sensing patch was studied. Experiments were performed in 0.1 M PBS by measuring the sensor response to 2 mM glucose for 10 consecutive times using the same patch (Figure S4.4). The MNA glucose sensing patch was thoroughly rinsed with PBS and the testing solution was replaced with fresh glucose and PBS after each measurement. The biosensor kept 95% of its initial response during the first five consecutive measurements. Then, the response slowly decreased to 80% after ten measurements. The MNA glucose sensing patch exhibits good reproducibility and accuracy towards glucose during the first five measurements. However, the biosensor would require slight recalibration if used for long-term continuous measurement.

The selectivity of the glucose biosensor is important, especially when working with ISF due to the potential interference of electroactive molecules present in ISF such as uric acid (UA) and ascorbic acid (AA). In order to minimize interference, Fc was integrated into the enzyme immobilization matrix as redox mediator. This molecule did not just serve as an electron carrier between the enzyme active site and the electrode, but also allowed to decrease the required working potential of the glucose patch. The use of a high working potential can lead to oxidation of interfering electroactive compounds on the electrode surface leading to a false positive response. For this reason, we conducted an interference study with the MNA glucose sensing patch using 2 mM glucose and 0.1 mM AA, UA, dopamine (DA), lactic acid (LA) and glycine (gly) as interfering species. AA, UA, DA and LA are some of the most important potential interferences present in ISF because of their ability to oxidize at certain applied potential on the electrode surface, thus affecting the sensors response. As seen in Figure 4.4a, 0.1 mM of AA, UA, DA, LA, and gly had no significant effect on the electrochemical signal of the glucose patch. The optimization of the working

conditions shows that the MNA glucose patch exhibits a suitable performance for transdermal glucose measurements in relevant physiological pH and temperature. Additionally, the interference study data demonstrate the absence of significant interference from physiologically relevant species found in blood and/or ISF.

The analytical performance of the MNA glucose patch was validated in PBS (0.1 M pH 7.4) and in artificial ISF (aISF) (pH 7.4). The working potential of MNA glucose patch is dictated by the mediator and how it is tethered to the PAMAM dendrimers (Fc-PAMAM). Figure 4.4b shows the chronoamperometric plot obtained from the response of the MNA glucose patch to increasing concentrations of glucose prepared in 0.1 M PBS. The biosensor exhibits a well-defined response to glucose in PBS having a linear dynamic range from 1 to 11 mM with a sensitivity of 0.58 μA mM^{-1} cm^{-2}, a detection limit of 0.45 mM and a correlation coefficient of 0.9996 (Figure 4.4d). Since the MNA glucose patch will be used for transdermal glucose analysis from ISF, it is important to examine the performance of the biosensor in an environment similar to ISF. For this experiment, we used artificial ISF (aISF) prepared in dH_2O using 10 mM HEPES, 123 mM NaCl, 7.4 mM saccharose, 2.2 mM $CaCl_2$, 3.5 mM KCl, 0.7 mM $MgSO_4$, and 1.5 mM NaH_2PO_4 with pH adjusted to 7.4.[24,46] Figure 4.4c shows the chronoamperometric plot obtained from the response of the MNA glucose patch to increasing concentrations of glucose prepared in aISF. The linear response of the biosensor is characterized with a sensitivity of 0.1622 μA mM^{-1} cm^{-2}, a linear range and a detection limit of 1 to 9 mM and 0.66 mM (with a correlation coefficient of 0.9995), respectively. Notice that the glucose concentration found in ISF of healthy individuals ranges from 3.6 to 6 mM.[2] The limit of detection is well below harmful hypoglycemic levels (<3.0 mM) that should trigger immediate action from the patient. The sensitivity of our MNA system is such that it allows the detection of μM variations in glucose

levels. When compared to other reported MNs-based glucose sensors (Table S4.2), the sensitivity of our biosensor is one of the best, despite the low applied potential. This can be attributed to the use of Fc mediator and high surface area of the high density MNA. The observed differences in the sensor response (Figure 4.4d) in PBS and aISF are attributed to the different composition of the testing solutions. Although the complexity of the aISF affected enzyme activity, the sensing performance obtained in aISF was deemed sufficient to perform *in vivo* testing where we aim to observe an increase in the glucose concertation after intramuscular injection of glucose solution.

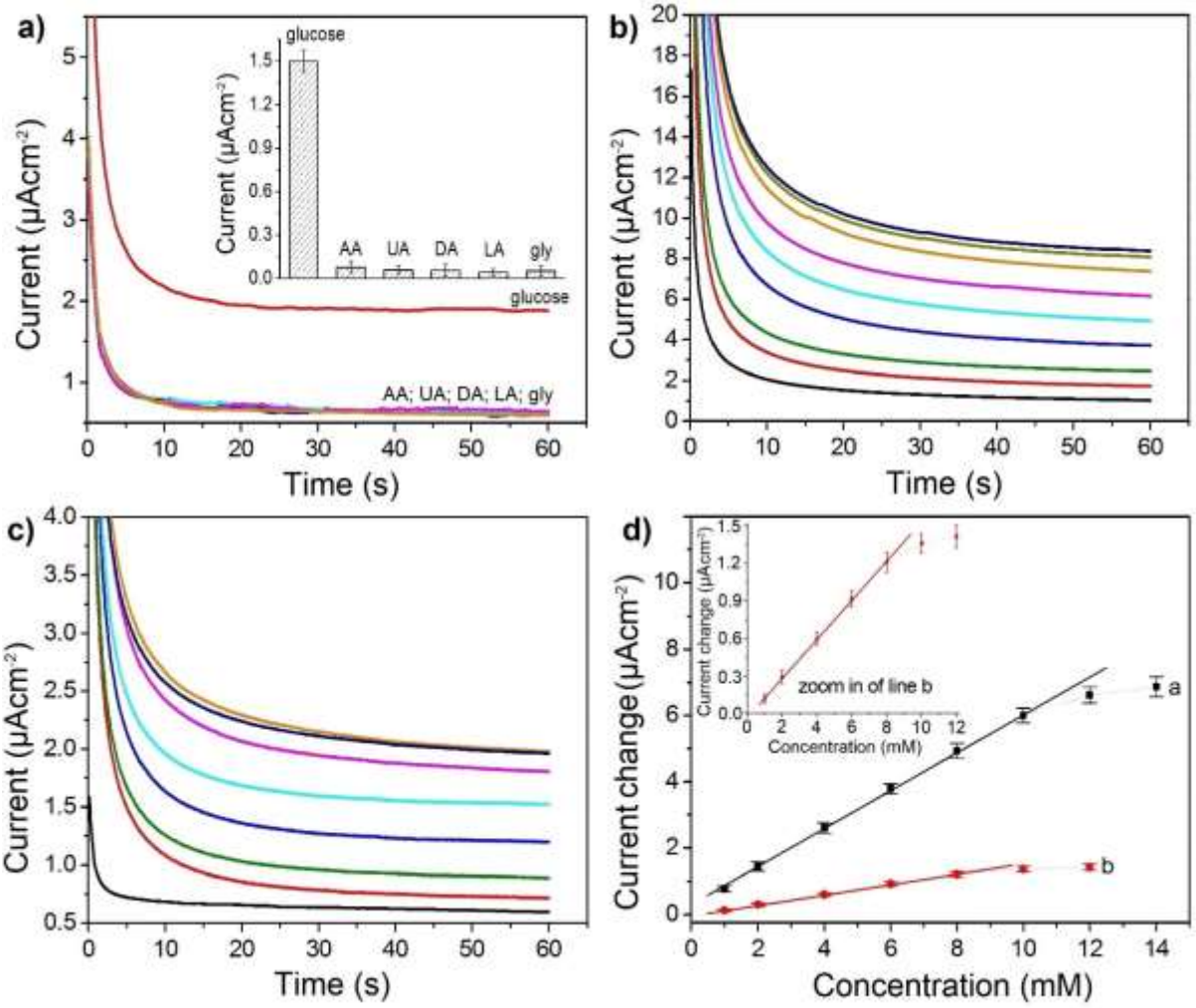

Figure 4.4: a) Interference study using 2 mM glucose and 0.1 mM AA, UA, DA, LA, and gly in 0.1 M PBS, pH 7.4 at applied potential of 0.35 V (n=3 for graph in inset). Chronoamperometric response of the MNA glucose patch to glucose in **b)** PBS (0.1 M, pH 7.4) and **c)** aISF (pH 7.4), and **d)** calibration curves obtained in PBS (a) and aISF (b). (SD, n=3).

4.3.4 *In Vivo* Glucose Monitoring

After the evaluation of the analytical performance of the glucose biosensor *in vitro*, as a proof of concept, we performed an *in vivo* test of the MNA glucose patch on mice. Prior to the *in vivo* measurements, mice were anesthetized and hair on the dorsal side of the mice was shaved off after which the MNA glucose patch was applied. Figure 4.5b shows the three-electrode MNA glucose sensing patch composed of counter and reference electrodes, and a working electrode previously modified with Fc-PAMAM and GOx enzyme. On-mouse application of the patch was gently supported by finger pressure, with a force which was previously measured off-site using a weight balance and estimated to be 6-7 N (Figure 4.5c). The patch was left onto the mouse skin for the whole duration of the experiment (approximately 1 h). After removal of the MNA glucose patch, the resulting indentations were clearly observed with no sign of bleeding or inflammation (Figure 4.5d). Immediately after patch application, the amperometric response was recorded for 5 min at constant 0.35 V potential to ensure a stable electrochemical signal. The last 60 s of this recording was considered the baseline signal. Figure 4.5a displays the electrochemical results of on-mouse MNA glucose patch obtained from three mice. First, measurements were recorded for 5 min in order to ensure a stable electrochemical signal and at the same time to record the base line for 60 s before glucose injection. Then, 120 µL of glucose solution (30% w/v) were administered via intramuscular injection, allowing ~30 min in order for the blood glucose level to be reflected in the ISF and then amperometric measurements were performed once again. Note that the glucose concentration found in blood is similar to ISF, but the increase in glucose concentration in ISF has a slight lag time due to the low capillary density in the dermis layer and the slow metabolic activity in the epidermis layer.[6] To validate the performance of the MNA patch, the blood glucose level of the

mice was recorded in parallel to the electrochemical measurements using a commercial glucometer. The increase in blood glucose after intramuscular injection of the glucose solution is not immediate, thus a conventional glucometer was used to monitor the change and determine the time to proceed with the electrochemical recording using the MNA glucose patch. The inset of Figure 4.5a shows the glucose concentration change (representing increase in glucose concentration after glucose solution injection) recorded with both the MNA sensing patch and commercial glucometer. From the represented results, it can be seen that ISF glucose level detected by the MNA patch and the blood glucose level recorded with the commercial glucometer have very good correlation. Even though the intramuscular injection of glucose solution was performed in exactly the same way for all three mice, their glucose levels varied slightly, possibly due to their different metabolism, difference in their diet and stress developed during the experimental procedure. Overall, the *in vivo* study results suggest that the glucose level in ISF detected by the MNA patch corresponds to the glucose level found in blood which illustrates the successful proof-of-concept application of the glucose MNA sensing patch. In contrast to the majority of previously reported MNA-based glucose sensors (see Table S4.2), this study provides a successful demonstration of the *in vivo* application. We attribute this to the design of the MNA sensing patch and its analytical performance, which provided a robust sensing platform required for the *in vivo* measurements. Future investigations will focus on the continuous transdermal monitoring of glucose using MNA.

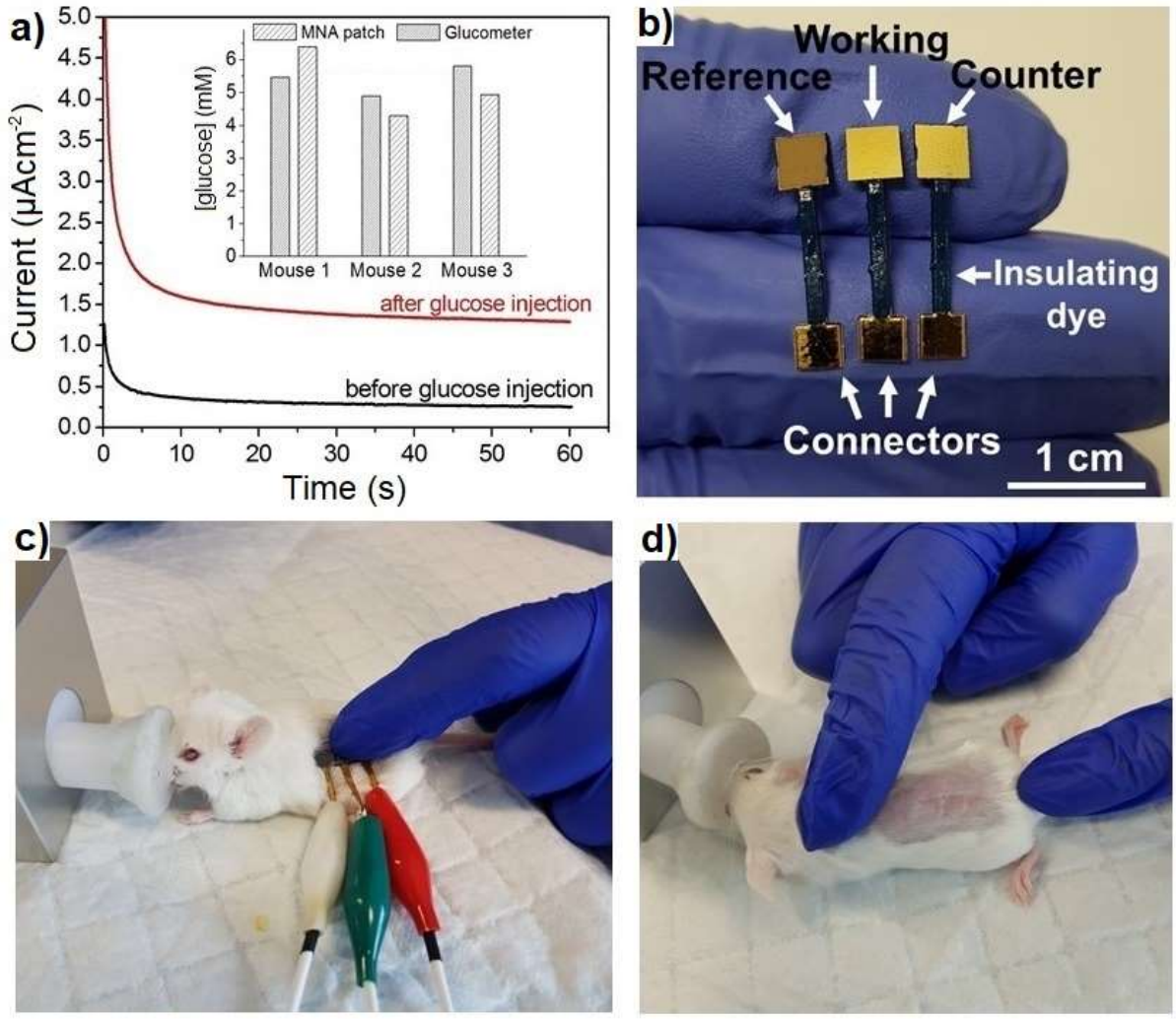

Figure 4.5: *In vivo* testing of MNA glucose sensing patch. **a)** Amperometric signal (applied potential 0.35 V) recorded during the application of the patch on mice skin before (a) and 30 min after (b) intramuscular injection of 120 µL of glucose solution (30% w/v). Optical images of **b)** the three-electrode system used as a patch for transdermal monitoring of glucose in mice, **c)** application of the patch on shaved mice skin, and **d)** mice skin after the application of the needles illustrating successful penetration.

4.4 Conclusions

In this chapter, the use of a high-density MNA sensing patch for transdermal glucose monitoring is reported for the first time. Our MNA sensing patch enabled minimally invasive, *in situ* glucose detection from ISF without the need for extraction or collection. The analytical characterization of the MNA glucose patch in aISF showed very good selectivity, with a sensitivity of 0.1622 μA mM^{-1} cm^{-2} over a working range of 1 to 9 mM glucose, and a detection limit of 0.66 mM. Successful *in vivo* application of the biosensor on mouse demonstrated that the MNA patch has the ability to detect changes in the ISF glucose levels. Furthermore, the glucose values obtained by the MNA patch correlated very well with the blood glucose values obtained with a commercial glucometer. We believe that the proposed MNA sensing patch provides an alternative transdermal diagnostic tool to the invasive existing techniques. Having successful proof-of-concept demonstration, our future work will focus on developing a more compact MNA patch with the ability to target multiple biomarkers from ISF.

4.5 References

(1) Liu, G.-S.; Kong, Y.; Wang, Y.; Luo, Y.; Fan, X.; Xie, X.; Yang, B.-R.; Wu, M. X. Microneedles for transdermal diagnostics: Recent advances and new horizons, *Biomaterials* **2020**, *232*, 119740.

(2) Dervisevic, M.; Alba, M.; Prieto-Simon, B.; Voelcker, N. H. Skin in the diagnostics game: Wearable biosensor nano- and microsystems for medical diagnostics, *Nano Today* **2020**, *30*, 100828.

(3) Fenner, J.; Clark, R. A. F. In Skin Tissue Engineering and Regenerative Medicine, Iv, J. H. H., Ed.; Academic Press: Boston, 2016, pp 1-17.

(4) Whitton, J. T.; Everall, J. D. The thickness of the epidermis, *British Journal of Dermatology* **1973**, *89*, 467-476.

(5) Bariya, M.; Nyein, H. Y. Y.; Javey, A. Wearable sweat sensors, *Nature Electronics* **2018**, *1*, 160-171.

(6) Heikenfeld, J.; Jajack, A.; Feldman, B.; Granger, S. W.; Gaitonde, S.; Begtrup, G.; Katchman, B. A. Accessing analytes in biofluids for peripheral biochemical monitoring, *Nature Biotechnology* **2019**, *37*, 407-419.

(7) Tran, B. Q.; Miller, P. R.; Taylor, R. M.; Boyd, G.; Mach, P. M.; Rosenzweig, C. N.; Baca, J. T.; Polsky, R.; Glaros, T. Proteomic Characterization of Dermal Interstitial Fluid Extracted Using a Novel Microneedle-Assisted Technique, *Journal of Proteome Research* **2018**, *17*, 479-485.

(8) Bailey, T.; Bode, B.W.; Christiansen, M. P.; Klaff, L. J.; Alva, S. The perfromance and usability of factory-calibrated flash glucose monitoirng system, *Diabetes Technology and Therapy* **2015**, *17*, 787-794.

(9) Yang, Y.; Song, Y.; Bo, X.; Min, J.; Pak, O. S.; Zhu, L.; Wang, M.; Tu, J.; Kogan, A.; Zhang, H.; Hsiai, T. K.; Li, Z.; Gao, W. A laser-engraved wearable sensor for sensitive detection of uric acid and tyrosine in sweat, *Nature Biotechnology* **2020**, *38*, 217-224.

(10) Gao, W.; Emaminejad, S.; Nyein, H. Y. Y.; Challa, S.; Chen, K.; Peck, A.; Fahad, H. M.; Ota, H.; Shiraki, H.; Kiriya, D.; Lien, D.-H.; Brooks, G. A.; Davis, R. W.; Javey, A. Fully integrated wearable sensor arrays for multiplexed in situ perspiration analysis, *Nature* **2016**, *529*, 509-514.

(11) Lin, Y.; Bariya, M.; Nyein, H. Y. Y.; Kivimäki, L.; Uusitalo, S.; Jansson, E.; Ji, W.; Yuan, Z.; Happonen, T.; Liedert, C.; Hiltunen, J.; Fan, Z.; Javey, A. Porous Enzymatic Membrane for Nanotextured Glucose Sweat Sensors with High Stability toward Reliable Noninvasive Health Monitoring, *Advanced Functional Materials* **2019**, *29*, 1902521.

(12) Hong, Y. J.; Lee, H.; Kim, J.; Lee, M.; Choi, H. J.; Hyeon, T.; Kim, D.-H. Multifunctional Wearable System that Integrates Sweat-Based Sensing and Vital-Sign Monitoring to Estimate Pre-/Post-Exercise Glucose Levels, *Advanced Functional Materials* **2018**, *28*, 1805754.

(13) Ranamukhaarachchi, S. A.; Padeste, C.; Dübner, M.; Häfeli, U. O.; Stoeber, B.; Cadarso, V. J. Integrated hollow microneedle-optofluidic biosensor for therapeutic drug monitoring in sub-nanoliter volumes, *Scientific Reports* **2016**, *6*, 29075.

(14) Strambini, L. M.; Longo, A.; Scarano, S.; Prescimone, T.; Palchetti, I.; Minunni, M.; Giannessi, D.; Barillaro, G. Self-powered microneedle-based biosensors for pain-free high-accuracy measurement of glycaemia in interstitial fluid, *Biosensors and Bioelectronics* **2015**, *66*, 162-168.

(15) Zhang, X.; Chen, G.; Bian, F.; Cai, L.; Zhao, Y. Encoded Microneedle Arrays for Detection of Skin Interstitial Fluid Biomarkers, *Advanced Materials* **2019**, *31*, 1902825.

(16) GhavamiNejad, A.; Li, J.; Lu, B.; Zhou, L.; Lam, L.; Giacca, A.; Wu, X. Y. Glucose-Responsive Composite Microneedle Patch for Hypoglycemia-Triggered Delivery of Native Glucagon, *Advanced Materials* **2019**, *31*, 1901051.

(17) Ventrelli, L.; Marsilio Strambini, L.; Barillaro, G. Microneedles for Transdermal Biosensing: Current Picture and Future Direction, *Advanced Healthcare Materials* **2015**, *4*, 2606-2640.

(18) Brown, S.; Zambrana, P. N.; Ge, X.; Bagdure, D.; Stinchcomb, A. L.; Rao, G.; Tolosa, L. Minimally invasive technique for measuring transdermal glucose with a fluorescent biosensor, *Analytical and Bioanalytical Chemistry* **2018**, *410*, 7249-7260.

(19) Yan, L.; Alba, M.; Tabassum, N.; Voelcker, N. H. Micro- and Nanosystems for Advanced Transdermal Delivery, *Advanced Therapeutics* **2019**, *2*, 1900141.

(20) Prausnitz, M. R. Microneedles for transdermal drug delivery, *Advanced Drug Delivery Reviews* **2004**, *56*, 581-587.

(21) Larrañeta, E.; Lutton, R. E. M.; Woolfson, A. D.; Donnelly, R. F. Microneedle arrays as transdermal and intradermal drug delivery systems: Materials science, manufacture and commercial development, *Materials Science and Engineering: R: Reports* **2016**, *104*, 1-32.

(22) Takeuchi, K.; Kim, B. Functionalized microneedles for continious glucose monitoirng, *Nano Convergence* **2018**, *5*, 28.

(23) Invernale, M. A.; Tang, B. C.; York, R. L.; Le, L.; Hou, D. Y.; Anderson, D. G. Microneedle Electrodes Toward an Amperometric Glucose-Sensing Smart Patch, *Advanced Healthcare Materials* **2014**, *3*, 338-342.

(24) Bollella, P.; Sharma, S.; Cass, A. E. G.; Tasca, F.; Antiochia, R. Minimally Invasive Glucose Monitoring Using a Highly Porous Gold Microneedles-Based Biosensor: Characterization and Application in Artificial Interstitial Fluid, *Catalysts* **2019**, *9*, 580.

(25) Valdés-Ramírez, G.; Li, Y.-C.; Kim, J.; Jia, W.; Bandodkar, A. J.; Nuñez-Flores, R.; Miller, P. R.; Wu, S.-Y.; Narayan, R.; Windmiller, J. R.; Polsky, R.; Wang, J. Microneedle-based self-powered glucose sensor, *Electrochemistry Communications* **2014**, *47*, 58-62.

(26) Kim, K. B.; Lee, W.-C.; Cho, C.-H.; Park, D.-S.; Cho, S. J.; Shim, Y.-B. Continuous glucose monitoring using a microneedle array sensor coupled with a wireless signal transmitter, *Sensors and Actuators B: Chemical* **2019**, *281*, 14-21.

(27) Hopcroft, M. A.; Nix, W. D.; Kenny, T. W. What is the Young's Modulus of Silicon?, *Journal of Microelectromechanical Systems* **2010**, *19*, 229-238.

(28) Rao Kondapally Seshasai, S.; Kaptoge, S.; Thompson, A.; Di Angelantonio, E.; Gao, P.; Sarwar, N.; Whincup, P. H.; Mukamal, K. J.; Gillum, R. F.; Holme, I.; Njolstad, I.; Fletcher, A.; Nilsson, P.; Lewington, S.; Collins, R.; Gudnason, V.; Thompson, S. G.; Sattar, N.; Selvin, E.; Hu, F. B., et al. Diabetes mellitus, fasting glucose, and risk of cause-specific death, *The New England Journal of Medicine* **2011**, *364*, 829-841.

(29) Visca, D.; Pignatti, P.; Spanevello, A.; Lucini, E.; La Rocca, E. Relationship between diabetes and respiratory diseases—Clinical and therapeutic aspects, *Pharmacological Research* **2018**, *137*, 230-235.

(30) Lee, H.; Song, C.; Hong, Y. S.; Kim, M. S.; Cho, H. R.; Kang, T.; Shin, K.; Choi, S. H.; Hyeon, T.; Kim, D. H. Wearable/disposable sweat-based glucose monitoring device with multistage transdermal drug delivery module, *Science Advances* **2017**, *3*, e1601314.

(31) Koschinsky, T.; Jungheim, K.; Heinemann, L. Glucose sensors and the alternate site testing-like phenomenon: relationship between rapid blood glucose changes and glucose sensor signals, *Diabetes Technology and Therapeutics* **2003**, *5*, 829-842.

(32) Chang, H.; Zheng, M.; Yu, X.; Than, A.; Seeni, R. Z.; Kang, R.; Tian, J.; Khanh, D. P.; Liu, L.; Chen, P.; Xu, C. A Swellable Microneedle Patch to Rapidly Extract Skin Interstitial Fluid for Timely Metabolic Analysis, *Advanced Materials* **2017**, *29*, 1702243.

(33) Coffey, J. W.; Meliga, S. C.; Corrie, S. R.; Kendall, M. A. F. Dynamic application of microprojection arrays to skin induces circulating protein extravasation for enhanced biomarker capture and detection, *Biomaterials* **2016**, *84*, 130-143.

(34) Xiao, X.; Si, P.; Magner, E. An overview of dealloyed nanoporous gold in bioelectrochemistry, *Bioelectrochemistry* **2016**, *109*, 117-126.

(35) Senel, M.; Dervisevic, M.; Voelcker, N. H. Gold microneedles fabricated by casting of gold ink used for urea sensing, *Materials Letters* **2019**, *243*, 50-53.

(36) Holzer, B.; Manoli, K.; Ditaranto, N.; Macchia, E.; Tiwari, A.; Di Franco, C.; Scamarcio, G.; Palazzo, G.; Torsi, L. Characterization of Covalently Bound Anti-Human Immunoglobulins on Self-Assembled Monolayer Modified Gold Electrodes, *Advanced Biosystems* **2017**, *1*, 1700055.

(37) Fail, C. A.; Evenson, S. A.; Ward, L. J.; Schofield, W. C. E.; Badyal, J. P. S. Controlled Attachment of PAMAM Dendrimers to Solid Surfaces, *Langmuir* **2002**, *18*, 264-268.

(38) Beamson, G.; Briggs, D. High Resolution XPS of Organic Polymers: The Scienta ESCA300 Database; Wiley, 1992.

(39) Hermanson, G. T. In Bioconjugate Techniques (Third Edition), Hermanson, G. T., Ed.; Academic Press: Boston, 2013, pp 951-957.

(40) Kucherenko, D. Y.; Kucherenko, I. S.; Soldatkin, O. O.; Topolnikova, Y. V.; Dzyadevych, S. V.; Soldatkin, A. P. A highly selective amperometric biosensor array for the simultaneous determination of glutamate, glucose, choline, acetylcholine, lactate and pyruvate, *Bioelectrochemistry* **2019**, *128*, 100-108.

(41) Şenel, M.; Nergiz, C.; Çevik, E. Novel reagentless glucose biosensor based on ferrocene cored asymmetric PAMAM dendrimers, *Sensors and Actuators B: Chemical* **2013**, *176*, 299-306.

(42) Şenel, M.; Nergiz, C.; Dervisevic, M.; Çevik, E. Development of Amperometric Glucose Biosensor Based on Reconstitution of Glucose Oxidase on Polymeric 3-Aminophenyl Boronic Acid Monolayer, *Electroanalysis* **2013**, *25*, 1194-1200.

(43) Araque, E.; Arenas, C. B.; Gamella, M.; Reviejo, J.; Villalonga, R.; Pingarrón, J. M. Graphene–polyamidoamine dendrimer–Pt nanoparticles hybrid nanomaterial for the preparation of mediatorless enzyme biosensor, *Journal of Electroanalytical Chemistry* **2014**, *717-718*, 96-102.

(44) Vieira, N. C.; Figueiredo, A.; de Queiroz, A. A.; Zucolotto, V.; Guimaraes, F. E. Self-assembled films of dendrimers and metallophthalocyanines as FET-based glucose biosensors, *Sensors* **2011**, *11*, 9442-9449.

(45) Liu, Y.; Wang, L.; Liu, J.; Di, Y. A study of human skin and surface temperatures in stable and unstable thermal environments, *Journal of Thermal Biology* **2013**, *38*, 440-448.

(46) Dawes, J. M.; Weir, G. A.; Middleton, S. J.; Patel, R.; Chisholm, K. I.; Pettingill, P.; Peck, L. J.; Sheridan, J.; Shakir, A.; Jacobson, L.; Gutierrez-Mecinas, M.; Galino, J.; Walcher, J.; Kuhnemund, J.; Kuehn, H.; Sanna, M. D.; Lang, B.; Clark, A. J.; Themistocleous, A. C.; Iwagaki, N., et al. Immune or Genetic-Mediated Disruption of CASPR2 Causes Pain Hypersensitivity Due to Enhanced Primary Afferent Excitability, *Neuron* **2018**, *97*, 806-822.e810.

(47) Chang, H.; Zheng, M.; Yu, X.; Than, A.; Seeni, R. Z.; Kang, R.; Tian, J.; Khanh, D. P.; Liu, L.; Chen, P.; Xu, C. A Swellable Microneedle Patch to Rapidly Extract Skin Interstitial Fluid for Timely Metabolic Analysis, *Advanced Materials* **2017**, *29*, 1702243.

(48) Bhargav, A.; Muller, D. A.; Kendall, M. A. F.; Corrie, S. R. Surface Modifications of Microprojection Arrays for Improved Biomarker Capture in the Skin of Live Mice, *ACS Applied Materials & Interfaces* **2012**, *4*, 2483-2489.

(49) Zhang, B.L.; Yang, Y.; Zhao, Z.Q.; Guo, X.D. A gold nanoparticles deposited polymer microneedle enzymatic biosensor for glucose sensing, *Electrochimica Acta* **2020**, *358*, 136917.

(50) Gao, J.; Huang, W.; Chen, Z.; Yi, C.; Jiang, L. Simultaneous detection of glucose, uric acid and cholesterol using flexible microneedle electrode array-based biosensor

and multi-channel portable electrochemical analyzer, *Sensors and Actuators B: Chemical* **2019**, *287*, 102-110.

(51) Kim, K.B.; Lee, W.C.; Cho, C.H.; Park, D.S.; Cho, S.J.; Shim, Y.B. Continous glucose monitoring using a microneedle array sensor coupled with a wireless signal transmitter, *Sensors and Actuators B: Chemical* **2019**, *281*, 14-21.

(52) Yoon, Y.; Lee, G.S.; Yoo, K.; Lee, J.B. Fabrication of a microneedle/CNT hierarchical micro/nano surface electrochemical sensor and its In-Vitro glucose sensing characterization, *Sensors* **2013**, *13*, 16672-16681.

(53) Invernale, M.A.; Tang, B.C.; York, R.L.; Le, L.; Hou, D.Y.; Anderson, D.G. Micorneelde electrodes towards an amperometric glucose-sensing smart patch, *Advanced Healthcare Materials* **2014**, *3*, 338-342.

(54) Lee, S.J.; Yoon, H.S.; Xuan, X.; Park, J.Y.; Paik, S.J.; Allen, M.G. A patch type non-enzymatic biosensor based on 3D SUS micro-needl electrode array for minimally invasive continous glucose monitoring, *Sensors and Actuators B: Chemical* **2016**, *222*, 1144.

(55) Windmiller, J.R.; Ramirez, G.V.; Zhou, N.; Zhou, M.; Miller, P.R.; Jin, C. ; Brozik, S.M.; Polsky, R.; Katz, E.; Narayan, R.; Wang, J. Biocomponent microneedle array biosensor for minimally-invasive glutamate monitoring, *Electroanalysis* **2011**, *23*, 2302-2309.

(56) Calio, A.; Dardano, P.; Di Palma, V.; Bevilacqua, M.F.; Di Matteo, A.; Iuele, H.; De Stefano, L. Polymeric microneedles based enzymatic electrodes for electrochemical biosensing of glucose and lactic acid, *Sensors and Actuators B: Chemical* **2016**, *236*, 343-349.

Appendices

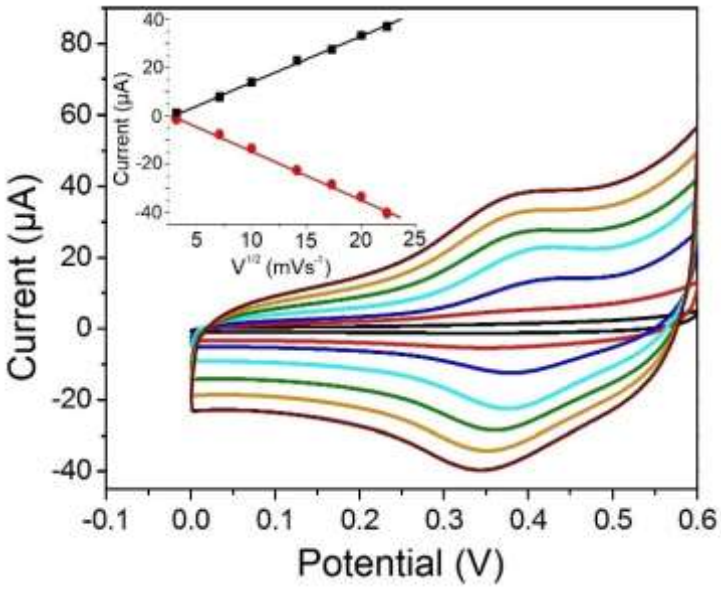

Figure S4.1: CV plot of Au-Si-MNA/Fc-PAMAM electrode at different scan rates, inset: anodic and cathodic peak currents versus the square root of the scan rate.

Table S4.1: Atomic ratios (X/C) calculated from average elemental compositions based on three replicates.

	Samples			
Atomic ratio (X/C)	**Au**	**Au/SAM**	**Au/SAM/Fc-PAMAM**	**Au/SAM/Fc-PAMAM/GOx**
Au	1.625 ± *0.194*	1.596 ± *0.069*	0.436 ± *0.181*	0.218 ± *0.046*
C1	0.734 ± *0.065*	0.713 ± *0.024*	0.596 ± *0.034*	0.517 ± *0.007*
C2	0.192 ± *0.063*	0.114 ± *0.023*	0.285 ± *0.028*	0.337 ± *0.004*
C3	0.036 ± *0.003*	0.048 ± *0.009*	0.100 ± *0.005*	0.124 ± *0.008*
C4	0.038 ± *0.005*	0.125 ± *0.008*	0.019 ± *0.002*	0.022 ± *0.003*
O	0.186 ± *0.018*	0.362 ± *0.021*	0.345 ± *0.054*	0.311 ± *0.007*
N	0.042 ± *0.002*	0.021 ± *0.004*	0.182 ± *0.038*	0.184 ± *0.010*
S	0.027 ± *0.009*	0.093 ± *0.012*	0.027 ± *0.011*	0.015 ± *0.002*
Fe			0.070 ± 0.*016*	0.022 ± *0.003*

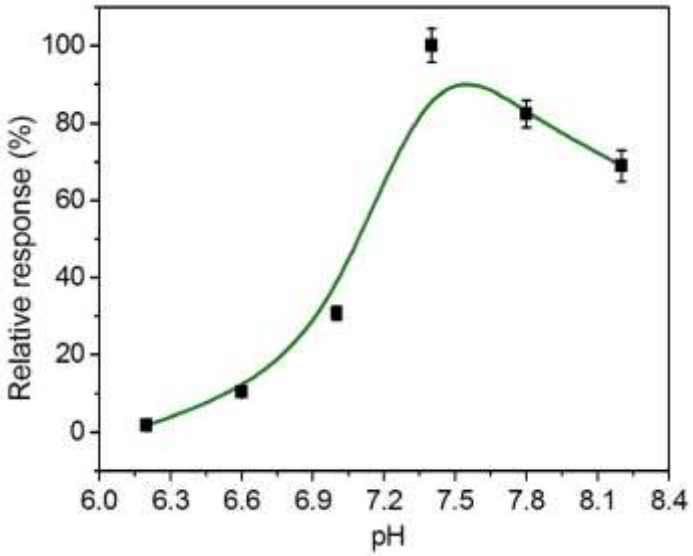

Figure S4.2: Electrochemical response of MNA glucose sensing patch with 0.35 V applied potential to 2 mM glucose in 0.1 M PBS at different pH ranging from 6.2 to 8.2 (SD n=3).

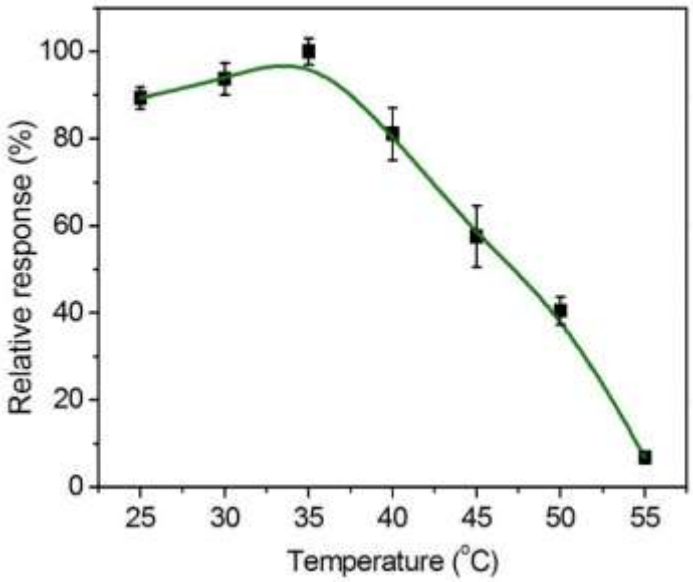

Figure S4.3: Electrochemical response of MNA glucose sensing patch with 0.35 V applied potential to 2 mM glucose in 0.1 M PBS at different temperatures ranging from 25ºC to 55ºC (SD n=3).

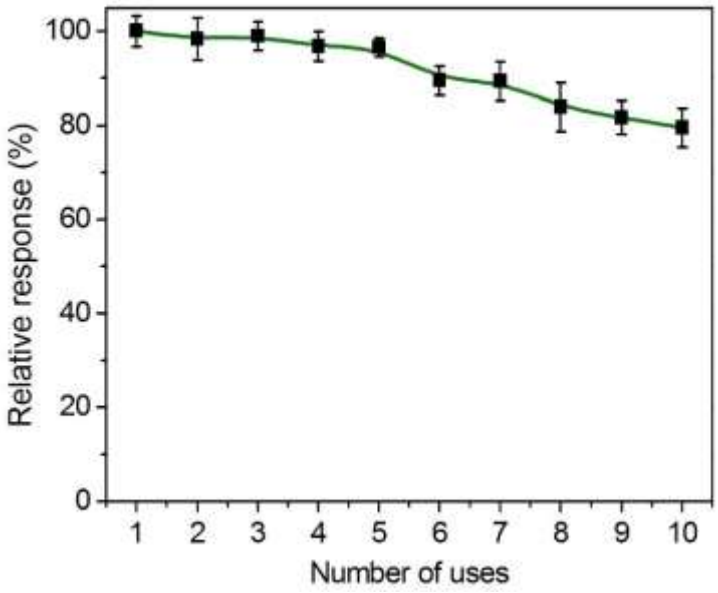

Figure S4.4: Reusability of the MNA-based biosensor preformed in 0.1 M PBS (pH 7.4) with 2 mM glucose and applied potential of 0.35 V (SD n=3).

Table S2. A comparison of the microneedle design, analytical performance parameters, and real sample application of Au-Si-MNA-based glucose sensor with previous reports.

Electrode	MN Height (µm)	MN Density (MN/cm^2)	E_{app} (V)	Sensitivity	Tested interference	Real sample	Ref.
PLA/Au/OPPy/ AuNPs	500	~22*	0.75	8.09 µA mM^{-1}	AA, Urea, Gly, AP	NR	[49]
GOx/Pt NPs/ PANI/MEA	600	NR	0.425	NR	UA, AA, Chol, Bil	In vitro: Serum	[50]
AuMN/pTCA	700	NR	0.45	0.017 and 0.22 µA mM^{-1} cm^{-2}	AA, AP, DA, UA, Hem, Cyto	In vitro: Blood	[51]
Pt/MWCNTs/MNs	380	~3500*	0.4	17.73 µA mM^{-1} cm^{-2}	NR	NR	[52]
Pt/Stainless steel-EDOT	680	~250*	0.4	NR	UA, AA, Cys, Urea, Fru	NR	[53]
Au/Pt black-Nafion	650	NR	0.4	1.62 µA mM^{-1}	AA, AP	In vivo: Rabbit	[54]
E200acryl-BMAE	1174	~450*	0.4	8 nA mM^{-1}	AA, UA, AP, Cys	NR	[55]
PEGDA	500	NR	0.3	18 nA mM^{-1}	NR	NR	[56]
Si-Au-MNA	~250	~9500	0.35	0.1622 µA mM^{-1} cm^{-2}	AA, UA, LA, DA, Gly	In vivo: Mice	This work

Abbreviations: NR= not reported, AA= ascorbic acid, UA= uric acid, LA= lactic acid, DA= dopamine, Gly=glycine, AP-acetaminophen, Hem- hemoglobin, Cyto= cytochrome C, Chol= Cholesterol, Bil= bilirubin, Fru=Fructose, PEGDA= poly(ethylene glycol) diacrylate, Cys= cystein.
* Calculated number of MN based on information provided in published work.

Chapter 5: Electrochemical Immunosensor for Breast Cancer Biomarker Detection Using High-density Silicon Microneedle Arrays

5.1 Introduction

Breast cancer is the most frequently encountered malignancy affecting women's health worldwide,[1] with almost 2.1 million newly recorded breast cancer cases in 2018 alone, according to the World Health Organization (WHO).[2,3] Breast cancer is an increasing problem worldwide, regardless of income, with an estimate of one new case diagnosed every 18 seconds.[1] This malignancy is curable in ~70-80% of early stage patients with a survival rate of 80% or greater in developed countries.[1] These figures underpin the importance of prompt diagnosis to ensure appropriate treatment and eventually improve the patient survival rate. In least developed countries, the survival rate decreases to below 40% [4] which is mainly attributed to the lack of tools for early diagnosis at an early stage of the disease, and the possibility to provide the required treatment.

Mammography, ultrasound imaging, and magnetic resonance imaging are among the methods commonly used for breast cancer diagnosis and to monitor its progression.[5] In order to support these technologies which can only perform image-based analysis localizing the cancer tissue, additional methods such as immunoblotting and immunohistochemistry,[6] enzyme-linked immunosorbent assay (ELISA),[7] fluorescence in-situ hybridization (FISH),[8] etc. are employed to specifically quantify breast cancer biomarkers. Indeed, to assist better with the diagnosis and establishment of cancer treatment, it is recommended to screen different breast cancer biomarkers such as the progesterone receptor (PR), estrogen receptor (ER), Ki-67, and human epidermal growth factor receptor.[9]

The human epidermal growth factor receptor 2 (HER2), also known as ErbB2, is a member of a family of human epidermal growth factors composed of ErbB1, ErbB2, ErbB3, and ErbB4, located on the surface of the epithelial cells.[10,11] The

interest of using ErbB2 as a breast cancer biomarker comes from its association with invasive breast cancers because it is involved in the signaling pathways that activate proliferation, cell survival, and metastasis.[1] Research data show that ErbB2 is overexpressed in ~20-25% of invasive breast cancers.[12] Healthy individuals have blood ErbB2 concentrations ranging from 2 to 15 ng/mL whereas ErbB2 concentration in breast cancer patients is above 15 ng/mL.[13,14] Shukla et al. evaluated the presence of ErbB2 oncoprotein in serum and tissue samples of 64 breast cancer patients using immunohistochemistry (IHC) and fluorescence in-situ hybridization (FISH) methods.[8] Reported results showed that ErbB2 concentrations in blood is ranging from 33.2 to 166.6 ng/mL, and ~ 65 ± 37 ng/mL (n=26) mean value was found in tissue samples of patients whereas the tissue of healthy individuals contained only ~19.6 ± 7.3 ng/mL (n=38).

Different technologies and sensing platforms such as nanotransistors,[15] photonic crystals,[16] microfluidics,[17] electrochemical biosensors,[3,18,19] etc. have been used for breast cancer biomarker detection. However, each one of these detection methods faces some limitations such as requiring high-cost equipment, sample pretreatment, or long analysis times. Therefore, a rapid, sensitive, and minimally invasive device for the detection of ErbB2 is expected to be a game-changer in the identification and follow-up of breast cancer patients.

This chapter describes a microneedle array (MNA)-based platform for the transdermal monitoring of the breast cancer biomarker ErbB2. MNA are a downsized form of conventional hypodermic needles which target interstitial fluid (ISF) or peripheral blood without causing pain or discomfort.[20] Up to date, MNA have been used for the electrochemical detection of different analytes such as glucose,[21] lactate,[22] urea,[23] L-dopamine, cholesterol,[24] and tyrosinase,[25] either by extracting ISF

or a specific biomarker followed by offline analysis, or by direct on skin ISF analysis without need for extraction or external analysis.[20] In this work, high-density silicon MNA (Si-MNA) are used to build sensing platform for simultaneously extraction and quantification of breast cancer biomarker ErbB2. The Si-MNA platform consists of ~9500 MNs/cm^2, conformally coated with a 150 nm thick gold (Au) layer, incorporated into a 3D printed holder to facilitate MNA application and used for extraction and electrochemical quantification of ErbB2 biomarker. The Au-Si-MNA electrode was functionalized by self-assembling of 3-mercaptopropionic acid which carboxylic groups were activated via carbodiimide chemistry to covalently bind anti-HER2 antibody. The Si-MNA-based immunosensor was able to detect ErbB2 in artificial ISF (aISF) with a linear range from 10 to 250 ng/mL and a detection limit of 4.8 ng/mL which is sufficient to cover the ErbB2 concentration range in both healthy individuals and cancer patients. Furthermore, a skin-mimicking phantom gel simulating epidermis and dermis layers of the skin was used to assess penetration efficiency and ErbB2 extraction. The Si-MNA-based immunosensor showed excellent skin model penetration ability as well as promising analytical performance in extraction and electrochemical quantification of ErbB2 biomarker. This type of technology shows promise for minimally invasive transdermal diagnosis and monitoring of cancer biomarkers and thus has high potential in early cancer detection.

5.2 Experimental Section

5.2.1 Materials

3-mercaptopropionic acid, 2-mercaptoethanol, 2-(N-morpholino)ethanesulfonic acid hydrate (MES), 1-ethyl-3-[3-dimethylaminopropyl] carbodiimide hydrochloride (EDC), N-hydroxysuccinimide (NHS), poly(ethylene glycol) (PEG) bis(amine), potassium hexacyanoferrate (III) ($K_3[FeCN_6]$), potassium hexacyanoferrate (II) trihydrate ($K_4[FeCN_6]\cdot 3H_2O$), 4-(2-hydroxyethyl)-1-piperazineethanesulfonic acid (HEPES), NaCl, NaOH, $MgSO_4$, $CaCl_2$, KCl, sucrose, sodium salt, gelatin, agar, glycerol, insulin, and IgG from goat were purchased from Sigma Aldrich Chemical Co. H_2O_2, Na_2HPO_4 and NaH_2PO_4 were purchased from Merck. Ammonia solution was obtained from AJAX. H_2SO_4 and HCl were purchased from J.T. Baker. All chemicals were of analytical grade and were used without further purification. Anti-HER2 antibody and ErbB2 were kindly supplied by Dr Adams from CSIRO.

5.2.2 Immunosensor Preparation

Si-MNA-based electrodes (Figure 5.1a) were fabricated using procedures described in Chapter 4 (see section 4.2.2). Prior to functionalization, the Au-Si-MNA electrode surface was cleaned first by thoroughly rinsing the electrode with ethanol and acetone, and then the electrode was immersed in base piranha solution composed of aqueous solution of 1.5 wt% ammonia, and 5.4 wt% H_2O_2, for 1 min at 80^{o}C, followed by rinsing with dH_2O [26]. The electrode was then incubated in a 2 mM aqueous solution of 3-mercaptopropionic acid overnight, allowing the formation of a self-assembled monolayer (SAM) via reaction of thiol groups with the Au surface. After rinsing the electrode with dH_2O, it was immersed in a 2 mM aqueous solution of 2-mercaptoethanol for 30 min for the purpose of the backfilling of any exposed Au

surface. Next, the electrode was immersed in a 1:1 mixture of 10 mg/mL EDC and 15 mg/mL NHS prepared in 10 mM MES buffer pH 5 for 45 min. The NHS ester functionalized Au-Si-MNA electrode was then immersed in 25 µg/mL anti-HER2 antibody solution prepared in 10 mM PBS for 4 h. The electrode was then rinsed with 10 mM PBS in order to remove unbound anti-HER2. The residual NHS sites were blocked by reaction with NH_2 functionalized PEG (1 mg/mL solution) for 30 min. Finally, the Au-Si-MNA/anti-HER2 electrode was once more rinsed with 10 mM PBS and, when not in use, it was stored in 10 mM PBS at 5^{o}C.

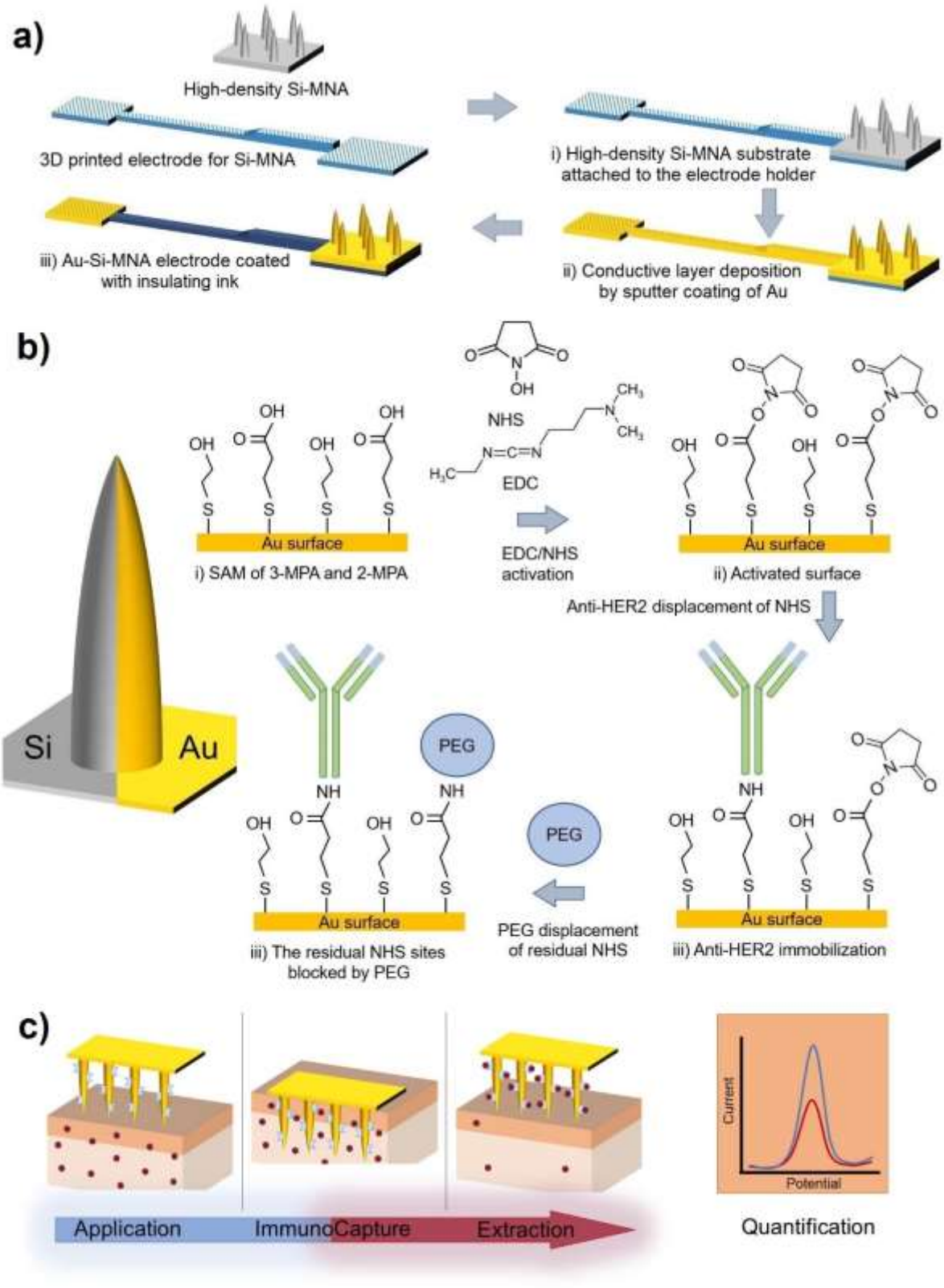

Figure 5.1: Schematic illustrations of **a)** MNA electrode preparation, **b)** surface modification and anti-HER2 monoclonal antibody immobilization on Au-Si-MNA electrode, and **c)** detection principle of MNA-based immunosensor.

5.2.3 Electrochemical Detection

A CHI 650E (CH Instruments, USA) electrochemical analyzer was used for all electrochemical measurements. Differential pulse voltammetry (DPV) measurements were performed by scanning the potential from -0.3 to 0.5 V in an electrochemical setup including Au-Si-MNA/anti-HER2, Au-Si-MNA, and Au-Si-MNA modified with AgCl ink, as working, counter and reference electrodes, respectively. All measurements were performed in a solution of 5 mM $K_4[Fe(CN)_6]$ and 5 mM $K_3[Fe(CN)_6]$ in 0.1 M KCl. The anti-HER2-modified Au-Si-MNA working electrode was incubated during 1 h in artificial interstitial fluid (aISF) spiked with known concentrations of ErbB2 ranging from 10 to 250 ng/mL. aISF consisted of 10 mM HEPES, 3.5 mM KCl, 123 mM NaCl, 1.5 mM NaH_2PO_4, 7.4 mM sucrose, 2.2 mM $CaCl_2$, and 0.7 mM $MgSO_4$ prepared in dH_2O and the pH was adjusted to 7.4 [27]. The antibody-antigen binding was monitored through the changes in the current intensities obtained from DPV measurements performed before and after incubation of aISF spiked with ErbB2 (Figure 5.1c). Control experiments were carried out using a working electrode modified with a goat IgG, following the same immobilization method used for the anti-HER2-modified Au-Si-MNA electrode. Error bars illustrate the standard deviation (SD) of three measurements (n = 3) unless otherwise stated.

5.2.4 Preparation of Skin-Mimicking Phantom Gel

Phantom gels composed of epidermis and dermis layers were prepared according to a procedure reported by Chen et al.[28] with slight modifications. The epidermis mimicking layer is composed of 10 wt% gelatin and 5 wt% of glycerol prepared in aISF, after which 0.1 wt% glutaraldehyde was added to the mixture. Dermis mimicking layer is composed of 24 wt% gelatin and 1 wt% agar prepared in

aISF. The phantom gel was fabricated using 3D printed molds. The molds used for epidermis and dermis layer fabrication had a height of 120 µm and 1.5 mm, respectively. The mixture used for dermis layer fabrication was initially heated up to ~70^{o}C under constant mixing until all constituents completely dissolved. The final solution was cooled to 40^{o}C and then it was casted onto the mold and left to cool for 2 h at room temperature. The gel samples used for the calibration plot experiments were prepared by spiking them with known concentrations of ErbB2 biomarker (10-250 ng/mL). Later on, the epidermis layer mixture, also heated up to ~70^{o}C and cooled to 40^{o}C under constant stirring, was poured on top of the solidified dermis layer and left to cool down at room temperature. Detection of ErbB2 using Au-Si-MNA/anti-HER2 immunosensor was performed by extracting the biomarker from the phantom gel and analyzing the changes observed in the DPV signal caused by the binding of ErbB2. The immunosensor was gently inserted in the phantom gel, incubated for 1 h, thoroughly washed with PBS after removing it from the phantom gel, and finally used for DPV analyses in K_4[Fe $(CN)_6$]/K_3[$Fe(CN)_6$] solution.

5.3 Results and Discussion

5.3.1 Morphological Characterization of MNA-based Immunosensor

A field-emission gun scanning electron microscope (FEG-SEM, FEI NovaNano SEM 430) was used to characterize the Au-Si-MNA electrode. Figure 5.2 illustrates SEM micrographs of tilted (Figure 5.2a), top (Figure 5.2b), and cross-sectional (Figure 5.2c) views of Au-Si-MNA. Micrographs show hexagonal arrangement of MN with a density of ~9500 MNs/cm^2 with MN height of ~250 µm, a base diameter of ~50 µm, and space between two adjacent cone centers of ~110 µm. At increased magnification represented in the inset of Figure 5.2c, the sharpness of individual needle tips of ~2

µm diameter was apparent. Density, shape, size, and sharpness of fabricated MNA are ideal for the painless penetration of stratum corneum and interfacing the ISF in the epidermis and dermis layers of the skin, since the thickness of the epidermal layer can range from 36 to 61 µm on human forearm and 100 µm on the wrist [29,30], with the dermis layer ranging from 500 to 2000 µm [20].

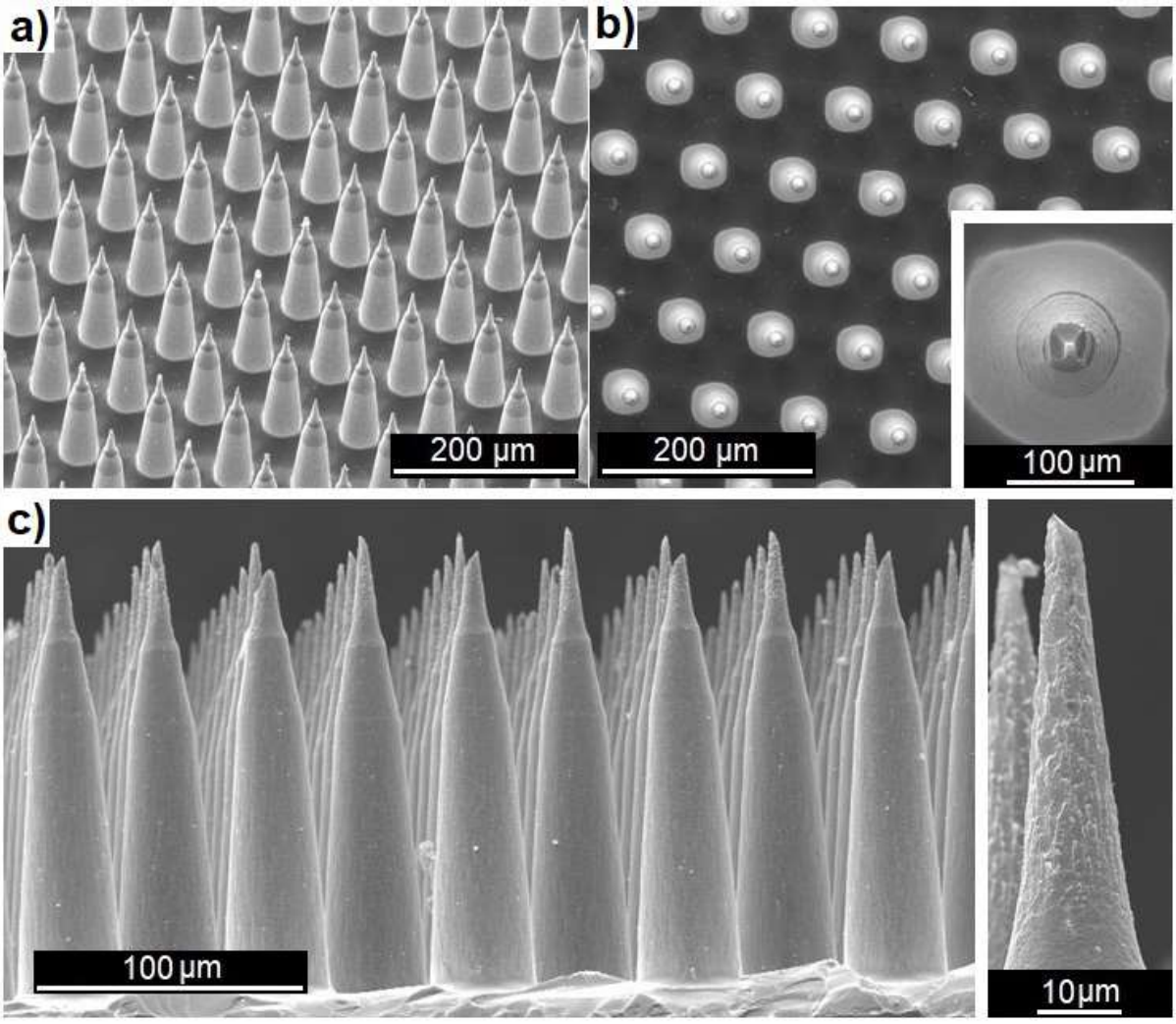

Figure 5.2: SEM micrographs of **a)** tilted view, **b)** top view (inset: top view of single microneedle) and **c)** cross-sectional view (inset: cross-sectional view of microneedle tip) of Au-Si-MNA.

5.3.2 Electrochemical Characterization

The preparation of Au-Si-MNA electrodes was electrochemically characterized using cyclic voltammetry (CV), DPV, and electrochemical impedance spectroscopy (EIS) using Au-Si-MNA as working and counter electrodes, and Au-Si-MNA modified with AgCl ink as reference electrode. First, a CV in 0.5 M H_2SO_4 was applied to determine the active surface area of the working electrode (Figure 5.3a) [31]. The active surface area can be calculated using the charge of the reduction peak divided by the charge per microscopic unit area of Au which was previously determined to be 390 µC cm^{-2} [31]. In Figure 5.3a, the oxidation peaks of the deposited Au layer can be observed within 0.93 to 1.20 V, and reduction of oxidized Au can be seen at 0.7 V. The active surface area of Au-Si-MNA electrode is illustrated in the inset of Figure 5.3a and was found to be 0.97 cm^2, four times higher than the geometric surface area. This increase in active surface area is attributed to the high density of MNA which allows to fit ~9,500 microneedles/cm^2.

The surface modification of the Au-Si-MNA electrode was electrochemically characterized to confirm the immobilization of anti-HER2 antibody on MNA and binding of ErbB2 antigen. DPV and EIS measurements, represented in Figure 5.3b and 5.3c, respectively, show step-by-step modification of MNA by SAM formation and immobilization of anti-HER2 antibody, and binding of ErbB2 antigen. As expected, the current intensity decreased and charge transfer resistance (Rct) increased for the Au-Si-MNA electrode upon Au surface functionalization with SAM and immobilization of anti-HER2 antibody. Besides, to demonstrate the feasibility of the Au-Si-MNA/anti-HER2 electrode to detect ErbB2, ErbB2 antigen was incubated on the surface, causing further decrease in the peak current and increase in Rct which indicates successful antigen-antibody interaction. Both DPV and EIS results confirm immobilization of anti-

HER2 on the electrode surface as well as successful binding of ErbB2 antigen. Furthermore, the redox properties of the Au-Si-MNA/anti-HER2 electrode were studied using CV by applying different scan rates ranging from 10 to 150 mV/s. Figure S5.1 in the Appendix shows well-defined oxidation-reduction peaks of the ferro/ferricyanide redox couple. Increase in scan rate resulted in increase of oxidation and reduction peaks with potentials shifted in positive and negative directions, respectively, indicating a quasi-reversible process. Current peak values of oxidation-reduction peaks are represented in Figure S5.2 in the form of a linear plot of current *versus* square root of the scan rates and the linearity of both oxidation and reduction peaks show a diffusion-controlled electron transfer process occurring at the MNA electrode surface.

5.3.3 Spectroscopic Analysis

XPS analysis was used to characterize the surface modification of Au-Si-MNA working electrode at each step of the functionalization process: pre-cleaned Au, SAM of 3-mercaptopropionic acid, and immobilization of anti-HER2 antibody (Figure 5.3d). A summary of the results, represented as atomic ratios with respect to elemental carbon, is shown in Table S5.1. The atomic composition of Au decreases as the functionalization progresses, as represented by the significant decrease in the Au/C ratio, which is consistent with the modification of the bare Au-Si-MNA surface with SAMs and the attachment of the HER2 antibody [32]. The efficient coverage of precleaned Au-Si-MNAs with carboxylic acid terminated alkanethiols was confirmed by the increase in sulfur and oxygen atomic concentrations. The S/C and O/C atomic ratio after SAM functionalization are distinctly above the ratios of untreated Au-Si-MNA, confirming the presence of –COOH terminated SAMs. The high-resolution C 1s

XPS curves (Figure 5.3d) shows a main peak centered at ~285 eV (C1 component), which can be ascribed to aliphatic carbons from alkyl chains. The carbon present on pre-cleaned Au-Si-MNAs most likely indicates the presence of adventitious carbon. After SAM modification, a significant increase in the C4 component (representative of O–C=O– functionalities centered at ~288.5 eV) becomes evident. The shoulder centered at ~286.5 eV (C2 component) represents the carbon next to the sulfur atoms. Following EDC/NHS activation and incubation with anti-HER2, the bioconjugated MNA displayed a significantly higher carbon and nitrogen content compared to SAM-modified Au-Si-MNA. After anti-HER2 immobilization, the C 1s spectrum is significantly modified. While the C1 component can still be attributed to aliphatic carbons, the higher binding energy peaks can be assigned to the various C-N and C-O based functional groups in the polypeptide (C2) and the characteristic peptide bonds of the immobilized antibody (C3). The latter components (C2, C3) were observed to increase significantly in intensity, confirming the presence of the antibody [32]. The carboxylic acid signal originating from the SAM is no longer detectable, indicating an efficient immobilization of the antibody onto the activated SAM layer.

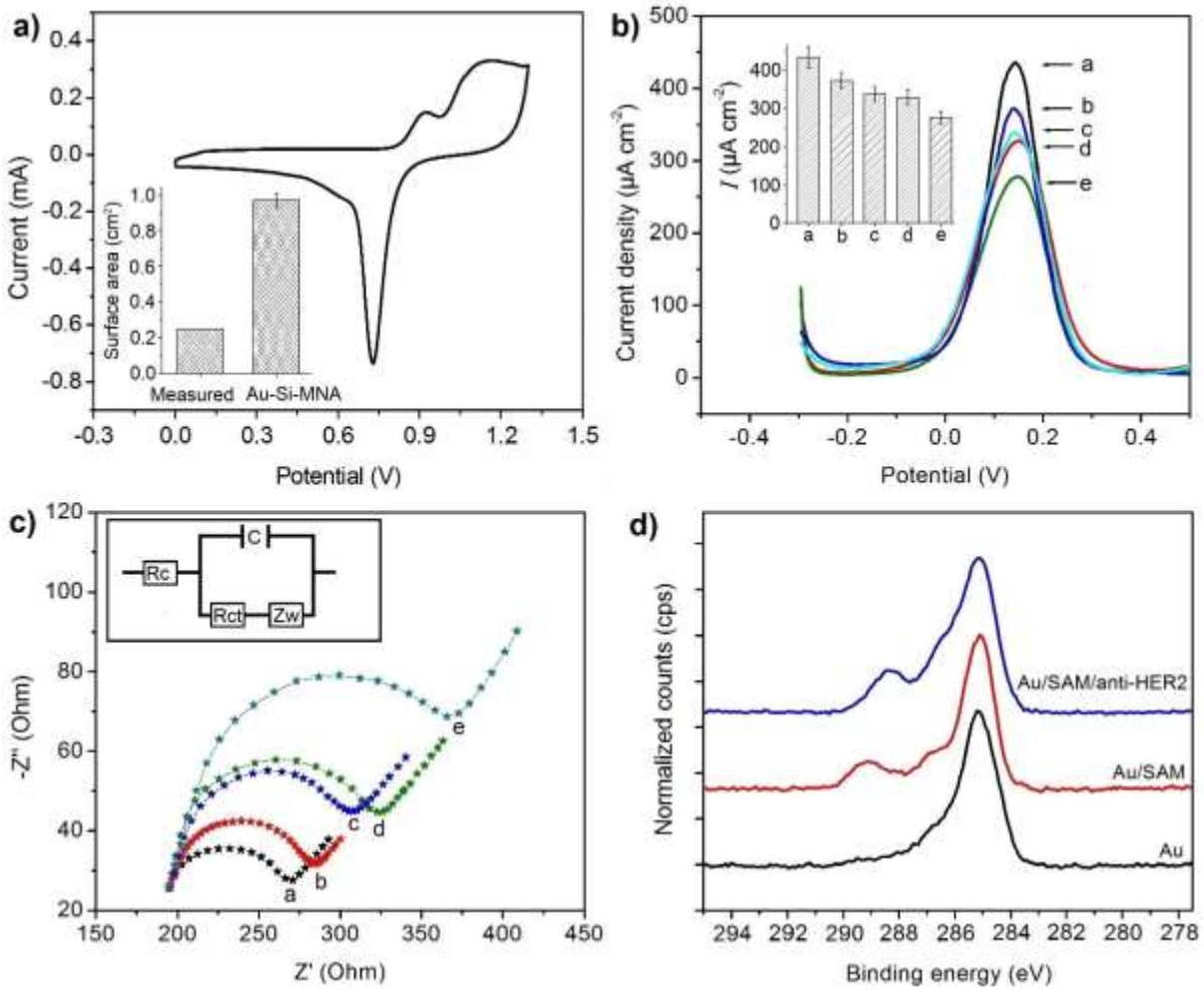

Figure 5.3: Characterization of MNA-based immunosensor. **a)** CV recorded in a 0.5 M H_2SO_4 solution (inset: histogram showing a comparison of the measured surface area and calculated active surface area (SD of n=3)). **b)** DPV and **c)** EIS plots obtained after each step of the electrode modification: a) Au-Si-MNA, b) SAM, c) after immobilization of anti-HER2 antibody, d) PEG, and e) after ErbB2 conjugation (150 ng/mL) (insets: of B) histogram showing current comparison of DPV peaks (SD of n=3), and C) Randles equivalent circuit used for fitting). Measurements were performed in 5 mM $K_4[Fe(CN)_6]/K_3[Fe(CN)_6]$ (1:1 ratio) in 0.1 M KCl. **d)** XPS high resolution spectra of the C 1s obtained after each functionalization step: pre-cleaned Au (black); SAM modification (red); and immobilization of anti-HER2 (blue).

5.3.4 Optimization of the MNA-Based Immunosensor

In order to maximize the performance of the immunosensor, the experimental parameters such as the concentration of anti-HER2 used for the electrode modification and ErbB2 incubation time were optimized. To evaluate the immobilization of anti-HER2 antibody, electrodes were prepared as previously described in section 5.2.2 and then incubated in 10 mM PBS solutions containing different concentrations of antibody for 1 h. Antibody concentrations used in this study ranged from 4 to 75 µg/mL. Figure S5.3 shows the increase in current density change (ΔI) with increase of the antibody concentration. ΔI is difference of the oxidation current density measured before (I_0) and after incubation (I) of Au-Si-MNA/anit-HER2 with ErbB2 biomarker ($\Delta I = I_0 - I$). Current change reached a plateau for the immunosensor prepared with 25 µg/mL anti-HER2 antibody which indicates saturation of the electrode surface with antibody. Thus, 25 µg/mL was selected as the optimum concentration for the fabrication of the immunosensor. Various ErbB2 incubation times were tested to determine the optimum time to maximize the binding of ErbB2 to immobilized anti-HER2. Figure S5.4 shows the change in current density of the recorded DPV of Au-Si-MNA/anti-HER2 incubated with the same concentration of ErbB2 biomarker (150 ng/mL) for different time intervals ranging from 10 min to 2 h. The change in current density drastically increased during the first 40 min of incubation and later reached its maximum at 60 min. Further increase in the incubation time did not have significant effect on the current change. Therefore, 60 min was selected as optimum incubation time.

5.3.5 Detection of ErbB2 Breast Cancer Biomarker

A set of control experiments was performed using goat IgG in order to confirm the affinity of immobilized anti-HER2 antibody towards ErbB2. Figure 5.4a shows DPV plots of Au-Si-MNA/anti-HER2 and Au-Si-MNA/IgG electrodes, recorded before and after incubation in aISF containing 150 ng/mL of ErbB2 biomarker. The current density change for IgG modified electrode (control) was insignificant comparing to anti-HER2 modified electrode (inset of the Figure 5.4a). This result confirms that Au-Si-MNA/anti-HER2 electrode has high affinity towards targeted breast cancer biomarker, ErbB2.

The analytical performance of MNA immunosensors was studied by incubating Au-Si-MNA/anti-HER2 electrode in aISF spiked with different concentrations of ErbB2 biomarker. The sensing principle of the MNA immunosensor is based on determining the changes in the diffusion of the redox probe towards the electrode surface as a result of the ErbB2 biomarker binding of to the antibody modified Au-Si-MNA. Figure 5.4b shows the DPV signal obtained by scanning the potential from -0.3 to 0.5 V after incubating the working electrode in aISF with different concentrations of ErbB2 ranging from 10 to 250 ng/mL for 1 h. Increase in ErbB2 concentration gradually decreased the intensity of the current peak produced by the oxidation of $K_4[Fe(CN)_6]$. This correlation is demonstrated in Figure 5.4c, where a linear increase in the current density change is observed with increasing ErbB2 concentrations. The change in current density (ΔI) represented in Figure 5.4c corresponds to the difference of the oxidation current density measured before and after incubation of Au-Si-MNA/anit-HER2 with ErbB2 biomarker ($\Delta I = I_0 - I$) at 0.15 V. The dynamic range of the immunosensor ranged from 10 to 250 ng/mL with a correlation coefficient of 0.9987 and linear regression equation of ΔI = 0.3978[ErbB2] + 10.282. This linear range of MNA-based immunosensor is suitable for the detection of ErbB2 in breast cancer

patients since the ErbB2 concentration in serum ranges from 33.2 to 166.6 ng/mL and in cancer tissue can reach 65.38 ng/mL.[8] The limit of detection of MNA-based immunosensor is 4.8 ng/mL which is similar to the concentration of ErbB2 found in healthy individuals.[33]

The MNA-based immunosensor was tested against potentially interfering components prepared in aISF such as glucose (4 mM), glycine (100 µM), insulin (150 ng/mL), T4 bacteriophage (10^5 pfu/mL), and NaCl (123 mM). Selected potentially interfering molecules such as glucose, glycine, and insulin are most likely to be found in ISF of the skin, whereas T4 bacteriophage is selected based on its size and likeliness that similar seized spices potentially could affect the sensors performance. Figure 5.4d shows a column plot derived from the obtained DPV signal from which no significant changes are observed for components other than ErbB2, suggesting that the MNA-based immunosensor has an excellent selectivity for ErbB2 biomarker in the presence of different molecules at high concentrations. Furthermore, the effect of different types of media such as 0.1 M PBS (pH 7.4) and aISF (pH 7.4) on the performance of the immunosensor was tested. As shown in Figure 5.4d no significant change in current response was observed showing that functionality of immunosensor does not depend on the medium which also confirms its stability.

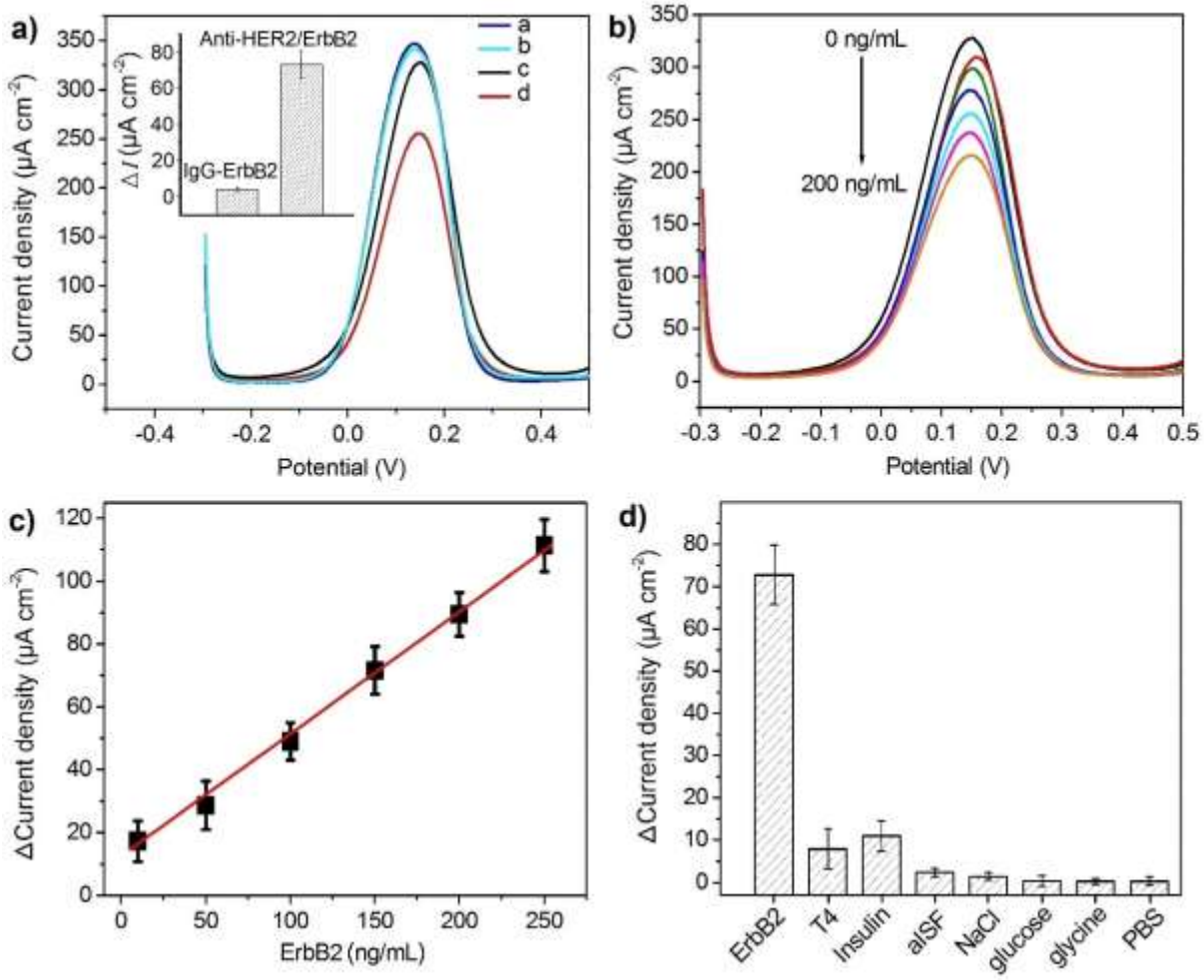

Figure 5.4: a) DPV plots of control experiments carried out using Au-Si-MNA electrodes modified with IgG (a, b) and anti-HER2 (c, d) antibodies before (a, c) and after (b, d) incubation; inset: histogram illustrates the change in the DPV current density after incubation with ErbB2 (SD of n=3)). ErbB2 breast cancer biomarker detection and quantification with a MNA-based immunosensor. **b)** DPV of Au-Si-MNA/anti-HER2 electrode with different concentrations of ErbB2 ranging from 10 to 250 ng/mL in aISF and **c)** calibration curve of Au-Si-MNA/anti-HER2 sensing electrode obtained at 0.15 V (SD, n=3). **d)** Selectivity of Au-Si-MNA/anti-HER2 immunosensor upon incubation in 150 ng/mL of Erbb2, 10^5 pfu/mL T4 bacteriophage, 150 ng/mL insulin, aISF, 5 mM glucose, and 100 μM glycine, all prepared in aISF, 123 mM NaCl prepared in dH_2O, and 0.1 M PBS (SD of n=3).

5.3.6 Detection of ErbB2 Biomarker in Skin-Mimicking Phantom Gel

The performance of Au-Si-MNA/anti-HER2 electrode was studied implementing a skin-mimicking phantom gel that was fabricated using a 3D printed mold (Figure 5.5c). The phantom gel was prepared containing ErbB2 biomarker at a 10-250 ng/mL concentration. Due to the differences in the chemical composition of the phantom model (described in section 5.2.4) we could model both epidermis and dermis layers, with the mock epidermis layer (100 ± 40 µm thickness) being clearly distinguished on top of the mock dermis layer in the fabricated phantom gel (Figure 5.5d). First, this gel was used for testing the penetration of the MNA-based electrode. The footprint of the MNA in the form of hexagonally arranged circular microscale craters can be observed in Figure 5.5e, demonstrating successful penetration of the MNA that is critical for our transdermal biosensor. The size and design of the current microneedles allowed for a sufficient skin penetration and are long enough to be used for the extraction of a biomarker from skin ISF based on the previous studies that achieved extraction when using ~150 µm long MNA. [34] Figure 5.5a shows the calibration curve derived from the DPV plots that was obtained after ErbB2 extraction from the phantom gel and subsequent electrochemical detection. The linear range of the immunosensor in skin-mimicking phantom gel is from 50 to 250 ng/mL with detection limit of 25 ng/mL, allowing the detection of ErbB2 biomarker in breast cancer tissue.[8] When compared to the analytical performance obtained in aISF, the performance of the immunosensor in phantom gel is slightly lower due to the difference in antibody-antigen binding environment. In other words, aISF solution allows for a faster diffusion of the antigen towards the antibodies immobilized on the electrode surface. This diffusion is limited in phantom gel because of its higher viscosity. Overall, these results indicate the high potential of the MNA-based immunosensor towards the point-of-care diagnostics by

extraction and quantification of ErbB2 biomarker without needing further sample treatment. In the literature, the detection of biomarkers from ISF has been performed using two different MN-based approaches that involve the extraction and quantification of the biomarkers. The first approach uses hollow MN to extract complete ISF whilst the second one employs antibody-modified MN to extract biomarkers only.[20,34,35] Both methods require post extraction quantification of the biomarker. A disadvantage of the ISF extraction approach is the requirement of the additional sample pre-treatment steps due to the biological complexity of the ISF, and current major drawback of the direct extraction of the biomarkers using MN is the requirement for long and labor-intensive analysis techniques such as ELISA. We believe that Au-Si-MNA/anti-HER2 electrochemical immunosensor can provide efficient solution for both problems mentioned above. High-density MNA not only serves as a method for extraction of biomarker from the skin that is completed within 1 h, but also as an electrochemical transducer which simplifies the quantification of the biomarker providing response in only ~1 min and avoids the complexity of ELISA-like methods.

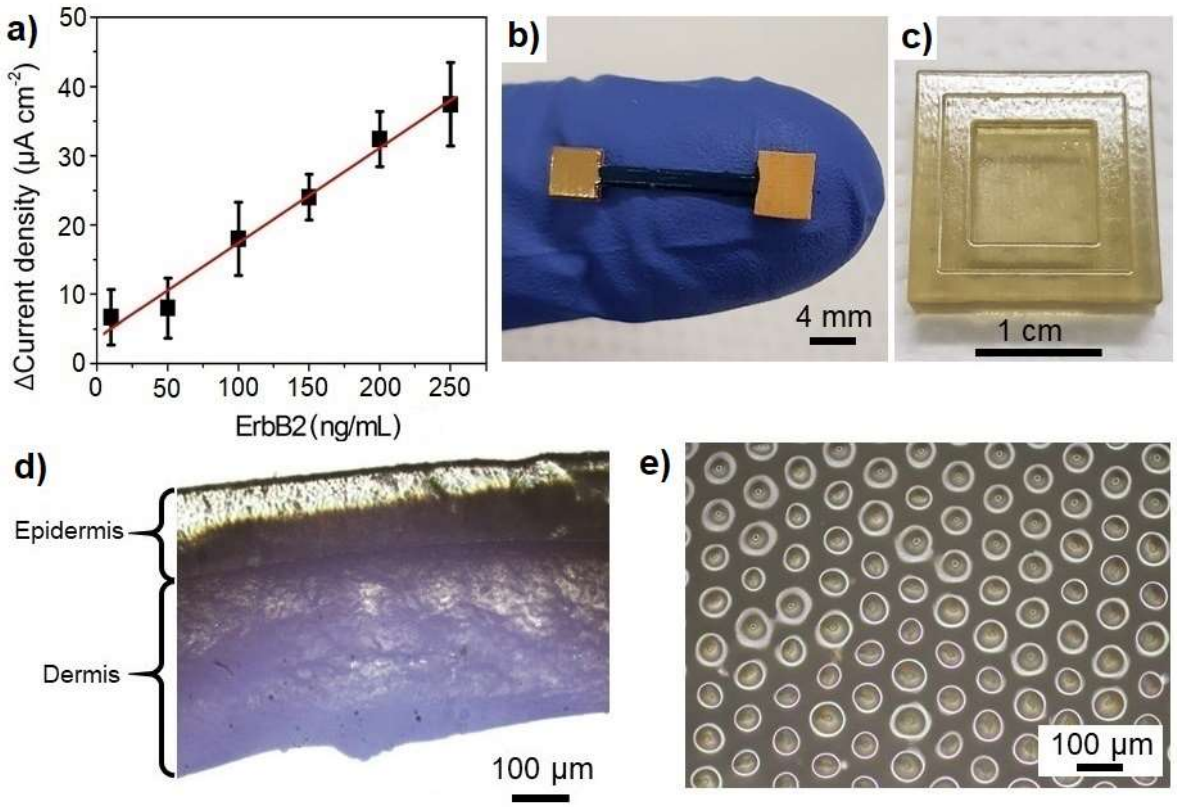

Figure 5.5: Testing of Au-Si-MNA/anti-HER2 immunosensor using skin-mimicking phantom gel. **a)** Calibration curve of DPV signals obtained after incubation of immunosensor in phantom gel (SD of n=3). Optical images of **b)** Au-Si-MNA electrode and **c)** 3D printed mold used for the preparation of the phantom gel. Light-microscope images of **d)** cross section of the phantom gel mimicking epidermis and dermis layers, and **E)** top view of the phantom gel after applying Au-Si-MNA electrode.

5.4 Conclusions

This chapter presents a high-density MNA-based electrochemical immunosensor for the detection of ErbB2 breast cancer biomarker. For the first time, high-density Au-Si-MNA were simultaneously used as a biomarker extraction platform and also as an *in situ* electrochemical transducer for the quantification of the captured biomarker. The size, shape, and conformation of MNA were characterized with SEM while the surface functionalization and the antibody immobilization were analyzed with XPS and electrochemical methods. As a proof of concept, the MNA-based immunosensor was tested using a carefully designed phantom gel that mimics the epidermis and dermis layers from where ErbB2 biomarker was extracted and quantified via DPV. MNA-based immunosensors allow for the detection of ErbB2 biomarker over a wide concentration range from 10 to 250 ng/mL with a detection limit of 4.8 ng/mL in aISF and 50 to 250 ng/mL a detection limit of 25 ng/mL in the phantom gel, and response time of ~1 min. These analytical performance of immunosensor is sufficient for detecting ErbB2 biomarker in the interstitial fluid and tissue of breast cancer patients. This MNA-based sensing platform is suitable for the modification with various biological recognition elements and can be applied for the sensing of different cancer biomarkers. Future work will focus on *in-vivo* application of the MNA-based transdermal sensing platform for the extraction and quantification of significant biomarkers from the ISF.

5.5 References

(1) Harbeck, N.; Penault-Llorca, F.; Cortes, J.; Gnant, M.; Houssami, N.; Poortmans, P.; Ruddy, K.; Tsang, J.; Cardoso, F. Breast cancer, *Nature Reviews Disease Primers* **2019**, *5*, 66.

(2) World Health Organization (WHO). Cancer, https://www.who.int/news-room/fact-sheets/detail/cancer, **2018**.

(3) Senel, M.; Dervisevic, M.; Kokkokoğlu, F. Electrochemical DNA biosensors for label-free breast cancer gene marker detection, *Analytical and Bioanalytical Chemistry* **2019**, *411*, 2925-2935.

(4) Coleman, M. P.; Quaresma, M.; Berrino, F.; Lutz, J.-M.; De Angelis, R.; Capocaccia, R.; Baili, P.; Rachet, B.; Gatta, G.; Hakulinen, T.; Micheli, A.; Sant, M.; Weir, H. K.; Elwood, J. M.; Tsukuma, H.; Koifman, S.; e Silva, G. A.; Francisci, S.; Santaquilani, M.; Verdecchia, A., et al. Cancer survival in five continents: a worldwide population-based study (CONCORD), *The Lancet Oncology* **2008**, *9*, 730-756.

(5) Ali, M. A.; Mondal, K.; Singh, C.; Dhar Malhotra, B.; Sharma, A. Anti-epidermal growth factor receptor conjugated mesoporous zinc oxide nanofibers for breast cancer diagnostics, *Nanoscale* **2015**, *7*, 7234-7245.

(6) Kerns, B. J.; Pence, J. C.; Huper, G.; Kinney, R. B.; Iglehart, J. D. c-erbB-2 expression in breast cancer detected by immunoblotting and immunohistochemistry, *Journal of Histochemistry & Cytochemistry* **1990**, *38*, 1823-1830.

(7) Agnolon, V.; Contato, A.; Meneghello, A.; Tagliabue, E.; Toffoli, G.; Gion, M.; Polo, F.; Fabricio, A. S. C. ELISA assay employing epitope-specific monoclonal antibodies to quantify circulating HER2 with potential application in monitoring cancer patients undergoing therapy with trastuzumab, *Scientific Reports* **2020**, *10*, 3016.

(8) Shukla, S.; Singh, B. K.; Pathania, O. P.; Jain, M. Evaluation of HER2/neu oncoprotein in serum & tissue samples of women with breast cancer, *The Indian Journal of Medical Research* **2016**, *143*, S52-S58.

(9) Colomer, R.; Aranda-López, I.; Albanell, J.; García-Caballero, T.; Ciruelos, E.; López-García, M. Á.; Cortés, J.; Rojo, F.; Martín, M.; Palacios-Calvo, J. Biomarkers in breast cancer: A consensus statement by the Spanish Society of Medical Oncology and the Spanish Society of Pathology, *Clinical and Translational Oncology* **2018**, *20*, 815-826.

(10) Leyland-Jones, B.; Smith, B. R. Serum HER2 testing in patients with HER2-positive breast cancer: the death knell tolls, *Lancet Oncol* **2011**, *12*, 286-295.

(11) Roskoski, R. The ErbB/HER family of protein-tyrosine kinases and cancer, *Pharmacological Research* **2014**, *79*, 34-74.

(12) Esteva, F. J.; Cheli, C. D.; Fritsche, H.; Fornier, M.; Slamon, D.; Thiel, R. P.; Luftner, D.; Ghani, F. Clinical utility of serum HER2/neu in monitoring and prediction of progression-free survival in metastatic breast cancer patients treated with trastuzumab-based therapies, *Breast cancer research : BCR* **2005**, *7*, R436-443.

(13) Meenakshi, A.; Suresh Kumar, R.; Siva Kumar, N. ELISA for quantitation of serum C-erbB-2 oncoprotein in breast cancer patients, *Journal of Immunoassay and Immunochemistry* **2002**, *23*, 293-305.

(14) Capobianco, J. A.; Shih, W. Y.; Yuan, Q.-A.; Adams, G. P.; Shih, W.-H. Label-free, all-electrical, in situ human epidermal growth receptor 2 detection, *The Review of Scientific Instruments* **2008**, *79*, 076101.

(15) Yu, X.; Munge, B.; Patel, V.; Jensen, G.; Bhirde, A.; Gong, J. D.; Kim, S. N.; Gillespie, J.; Gutkind, J. S.; Papadimitrakopoulos, F.; Rusling, J. F. Carbon nanotube

amplification strategies for highly sensitive immunodetection of cancer biomarkers, *Journal of the American Chemical Society* **2006**, *128*, 11199-11205.

(16) Chan, L. L.; Gosangari, S. L.; Watkin, K. L.; Cunningham, B. T. A label-free photonic crystal biosensor imaging method for detection of cancer cell cytotoxicity and proliferation, *Apoptosis* **2007**, *12*, 1061-1068.

(17) Ali, M. A.; Mondal, K.; Jiao, Y.; Oren, S.; Xu, Z.; Sharma, A.; Dong, L. Microfluidic Immuno-Biochip for Detection of Breast Cancer Biomarkers Using Hierarchical Composite of Porous Graphene and Titanium Dioxide Nanofibers, *ACS Applied Materials & Interfaces* **2016**, *8*, 20570-20582.

(18) Zhong, H.; Zhao, C.; Chen, J.; Chen, M.; Luo, T.; Tang, W.; Liu, J. Electrochemical immunosensor with surface-confined probe for sensitive and reagentless detection of breast cancer biomarker, *RSC Advances* **2020**, *10*, 22291-22296.

(19) Bezerra, G.; Córdula, C.; Campos, D.; Nascimento, G.; Oliveira, N.; Seabra, M. A.; Visani, V.; Lucas, S.; Lopes, I.; Santos, J.; Xavier, F.; Borba, M. A.; Martins, D.; Lima-Filho, J. Electrochemical aptasensor for the detection of HER2 in human serum to assist in the diagnosis of early stage breast cancer, *Analytical and Bioanalytical Chemistry* **2019**, *411*, 6667-6676.

(20) Dervisevic, M.; Alba, M.; Prieto-Simon, B.; Voelcker, N. H. Skin in the diagnostics game: Wearable biosensor nano- and microsystems for medical diagnostics, *Nano Today* **2020**, *30*, 100828.

(21) Kim, K. B.; Lee, W.-C.; Cho, C.-H.; Park, D.-S.; Cho, S. J.; Shim, Y.-B. Continuous glucose monitoring using a microneedle array sensor coupled with a wireless signal transmitter, *Sensors and Actuators B: Chemical* **2019**, *281*, 14-21.

(22) Windmiller, J. R.; Zhou, N.; Chuang, M.-C.; Valdés-Ramírez, G.; Santhosh, P.; Miller, P. R.; Narayan, R.; Wang, J. Microneedle array-based carbon paste amperometric sensors and biosensors, *Analyst* **2011**, *136*, 1846-1851.

(23) Senel, M.; Dervisevic, M.; Voelcker, N. H. Gold microneedles fabricated by casting of gold ink used for urea sensing, *Materials Letters* **2019**, *243*, 50-53.

(24) Gao, J.; Huang, W.; Chen, Z.; Yi, C.; Jiang, L. Simultaneous detection of glucose, uric acid and cholesterol using flexible microneedle electrode array-based biosensor and multi-channel portable electrochemical analyzer, *Sensors and Actuators B: Chemical* **2019**, *287*, 102-110.

(25) Ciui, B.; Martin, A.; Mishra, R. K.; Brunetti, B.; Nakagawa, T.; Dawkins, T. J.; Lyu, M.; Cristea, C.; Sandulescu, R.; Wang, J. Wearable Wireless Tyrosinase Bandage and Microneedle Sensors: Toward Melanoma Screening, *Advanced Healthcare Materials* **2018**, *7*, 1701264.

(26) Bhargav, A.; Muller, D. A.; Kendall, M. A. F.; Corrie, S. R. Surface Modifications of Microprojection Arrays for Improved Biomarker Capture in the Skin of Live Mice, *ACS Applied Materials & Interfaces* **2012**, *4*, 2483-2489.

(27) Dawes, J. M.; Weir, G. A.; Middleton, S. J.; Patel, R.; Chisholm, K. I.; Pettingill, P.; Peck, L. J.; Sheridan, J.; Shakir, A.; Jacobson, L.; Gutierrez-Mecinas, M.; Galino, J.; Walcher, J.; Kühnemund, J.; Kuehn, H.; Sanna, M. D.; Lang, B.; Clark, A. J.; Themistocleous, A. C.; Iwagaki, N., et al. Immune or Genetic-Mediated Disruption of CASPR2 Causes Pain Hypersensitivity Due to Enhanced Primary Afferent Excitability, *Neuron* **2018**, *97*, 806-822.e810.

(28) Chen, A. I.; Balter, M. L.; Chen, M. I.; Gross, D.; Alam, S. K.; Maguire, T. J.; Yarmush, M. L. Multilayered tissue mimicking skin and vessel phantoms with tunable mechanical, optical, and acoustic properties, *Medical Physics* **2016**, *43*, 3117-3131.

(29) Groenendaal, W.; von Basum, G.; Schmidt, K. A.; Hilbers, P. A. J.; van Riel, N. A. W. Qunitfying the Composition of Human Skin for Glucose Sensor Development, *Journal of Diabetes Science and Technology* ***2010****, 4,* 1032-1040.

(30) Whitton, J. T.; Everall, J. D. The thickness of the epidermis, *British Journal of Dermatology* **1973**, *89*, 467-476.

(31) Xiao, X.; Si, P.; Magner, E. An overview of dealloyed nanoporous gold in bioelectrochemistry, *Bioelectrochemistry* **2016**, *109*, 117-126.

(32) Holzer, B.; Manoli, K.; Ditaranto, N.; Macchia, E.; Tiwari, A.; Di Franco, C.; Scamarcio, G.; Palazzo, G.; Torsi, L. Characterization of Covalently Bound Anti-Human Immunoglobulins on Self-Assembled Monolayer Modified Gold Electrodes, *Advanced Biosystems* **2017**, *1*, 1700055.

(33) Capobianco, J. A.; Shih, W. Y.; Yuan, Q.-A.; Adams, G. P.; Shih, W.-H. Label-free, all-electrical, in situ human epidermal growth receptor 2 detection, *Review of Scientific Instruments* **2008**, *79*, 076101.

(34) Coffey, J.W.; Corrie, S.R.; Kendall, M.A.F. Rapid and selective sampling of IgG from skin in less than 1 min using a high surface area wearable immunoassay patch, *Biomaterials* **2018**, *170*, 49-57.

(35) Strambini, L.M.; Longo, A.; Scarano, S.; Prescimone, T.; Palchetti, I.; Minunni, M.; Giannessi, D.; Barillaro, G. Self-powered microneedle-based biosensors for pain-free high-accuracy measurement of glycaemia in interstitial fluid. *Biosensors and Bioelectronics* **2015**, *66*, 162-168.

Appendices

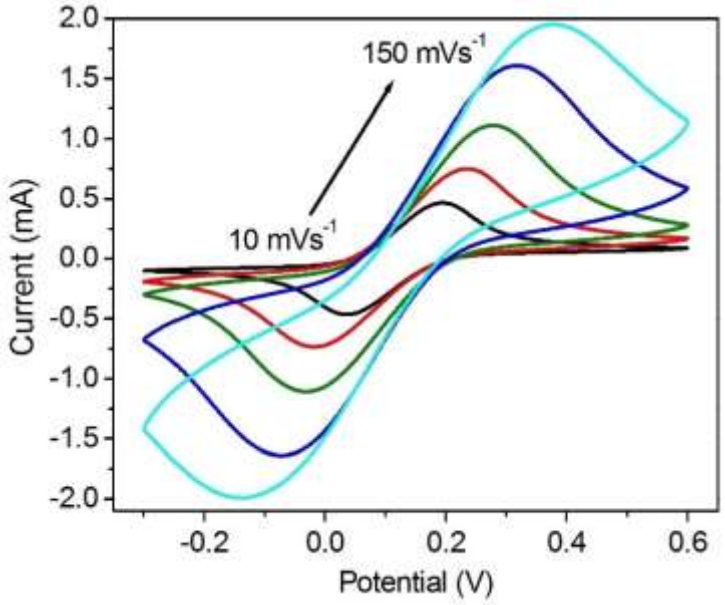

Figure S5.1: CV of Au-Si-MNA/anti-HER2 electrode at different scan rates, recorded in 5 mM of $K_4Fe(CN)_6$ / $K_3Fe(CN)_6$ (1:1 ratio) containing 0.1 M KCl.

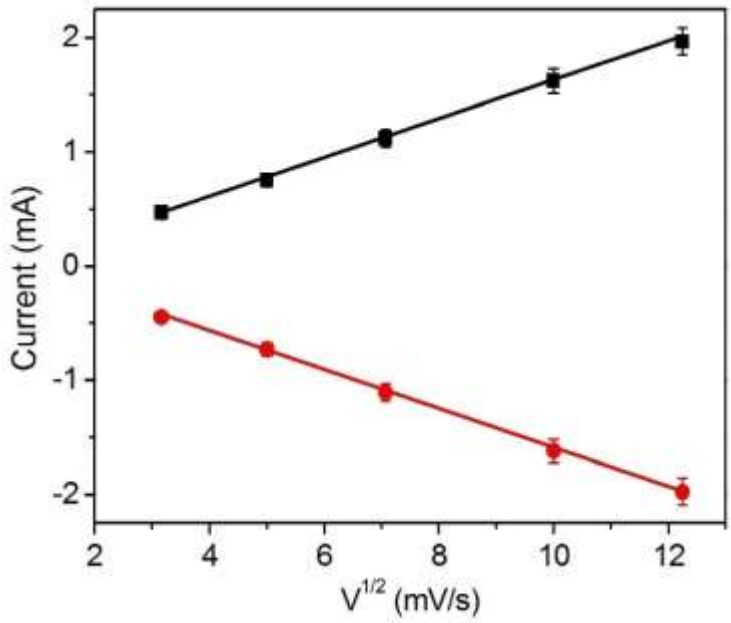

Figure S5.2: Anodic and cathodic peak currents obtained from Figure S5.1 versus the square root of scan rates (SD, n=3).

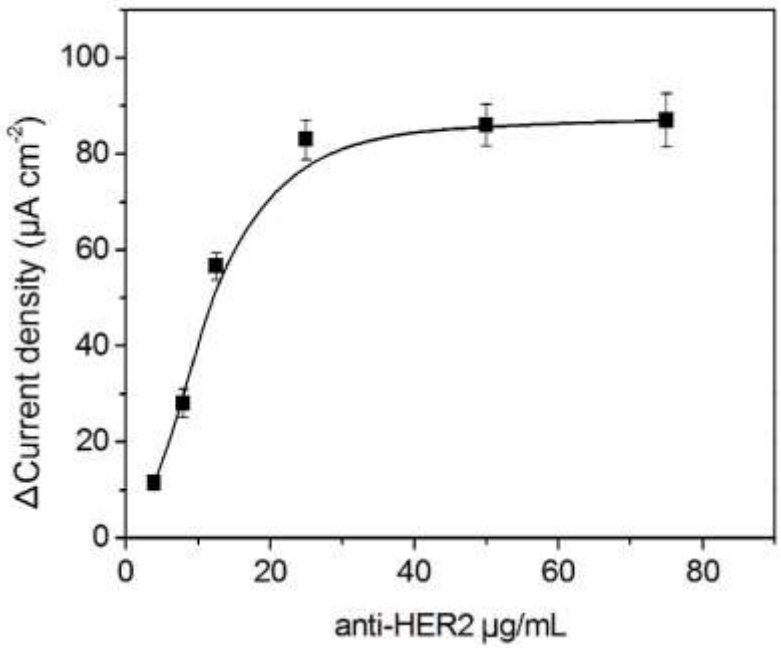

Figure S5.3: Optimum amount of anti-HER2 used for electrode modification (SD, n=3).

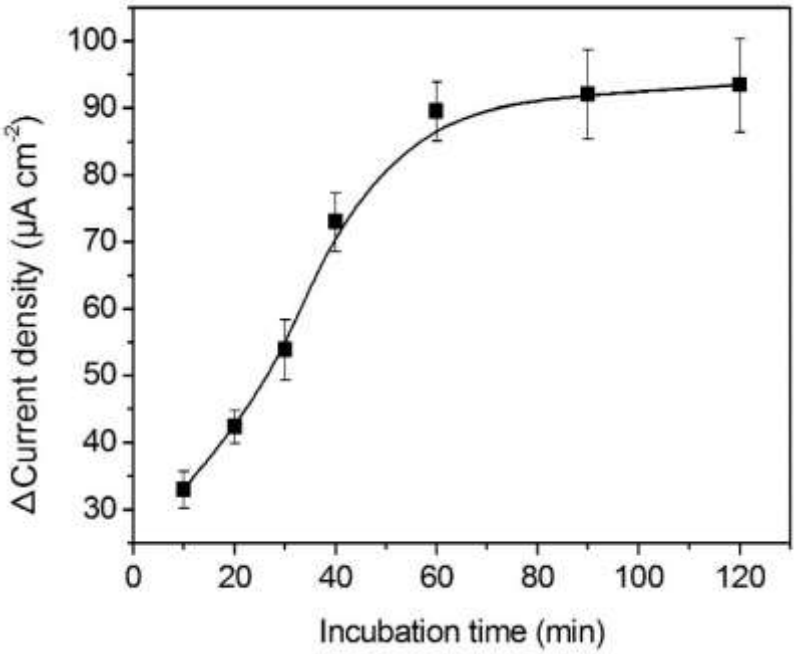

Figure S5.4: Optimum incubation time for Erbb2 (SD, n=3).

Table S5.1: Atomic ratios (X/C) calculated from average elemental compositions based on three replicates.

	Samples		
Atomic ratio (X/C)	**Au**	**Au/SAM**	**Au/SAM/anti-HER2**
Au	1.820 ± 0.023	1.690 ± 0.047	0.331 ± 0.000
C1	0.658 ± 0.009	0.741 ± 0.004	0.611 ± 0.004
C2	0.244 ± 0.018	0.091 ± 0.003	0.219 ±0.000
C3	0.054 ± 0.012	0.026 ± 0.004	0.160 ± 0.002
C4	0.044 ± 0.002	0.142 ± 0.005	0.009 ± 0.002
O	0.220 ± 0.007	0.336 ± 0.024	0.315 ± 0.005
N	0.060 ± 0.003	0.024 ± 0.018	0.167 ± 0.009
S	0.029 ± 0.003	0.101 ± 0.001	0.025 ± 0.000

Chapter 6: Conclusions and Future Directions

6.1 Conclusions

This thesis provides insights for developing wearable sensing platforms by utilizing high-density microstructured arrays. The fabrication of such sensing systems involves deep understanding, and therefore advances, in the structural engineering, electrochemical sensing, chemical biofunctionalization, and implementation of dense microarrays as efficient, user-friendly, and inexpensive platforms for epidermal and transdermal point-of-care disease diagnosis and health monitoring. Two types of microarrays, named micropillar (MPA) and microneedle arrays (MNA), were used to obtain three-electrode wearable patches for the electrochemical detection of clinically relevant biomarkers from sweat and interstitial fluid. An enzymatic approach was used for the detection of glucose using MPA and MNA in sweat and interstitial fluid, respectively. And an immunosensing approach based on microneedle arrays was designed to detect breast cancer biomarker ErbB2. The following points outline the conclusions drawn from this work addressing specific objectives of the thesis;

1. ***The first objective was design and fabrication of microarray structures suitable to interface sweat or interstitial fluid.*** This objective is mainly focused on developing microstructures to be used for noninvasive or minimally invasive wearable platforms. Since the sensing platforms come into contact with skin, MPA and MNA were made of silicon due to its biocompatibility in addition to its versatility for nano- and microfabrication. Both microarrays were fabricated using UV lithography and deep reactive ion etching of monocrystalline Si wafers. UV lithography allowed patterning hexagonal arrangements of microarrays with different dimensions and densities, and deep reactive ion etching allowed adjusting the length and shape of the microarray for specific application. In Chapter 3, a high-density silicon MPA platform fabricated for developing a noninvasive biosensor for sweat analysis is presented. The MPA

contains micropillars with a height of ~22 µm, diameter of 13 µm, and density of 65,500 pillars/cm^2. Noninvasiveness was achieved due to the ability of the pillars to be in contact with the epidermal sweat without penetrating the skin. Furthermore, high-density silicon MNA were fabricated for developing a transdermal biosensor. An enzymatic sensor (presented in Chapter 4) and an immunosensor (Chapter 5) were used for the analysis of interstitial fluid. Both platforms consisted of silicon microneedles with a height of ~250 µm, a base diameter of ~50 µm, and a density of ~9500 microneedles/cm^2 where the microneedle tip had a sharpness of ~2 µm. The design of the microneedles used in these sensing platforms allowed easy penetration of the outermost layer of the skin and enabled the biological recognition element (e.g. glucose oxidase (GOx) enzyme and anti-HER2 antibody) to interface with the interstitial fluid without reaching nerve bundles or blood vessels. After developing suitable microarrays for targeting sweat and interstitial fluid, the next step was to develop wearable patches for electrochemical sensing.

2. ***The second objective was development of a wearable sensing patch by integrating microarrays into a three-electrode system suitable for effective electrochemical sensing.*** With the goal of developing wearable patches, the fabricated silicon microarray substrates were integrated into 3D printed holders. Later on, for the realization of electrochemical sensing platforms, a thin layer (150 – 200 nm) of gold was deposited on MPA and MNA electrode surface via sputter coating. The gold coating not only provide a continuous conductive layer necessary for the use of silicon microarrays as electrochemical transducers, but also provided a suitable surface for further chemical modification and immobilization of the recognition element. Additionally, the Au-coated 3D printed holder provided a convenient electrical connection between microarray and the potentiostat. This process was applied for

both MPA and MNA electrodes. Having prepared functional microarray electrodes, the wearable patches were obtained by integrating three electrodes into a single patch. The final wearable patch consists of one working, one counter, and one reference electrode each made of microarrays suitable for sweat or interstitial fluid analysis.

3. ***The third objective was surface modification of the working electrode according to the specific application, and characterization and optimization the sensing patch***. The working electrodes were chemically modified and prepared for enzymatic sensing or immunosensing for their application in sweat or interstitial fluid analysis, respectively. In Chapter 3, the chemical modification of the MPA working electrode to be used for glucose detection in sweat involved the electrochemical deposition of a Prussian Blue layer followed by drop casting of a nanocomposite consisting of Au nanoparticles and chitosan. GOx enzyme was immobilized onto MPA electrode surface using glutaraldehyde as a crosslinker. This approach was shown to be effective for developing a sensitive glucose biosensor with a detection limit (26 µM) and linear range up to 1.4 mM. This sensing performance is suitable for the monitoring of sweat glucose the concentration of which is 100 times less than that in blood. In Chapter 4, the chemical modification of the MNA-based working electrode was designed for its application in transdermal glucose detection. The step-wise modification involved self-assembling monolayers of thiolated compounds on the Au surface after which ferrocene-cored poly(amidoamine) dendrimer (Fc-PAMAM) was immobilized after which GOx was immobilized via glutaraldehyde. Fc served as redox mediator between the enzyme and the working electrode surface. This approach enabled detection of glucose up to 10 mM making the sensing patch suitable for the monitoring of glucose in interstitial fluid. The surface biofunctionalization approach of each platform was tailored to the aimed application. Interstitial fluid contains glucose

in the mM range and hence this wearable patch required a different surface biofunctionalization approach than that implemented for MPA-based patch. The incorporation of Fc-PAMAM via self-assembling monolayers allowed higher levels of immobilization of enzyme onto MNA surface due to functional groups provided by dendrimers and therefore provided a much wider linear range. On the other hand, sweat contains glucose up to µM range and thus the MPA patch is needed to have µM sensitivity rather than a wide linear range, which was obtained using the Prussian Blue mediator. PB shows peroxidase activity which is excellent attributed to transducer platforms for H_2O_2 detection and during catalysis of glucose by GOx enzyme, gluconic acid and H_2O_2 are produced, where H_2O_2 is then reduced by PB (see Chapter 3). Having PB as an essential part of electrochemical transducer enables glucose detection in µM range since reaction occurs on the surface of electrochemical transducer whereas in MNA-based senor Fc served as electron mediator. The working electrode for the immunosensor was also based on MNA. In this case, the MNA electrode was modified using a similar self-assembling monolayers functionalization used to introduce Fc-PAMAM, followed by anti-HER2 antibody immobilization through EDC/NHS chemistry. Each step of the chemical modifications of the MNA-based working electrodes was characterized using XPS for elemental composition analysis, as well as electrochemical techniques such as CV, EIS, and DPV. The electrochemical optimizations of the analytical performance of the sensors such as sensitivity, linear range, detection limit, interference, and optimum parameters (pH, temperature, reusability, storage) were mainly performed using amperometry and DPV techniques.

4. ***The fourth objective was assessing the analytical performance of the wearable platforms using specific application scenarios***. In MPA-based platform for sweat analysis presented in Chapter 3, the electrochemical sensing mechanism relies on the transfer of the electrons from the reaction between glucose oxidase immobilized on the electrode surface and glucose present from sweat. The design and structure of the micropillars did not just provide high active surface area to enhance electrochemical sensing performance, but also a solution to an important issue that wearable sensors face: the loss of enzyme microlayer caused by the friction between skin and sensor surface. Prior to real-sample application, the MPA sensing patch was tested in artificial sweat where the sensor exhibited excellent analytical performance by detecting glucose in the range of 50 µM to 1.4 mM with detection limit of 26 µM and sensitivity of 4.7 µA/mM. The wearable MPA sensing patch was then tested using human sweat where glucose levels were successfully measured before and after meal consumption. The changes in measured glucose levels from sweat correlated very well with the changes in blood glucose levels measured using a commercial glucometer. MPA provided an alternative solution to the challenge faced by wearable technology regarding the delamination of the biological recognition element (e.g. enzyme) from the sensors surface due to the induced by friction between skin and the sensor surface. Additionally, the performance of the MPA sensing patch is such that is able to detect glucose levels not only in healthy individuals but also in diabetic patients owing to its wide linear range. Chapter 4 describes the MNA-based sensing patch for minimally invasive glucose detection from interstitial fluid without the need for extraction or collection. The analytical performance of the MNA glucose patch in artificial interstitial fluid showed very good selectivity towards glucose with a working range of 1 to 9 mM, detection limit of 0.66 mM, and sensitivity of 0.1622 µA/(mM $cm^{2)}$.

In vivo application of the MNA sensing patch on mouse demonstrated the ability of the sensor to detect changes in the interstitial fluid glucose levels. Moreover, the changes in glucose values obtained by the MNA sensing patch correlated very well with the blood glucose level changes obtained with a commercial glucometer. The developed MNA sensing patch provides an alternative transdermal diagnostic tool to the invasive existing techniques such as the finger-prick-based tests. In comparison with MPA based glucose patch, the MNA based patch had lower sensitivity. This is mainly due to the active surface area of the microarrays and the chemical modification approach of the electrode surface. Together to the conductive Au film, the MPA sensing patch incorporates a nanocomposite layer composed of AuNPs and chitosan. The electrical conductivity of AuNPs provides an enhanced the sensitivity and the chitosan matrix for immobilization of enzyme onto electrode surface. Instead, the MNA glucose sensing patch, apart from the Au conductive layer, incorporates a 2nd generation of non-conductive PAMAM dendrimers that facilitate the immobilization of the enzyme but might also have impacted on the electrode sensitivity despite providing a much wider linear range. Chapter 5 reports an MNA-based electrochemical immunosensor which can be used simultaneously as a biomarker extraction platform and electrochemical transducer for the quantification of the captured biomarker. The MNA-based immunosensor was tested, as a proof of concept, using a phantom gel that mimics the epidermis and dermis layers and contains a cancer biomarker, ErbB2. ErbB2 was extracted and quantified via DPV using the MNA sensing platform. As a result, the MNA-based immunosensor exhibited excellent analytical performance in the extraction and quantification of ErbB2 biomarker in a wide concentration range of 10 to 250 ng/mL and a detection limit of 4 ng/mL in aISF and 50 to 250 ng/mL with detection limit of 25 ng/mL in phantom gel. This analytical performance is sufficient for

detecting ErbB2 in the interstitial fluid and tissue of breast cancer patients which can range from 33.2 to 166.6 ng/mL. The MNA-based sensing platform is suitable for the modification with various biological recognition elements which can be applied for the sensing of other biomarkers. The simultaneous use of MNA as a tool for biomarker extraction and subsequent electrochemical quantification is described for the first time in this thesis. This sensing platfrom can provide an alternative method for the fast and simple protein biomarker screening and detection.

6.2 Future Directions

The works presented in this thesis describe new wearable sensing platforms which involve structural engineering, chemical surface modification, and development of high-performance electrochemical biosensors. At the same time, they provide solutions to some of the challenges faced in sweat and interstitial fluid analysis. The future work would involve managing some of the specific challenges which have to be addressed in order to produce cost-effective wearable devices with broad range of applications in health monitoring and diagnosis. The future work directions should be focused on the following:

1. To achieve continuous monitoring of sweat biomarkers, one of the remaining challenges is sweat manipulation in order to discard the analyzed sweat and collect a fresh sample. The integration of a microfluidic platform with the existing wearable sensing platform needs to be studied to resolve this issue.

2. The microneedle-based glucose sensing patch was used for the *in vivo* glucose monitoring for a relatively short time. Long-term applications will require further investigations to prevent detrimental effects such as biofouling and loss of enzymatic activity, which can hinder the analytical performance of the biosensor. Long-term studies of toxicity and biocompatibility of the sensing platform should also be performed.
3. The validation of the microneedle-based immunosensor was carried out using a phantom gel that mimics the density and horizontal alignment of the layers that form the skin. The optimum real application of this sensing system is an animal model that expresses the targeted breast cancer biomarker thus the future research could be focused on this direction.
4. The described sensing patches were optimized and used for the detection of glucose and ErbB2, as a proof of concept. However, analyzing the performance of this system in detecting different clinically relevant protein biomarkers including insulin and cortisol would be of high importance to the wider community.
5. Targeting relevant biomarkers, next to glucose, such as urea, lactate, and ions in form of multiplex system. Multiplex sensing platforms are particularly important in developing a closed loop system for diabetic patients that would involve the detection of both insulin and glucose in order to administer the most suitable amounts of insulin.
6. The current systems require the physical connection of the sensing patch electrodes to a potentiostat. For the purpose of increasing the patient compliance and portability of the system, the development of a wireless system with miniaturized power supply can be highly beneficial. This will be particularly important in integration of the sensors with other diagnostic systems.